

2013 Atomic spectrometry update—A review of advances in environmental analysis

Cite this: *J. Anal. At. Spectrom.*, 2014, 29, 17

Owen T. Butler,^{†*a} Warren R. L. Cairns,^b Jennifer M. Cook^c and Christine M. Davidson^d

Received 4th November 2013
Accepted 4th November 2013

DOI: 10.1039/c3ja90068a

www.rsc.org/jaas

1	Air analysis	3.4.3	Atomic fluorescence spectrometry
1.1	Review papers	3.4.4	Inductively coupled plasma mass spectrometry
1.2	Sampling techniques	3.4.5	Accelerator mass spectrometry
1.3	Sample preparation	3.4.6	Laser induced breakdown spectroscopy
1.4	Instrumental analysis	3.4.7	X-ray spectrometry
1.4.1	Atomic absorption spectrometry	4	Analysis of geological materials
1.4.2	Emission spectroscopy	4.1	Reference materials
1.4.3	Mass spectrometry	4.2	Solid sample introduction
1.4.3.1	Inductively coupled plasma mass spectrometry	4.2.1	Laser ablation
1.4.3.2	Other mass spectrometry techniques	4.2.2	Laser induced breakdown spectroscopy
1.4.4	X-ray spectrometry	4.3	Sample preparation
1.4.5	Combustion and spectrometric techniques	4.3.1	Sample dissolution
1.5	Data analysis and quality	4.3.2	Sample separation and preconcentration
2	Water analysis	4.4	Instrumental analysis
2.1	Sample preparation	4.4.1	Atomic emission spectrometry
2.2	Sample preconcentration and extraction	4.4.2	Inductively coupled plasma mass spectrometry
2.3	Speciation	4.4.3	Other mass spectrometric techniques
2.4	Instrumental analysis	4.4.3.1	Thermal ionisation mass spectrometry
2.4.1	Atomic absorption spectrometry	4.4.3.2	Secondary ion mass spectrometry
2.4.2	Inductively coupled plasma atomic emission spectrometry	4.4.3.3	Accelerator mass spectrometry
2.4.3	Inductively coupled plasma mass spectrometry	4.4.4	X-ray spectrometry
2.4.4	X-ray fluorescence spectrometry	5	Glossary of terms
2.4.5	Laser induced breakdown spectroscopy	6	References
3	Analysis of soils, plants and related materials		
3.1	Review papers		
3.2	Reference materials		
3.3	Sample preparation		
3.3.1	Sample dissolution and extraction		
3.3.2	Sample preconcentration		
3.4	Instrumental analysis		
3.4.1	Atomic absorption spectrometry		
3.4.2	Atomic emission spectrometry		

^aHealth and Safety Laboratory, Harpur Hill, Buxton, UK SK17 9JN. E-mail: owen.butler@hsl.gsi.gov.uk

^bCNR-IDPA, Università Ca' Foscari, 30123 Venezia, Italy

^cBritish Geological Survey, Keyworth, Nottingham, UK NG12 5GG

^dUniversity of Strathclyde, Cathedral Street, Glasgow, UK G1 1XL

[†] Review coordinator.

This is the 29th annual review of the application of atomic spectrometry to the chemical analysis of environmental samples. This Update refers to papers published approximately between September 2012 and July 2013 and continues the series of Atomic Spectrometry Updates (ASUs) in Environmental Analysis¹ that should be read in conjunction with other related ASUs in the series namely: clinical and biological materials, foods and beverages;² advances in atomic spectrometry and related techniques;³ elemental speciation;³ X-ray spectrometry⁴ and advances in the analysis of metals, chemicals and materials.⁵ In the field of air analysis, highlights within this review period include measuring the bioaccessible fraction of metals in particles and ongoing work in assessing the performance of optical and combustion techniques for the determination of the carbonaceous content of airborne



particulate matter. Developments in instrumentation included new sampler designs for the collection of nanoparticles, the coupling of FFF and hydrodynamic chromatography to ICP-MS for the sizing and compositional analysis of such particles and the ongoing development of aerosol mass spectrometry. In the field of water analysis, new procedures for the detection and quantification of emerging pollutants in water such as MRI contrast agents have been developed. Instrumental developments reported include the use of molecular absorption spectrometry, by exploiting the CS-AAS technique, for measuring halogen species in water. Numerous articles involving the application of atomic spectrometry to plants, soils and related materials appeared in this review period but, as usual, most were concerned with the environmental significance of the results, rather than the methodology used to obtain them. Nevertheless, there have been some interesting developments. Both LIBS and PXRF spectrometry have been used more widely, variants such as LA-LIBS and microwave assisted LIBS have appeared, and PXRF spectrometry has been applied for the first time in the analysis of plants. Developments in geochemical analysis include the production and (re)certification of new geological RMs for bulk, isotopic and microspatial analysis. Optimisation of LA-ICP-MS techniques for the interrogation of geochemical samples continues to be reported and a number of useful instrumental review articles (AMS, ICP-MS and SIMS) have been published. Feedback on this review is most welcome and the review coordinator can be contacted using the email address provided.

1 Air analysis

1.1 Review papers

Reviews have addressed: isotopic techniques and methodologies for assessing the origins and fate of pollutants⁶ (71 references); on-line aerosol MS for speciation analysis⁷ (31 references) and the chemical analysis of single particles in ambient ultrafine aerosols⁸ (88 references). Consolidation of knowledge regarding emerging pollutants is most welcome, such as the review by Harrison's group⁹ (271 references) on nanoparticle emissions from 11 non-vehicle exhaust sources and a review on the properties, production, uses, environmental fate, toxicity and analysis of phosphorus flame retardants¹⁰ (105 references). Studies on the bioaccessibility of metals in airborne particles have increased in number in recent years so a review¹¹ (86 references) on the approaches developed for the extraction of soluble metals was timely. The review also covered analytical techniques for the determination of dissolved species in the presence of complex sample matrix, *i.e.*, leachates, and included a useful compilation of published results for bio-accessible trace metals in airborne particles.

1.2 Sampling techniques

The development of *personal workplace air samplers*, used to monitor workers' exposure to airborne particles, continues to be a fertile area of research. The design of a new microtrap inertial impactor¹² utilised a high-density multijet plate to direct airflow and a matched mutiwell plate to collect particles by impaction.

The advantage of this system over current impactor samplers with fewer jets is a reduced pressure drop at comparable flow rates with favourable consequences for power consumption and potential for further miniaturisation. A microscale cascade-impactor using a novel soft lithography process¹³ included three impaction stages with 50% cut-points experimentally determined to be 1.19, 0.55 and 0.26 μm , when operating at a nominal 0.5 L min^{-1} . Particle bounce and re-entrainment were minimised by spin-coating of silicon oil onto the impaction targets. The overall particle losses were determined to be <10% for 0.2–2.5 μm particles and <12% for particles in the 0.05–0.2 μm range.

For the interrogation of nanoparticles, *TEM coupled with EDS* offers a powerful analytical tool for the determination of size, morphology and elemental composition. Sampling airborne particles directly onto TEM grids therefore makes sense as sample preparation time can be reduced and the potential for sample alteration or contamination minimised. Two commercially available TEM porous grids that allowed particles to be collected through filtration were evaluated.¹⁴ Collection efficiencies were *ca.* 18% for a nominal 30 nm size particle. A filter holder, the mini particle sampler, was specifically designed for this evaluation project to mount such grids and this new system was deemed suitable for sampling NPs in the size range 5–150 nm.

Following on from work reported in this ASU review last year on the development of field-portable FTIR systems¹⁵ for the determination of silica in coal dust, workers at NIOSH¹⁶ have now investigated the *uniformity of coal dust deposition on filters* and its effect on the accuracy of FTIR analysis. As with other microbeam techniques, use of FTIR analysis entails localised spot analysis and, as such, the spatial uniformity of dust deposition can affect accuracy and measurement repeatability. Three different sampler devices were evaluated using test filters loaded with silica and coal dust reference powders. The silica content was measured by FTIR spectrometry at nine locations across the face of each filter sample. Amongst a number of observations was the major conclusion that a single measurement shot at the centre of the filter was adequate for a field-based method. The average bias was *ca.* 10% and repeatability was *ca.* 15%.

Cascade impactor samplers are used to measure aerosol mass at different particle cuts and collected samples can further be analysed for chemical components. Concerns when using such samplers include solid particle bounce, overloading of collected particles on the impaction plate, interstage loss and clogging due to long-term or high-concentration sampling. Tests¹⁷ on a widely used system—MOUDI—showed that losses for particles <40 nm in size could be >20% and that nozzle plates with conventional step-shape nozzles could be prone to particle clogging. However, by using a lithographic technique to replace such nozzles with ones fabricated with smooth surfaces, the extent of clogging could be reduced. In addition, this new design was easier to clean between sampling exercises.

Passive samplers for collecting both gaseous and particle species from the atmosphere can be a cost-effective alternative to pumped samplers and are amenable for large-scale deployment in field sampling exercises. A disadvantage, however, is that the accuracy and precision of such devices may not meet



sampler performance standards often prescribed for regulatory measurements. A new calcium-aluminium oxide-based absorbent¹⁸ was designed for the diffusive sampling of atmospheric CO₂. Use of a range of techniques such as XRD analysis, electron microscopy and TGA showed that hydration of this absorbent was an essential part of the process of CO₂ absorption and subsequent conversion to carbonate. The diffusion uptake rate was $47 \pm 3 \text{ mL min}^{-1}$ and the LOD 40 ppm for samples collected over two days at 25 °C. When the samplers were deployed in triplicate in the field, the inter-sampler precision was *ca.* 6%. There was good correlation (Pearson's correlation coefficient = 0.879) between results obtained by this method and those obtained using a pumped sampler employing a reference NDIRS detection system. A passive aerosol sampler¹⁹ employed electron microscopy to measure concentrations and size distributions of airborne particulate matter. Measurement precision of this sampler, determined by deploying duplicate pairs of samplers in the field, was predominately <20% for both PM_{2.5} >5 $\mu\text{g m}^{-3}$ and PM₁₀ >20 $\mu\text{g m}^{-3}$. A new deposition sampler²⁰ employing industry standard 37 mm diameter filters could be used in different configurations such as suspension from a support with or without a protective windshield or as a suspended dust collection plate. An XRF ready option allowed sampling onto a filter cartridge assembly which could then be loaded directly into an XRF system for analysis. Initial wind tunnel tests using test aerosols of known particle size indicated that this sampler could collect representative particle size distributions.

Generation of *test particle atmospheres in a laboratory environment* is difficult and it is most informative to see publications describing the development and validation of aerosol test chambers. A system²¹ for source characterisation and controlled human exposure to NPs generated during gas-metal arc welding had an airtight 22 m³ climate-controlled stainless steel chamber at its core. A variety of on-line measurements, *e.g.*, using TEOM or SMPS, and offline measurements, *e.g.* using electron microscopy and PIXE techniques, could be made *via* sampling ports/samplers. Test particles were generated in a separate chamber and subsequently piped into the main chamber. Stable concentrations of atmospheric particles could be maintained for up to 6 h and concentrations could be varied from <5 $\mu\text{g m}^{-3}$ to >1000 $\mu\text{g m}^{-3}$ by dilution with clean filtered air. When this system was used²² to evaluate NPs generated from burning of scented candles in a simulated indoor environment, additional techniques such as IC, combustion and a TOF-MS were employed. There is increased concern that workers may be at risk of adverse health effects through exposure to CNTs which are increasingly being used in industry. Researchers at NIOSH designed a CNT aerosol respirator testing facility²³ for assessing the penetration of CNTs through half-mask and filtering-face-piece respirators commonly used to protect workers.

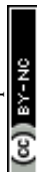
The *generation of test particles* within a laboratory setting can be achieved in many different ways. The most commonly used generators, spark device generators, and the theory of their operation have been reviewed²⁴ (60 references). These generators are already widely used in semi-conductor and materials research, and health and environmental studies and can

produce high-purity particles over the entire 1–100 nm range. The high-velocity impact²⁵ of Al or Cu cylinders of various lengths onto a steel anvil target (7.6 mm caliber, 23 or 38 mm in length, fired from a gas gun at velocities of up to 195 m s⁻¹) resulted in a particle number distribution with a mode of 10 nm. The goal of establishing a methodology for the production of soot particles resembling those emitted from internal combustion engines has led researchers²⁶ to evaluate the properties of particles produced under different operating conditions, using a commercially available and widely used combustion aerosol standard (CAST) generator. It was concluded that detailed and well-defined operational procedures were required if CAST systems were to be used to generate particles for instrument calibration.

1.3 Sample preparation

A *closed-vessel microwave-assisted* digestion method²⁷ was evaluated for the ICP-MS determination of trace and major elements in atmospheric aerosol samples collected on commonly used quartz-fibre filters. The use of HF was a prerequisite in dissolving the filter media but a consequence of its use was the potential for precipitation of insoluble fluoride compounds. Three approaches were examined for minimising this unwanted reaction: evaporation of excess HF using a microwave-assisted evaporation accessory; addition of boric acid to complex free fluoride ions; and a mixture of these two procedures. The hybrid approach was deemed to be the most successful based upon recoveries of 79–113% for elements in NIST SRM 1633b (constituent elements in coal fly ash) and 80–98% for elements in INCT CRM FFA-1 (elements in fine fly ash). Alternatively, a simple ultrasound-assisted extraction²⁸ involving a HNO₃–HF acid mixture has been proposed. Recoveries were 80–120% for a range of elements (Ag, Al, As, Ba, Be, Cd, Co, Cr, Cu, Fe, Mn, Mo, Ni, Pb, Sb, Se, Sr, U, V and Zn) in four RMs, namely NIST SRMs 1633b (constituent elements in coal fly ash), 1648 (urban particulate matter), 2584 (trace elements in indoor dust) and 2710 (Montana soil). Similar recoveries were obtained when the study was replicated in a different laboratory indicating that the method was both reliable and reproducible. As a further indicator of data quality, indoor air samples collected on filters were analysed initially by EDXRF spectrometry and then subsequently by ICP-MS using this extraction method. For the six elements detectable by EDXRF spectrometry (Cr, Cu, Fe, Ni, Pb and Zn), there were no significant differences in values between the two measurement approaches (paired *t*-test, *p* > 0.2, 95% CI). In summary, the authors concluded that this method was suitable for the high throughput analysis of lightly loaded air filter samples.

The *bioaccessible metal fraction* in urban aerosol particles may be a more informative metric than the total metal composition in assessing the potential health effects of exposure to inhaled particles. The bioaccessibility of nine elements (As, Cd, Co, Cr, Cu, Mn, Ni, Pb and Zn) in both TSP and PM_{2.5} filter samples were measured using a SBET *in vitro* extraction procedure.²⁹ Filter aliquots were extracted (1 h, 37 °C) in 0.4 M glycine (pH 1.5). Total concentrations were determined



following $\text{HNO}_3\text{--H}_2\text{O}_2$ digestion of separate filter sections using a closed-vessel microwave-assisted procedure. The mean bio-accessible fractions were 11% (Cr) to 65% (Cd) for both size fractions. The bioaccessible fractions of PGEs in airborne particulates were evaluated in two separate studies. In one,³⁰ a procedure using a synthetic gastric juice extractant was compared with closed-vessel microwave-assisted digestion with HCl--HF--HNO_3 . The Pd and Pt bioaccessible fractions were $41 \pm 17\%$ and $27 \pm 17\%$, respectively, in TSP filter samples and $26 \pm 17\%$ and $34 \pm 17\%$, respectively, in PM_{10} filter samples. The second study³¹ was similar but simulated human lung fluids, ALF and Gamble's solution, were used. Significant amounts of up to 29, 22 and 51% of Pd, Pt and Rh, respectively, were mobilised by ALF within 24 hours. The corresponding figures for exposure to Gamble's solution were 17, 18 and 44%. Interestingly, when sample leaching testing was performed on NIST SRM 2557 (used auto catalyst) test samples, much lower bio-accessible values were obtained. These results underline the danger of using RMs for leaching experiments, in which, despite best intentions, matrix matching between RMs and real world samples may not be as complete as believed.

1.4 Instrumental analysis

1.4.1 Atomic absorption spectrometry. Two papers advocated the use of *HR-CS-ETAAS* for the direct solid sample analysis of Ag^{32} and Pd^{33} in airborne particulate matter collected on glass fiber filter media which were ground for analysis. The characteristic mass M_0 for Ag was 4.4 pg when measured at the main absorption line of 338.289 nm and the LOD (3σ of the signal derived from ten atomisations of a ground blank filter) 17 ng g^{-1} equating to 0.05 ng m^{-3} in air for a sample air volume of 1440 m^3 . Using this optimised method, the airborne levels of Ag in Buenos Aires was determined to be $2\text{--}4.5 \text{ ng m}^{-3}$. The LOD for airborne levels of Pd was 0.07 pg m^{-3} . The airborne concentrations of Pd in Budapest and Istanbul were $0.3\text{--}0.9$ and $0.2\text{--}0.6 \text{ pg m}^{-3}$, respectively.

1.4.2 Emission spectroscopy. Investigation into the use of *LIBS* for the analysis of aerosol samples is a focus of a number of research groups. One attribute of this technique is its portability thereby providing *in situ* measurements. An interesting application of stand-off *LIBS* was an architectural survey³⁴ of the Cathedral in Malaga. Measurements made at an average distance of 35 m from stone structures were consistent with the mineralogical analysis of stones. The emission profiles for Al, Ca, Mg and Si confirmed that this particular structure was almost entirely built using sandstone. In addition, the different marbles used in the construction could be classified. Moreover, identification of pollutants, *e.g.*, Mn and Pb particles from vehicular emissions, on stone surfaces was possible, making it feasible to highlight hot-spots requiring repair and conservation. Exposure to airborne silica dust in coal mines can lead to silicosis, a potentially fatal lung disease. A *LIBS* system³⁵ was evaluated as a potential portable monitoring device for the rapid *in situ* analysis of personal filter samples from workers. Initial studies, using filter samples spiked with reference silica, kaolin and coal dust samples, and by undertaking

measurements at the Si 288.16 nm emission line, suggested that this approach had potential as an end-of-shift screening tool. In the hourly monitoring³⁶ of metals (*e.g.*, Al, Ca, Cr, Fe, Pb and Zn) in PM_{10} particles during Asian dust pollution episodes, the particles were sampled through a PM_{10} size-selective inlet, dried and focused as a spot onto a movable nylon filter. By moving a sample spot under a Nd:YAG laser it could be interrogated for their elemental composition. This process was repeated for subsequent spots thus providing time resolved data. Elemental emission intensities were normalised to carbon (measured at 247.856 nm) which could be used as an internal standard because the carbon emission from the underlying nylon filter was much larger and relatively more stable than the signal from the deposited carbonaceous particles. This approach was useful for minimising shot-to-shot variation common in laser-based systems. Metals were quantified using a calibration line established from *LIBS* and ICP-MS data for filter samples collected in parallel. The hourly data were successfully used to discriminate between various pollution episodes and their sources using elemental markers and employing chemometric techniques.

New AES instrumentation included: a *LIBS* system³⁷ employing a low-pressure rf-plasma discharge that had the potential for enhancing sensitivities over those obtained with plasmas operating at atmospheric pressure; a *LIBS* system³⁸ that used a triggering system to discharge the laser only when a particle was expected in the focal zone thereby improving the hit rate over current systems which commonly operate pulsed lasers at constant repetition rates; and a new portable dual-mode (OES and CRS) plasma spectrometer³⁹ which had the potential advantages of a large dynamic measurement range and an ability to cross-calibrate between the two modes of operation.

1.4.3 Mass spectrometry

1.4.3.1 Inductively coupled plasma mass spectrometry. The *multi-element capabilities* of ICP-MS were exploited in a newly developed DRC-ICP-MS method⁴⁰ employing a microwave-assisted digestion ($\text{HNO}_3\text{--HCl--HF}$ mixture) for the determination of 45 elements in road dust samples including PGEs (Pd, Pt and Rh), 13 main group elements, 15 transition metals and 14 lanthanoids. The recoveries of PGEs from IRMM BCR CRM 723 (road dust) and NIST SRM 2556 (used auto catalyst) were 105–111%. The recoveries of main group and transition elements from NIST SRM 1648a (urban particulate matter) were 85–115%. There was excellent correlation between analysis of digests using DRC-ICP-MS and re-analysis by SF-ICP-MS ($r^2 = 0.9\text{--}0.99$ for RMs and $0.99\text{--}1.00$ for road dust samples). The authors concluded that large element sets were needed to provide the necessary data to understand better anthropogenic influences on the wider environment. One source of metals in the atmosphere is the combustion of fuels in road vehicles. Because European national emission inventories have previously shown a very high variability in elemental emission factors (mass released per kg fuel burnt), a new survey⁴¹ analysed representative fuel samples, both diesel and petrol, from service stations in 9 nation states. Test samples were analysed using a collision cell ICP-MS system employing a HEN (ESI Apex Q). Use of a self-aspirating nebuliser with additional O_2 make-up gas ensured complete combustion and thus minimised potential for carbon



deposits on the cones. Although diesel samples could be analysed undiluted, petrol samples required dilution with Conostan PremisolTM solvent. Organometallic oil standards were used for calibration and NIST SRMs 1634c (trace elements in fuel oil) and 1084a (wear metals in lubricating oil) used as QC materials but the recoveries were not reported. Marked differences of up to two orders of magnitude in concentrations between samples remained but the proposed revised emission factors were generally lower than previously published values.

A technique⁴² for the detection and characterisation of *metal-containing NPs* coupled HDC, suitable for sizing NPs in the 5–300 nm range, to ICP-MS to provide a sensitive and selective analytical tool. Three calibration functions were required to measure NP size, number concentration and metal content, simultaneously. Reference Au NPs of various sizes were used as the model system. For water samples spiked with 60 nm sized Au NPs, the LOD was 2.2 ng L⁻¹ (600 NPs mL⁻¹). A working prototype⁴³ for the real-time size discrimination and elemental analysis of Au NPs consisted of a customised electrospray source and a differential mobility analyser to provide upstream particle size discrimination in real-time and CPC and ICP-MS instruments as downstream detectors to provide information on number density and elemental composition, respectively. A key design component in this system was the gas-exchange device for converting the air flow from the electrospray to the argon flow required to sustain the ICP-MS plasma. The Japanese research group led by Naoki Furuta,⁴⁴ continued their research into monitoring of elements in airborne particulates by direct introduction into an ICP-MS instrument. Calibrants were prepared using a desolvating USN to provide particle standards. Comparison of the results obtained with this real-time approach with those obtained for time-integrated samples collected using a more conventional filter sampling methodology gave good agreement for those elements (*e.g.*, As and Pb) with oxides that possess low melting points. In contrast, the real-time data were lower for elements (*e.g.*, Cr and Ni) with oxides with high melting points, indicating that such particles were not fully vaporised and ionised within the plasma. The authors suggested that this real-time approach could still be applicable if a correction factor based upon the ratio of real-time data to filter sampling data were used.

The use of quadrupole ICP-MS for isotopic measurements included the determination⁴⁵ of B isotopes in aerosol samples as tracers of emissions from coal burning. Water-soluble B was leached from filter samples, purified and concentrated using a B-specific resin and analysed using a bracketing calibration approach with normalisation to NIST SRM 951 (boric acid standard). The mean reproducibility (1 σ) of 3.0‰ for $\delta^{11}\text{B}$ was sufficient for B to be used as a discriminator. Isotopic data⁴⁶ for Nd, Pb and Sr were used in conjunction with elemental ternary diagrams to assess the relative contribution of particulate pollution from industrial point sources, such as an incinerator, a steel mill and a thermal power plant, in the air of two European cities (Kehl and Strasbourg). Suspended dust samples collected in passive samplers were digested in HNO₃-HF and elemental analysis undertaken using ICP-AES and ICP-MS. For isotope ratio measurements, MC-ICP-MS was used under dry

plasma conditions employing a HEN equipped with membrane desolvator. This combination of isotope tracers data with element triangle plots made it possible to identify specific point sources of pollution. The direct measurement⁴⁷ of U isotope ratios in single 10–20 μm U-doped glass particles used *ns* LA coupled to MC-ICP-MS. The analysis of 28 glass reference particles, measured under optimised conditions, yielded an average bias of <0.6% from certified values for $^{234}\text{U}/^{238}\text{U}$ and $^{235}\text{U}/^{238}\text{U}$. Results for the $^{236}\text{U}/^{238}\text{U}$ isotope ratio deviated by <2.5% from certified values. The calculated expanded measurement uncertainties ($k = 2$) were 2.6, 1.4 and 5.8% for $^{234}\text{U}/^{238}\text{U}$, $^{235}\text{U}/^{238}\text{U}$ and $^{236}\text{U}/^{238}\text{U}$, respectively.

1.4.3.2 Other mass spectrometry techniques. *New measurement tools* for nuclear safeguards will require new RMs to allow comparability of measurements by commonly used techniques such as LA-ICP-MS, SIMS and TIMS. To address this, IRMM, in collaboration with ITU, initiated a study⁴⁸ to investigate the feasibility of preparing and characterising a U-particle RM, certified for isotopic abundances and for U-mass per particle. To assist this process an improved ID-TIMS methodology was developed by IRMM to quantify the U-mass in single particles. Monodisperse U-oxide test particles were prepared by ITU using an aerosol-generation technique capable of producing particles of well-characterised size and isotopic composition. Experimental results demonstrated that it was possible to measure the U-mass per particle to a relative expanded uncertainty of *ca.* 10% ($k = 2$). The authors concluded that this enhanced method will be a valuable tool to assist in the certification of future RMs. It was possible⁴⁹ to distinguish between different valences states such as UO₂, U₃O₈ and UO₃ on surface layers and through depth profiles of U-oxide particles by interrogating the ion distributions measured by TOF-SIMS.

Developments and improvements in *gas-phase MS* included a new isotope ratio method⁵⁰ for the high-precision measurement of $^{17}\text{O}/^{16}\text{O}$ and $^{18}\text{O}/^{16}\text{O}$ in CO₂ to assist in tropospheric studies. The method was based on isotopic exchange equilibrium between H₂O and CO₂ in sealed glass ampoules followed by water fluorination to produce O₂. Dual inlet IRMS measurements of the $\delta^{17}\text{O}$ and $\delta^{18}\text{O}$ of O₂ in *ca.* 70 μmol of CO₂ allowed $\delta^{17}\text{O}$ values to be obtained with very high precision (0.01–0.3‰). In a rapid extractive ESI-MS method⁵¹ for the quantification of trace radioactive ^{129}I in ambient air, gaseous $^{129}\text{I}_2$ was initially converted into $^{129}\text{I}^-$ by passing it through an excess of Na₂SO₃. By adding an excess of $^{127}\text{I}_2$ into the solution, this $^{129}\text{I}^-$ was converted into a tri-iodate ion complex (I₃⁻). Quantification was based upon measurement of the characteristic $^{129}\text{I}^-$ fragment. The calibration curve had good linearity over a relatively wide range of 0.01–1000 ppbv ($r^2 = 0.991$), the LOD was 4.5 ppt and the RSD was 4–13%. The method was successfully applied to the detection of trace amounts of $^{129}\text{I}_2$ released in a simulated nuclear leakage accident.

Real-time measurements using *aerosol MS*, aided by the increased availability of new instrumentation, are providing more information on the origins and fate of particles in the atmosphere. Particulates containing trace elements emitted from vehicles are the focus of increasingly stringent air quality regulations but, to date, the emission rates and physiochemical



properties of such particles are not well characterised, largely as a result of difficulties in making such measurements. A newly developed instrument,⁵² the soot-particle aerosol mass spectrometer, employed a continuous 1064 nm laser beam to vaporise all particles, including the refractory ones, which were subsequently ionised by electron impact and analysed by HR-aTOF-MS. In contrast, commercially available aerosol MS systems that employ thermal desorption and electron impact ionisation methods can only quantify species that readily vaporise at up to 600 °C. The new soot-particle instrument also had a conical vaporiser used in more established aerosol MS systems so that only non-refractory components could be measured if the laser were switched off. The new instrument was considered a powerful tool for meeting future requirements for measurements at increasingly lower levels. The limitation⁵³ of a HR-aTOF-MS system that employed thermal desorption and electron impact ionisation for the on-line near-real-time detection of trace elements in airborne particles was that only elements with low melting and boiling points (*e.g.*, As, Cu, Zn) could be detected. With a nominal 5 minute sampling interval, the average LOD was *ca.* 0.3 ng m⁻³ (3 σ). In order to assess whether aerosol MS could be used as a quantitative tool, concentration data obtained were compared to those obtained by offline analysis of particles collected at the same times and locations using alternative methodologies. Two offline approaches were used: 12 h time-integrated PM_{2.5} filter samples collected using a high volume air sampler, subsequently digested for ICP-AES and ICP-MS analysis; and 6 h time-integrated PM_{0.07-0.34}, PM_{0.34-1.15}, PM_{1.15-2.5} filter samples collected using the IMPROVE DRUM sampler for PIXE analysis. Not unsurprisingly, the degree of correlation and agreement between the three measurement approaches varied depending upon the element in question, reflecting inherent limitations in each of the analytical approaches. The authors suggested that further intercomparison exercises, under controlled conditions, would be required to understand more fully the differences but that aerosol MS showed promise for the real-time detection of trace elements in air.

1.4.4 X-ray spectrometry. The *calibration and performance aspects of X-ray techniques* for characterisation of airborne particulate matter continue to attract attention. Initial studies⁵⁴ with a unit constructed at the Atominstut in Vienna for pipetting nL droplets onto flat surfaces, *e.g.*, quartz reflectors and wafers, for TXRF analysis suggested that the process was repeatable and that precise spatial patterns could be deposited on different sample carriers. More specifically, the system was able to produce calibrant standards for the quantification of aerosols collected by impactor samplers. Further developments are eagerly awaited. Historically, XRF techniques have been commonly used to analyse filter samples in a non-destructive manner, thus allowing further testing to be carried out. However, the validity of this approach⁵⁵ was questioned when it was observed that the EDXRF analysis under vacuum of particulate matter collected on commonly used quartz and Teflon filters led to mass losses of particulate matter, ionic compounds, VOCs and water. Although losses of NH₄⁺ and NO₃⁻ species have been previously reported, this was the first

time that losses of Ca²⁺, Cl⁻, Mg²⁺ and Na⁺ species had been observed. Further work to understand the mechanism of this mass loss will require additional measurements of, *e.g.*, organic/elemental carbon and water contents. Analysis in an inert atmosphere, rather than under vacuum, may alleviate the extent of the losses but could result in a decrease in sensitivity, particularly for lighter elements.

Novel but intriguingly simplistic applications of XRF for analysis of airborne particulates included the use⁵⁶ of a field-portable XRF spectrometer to determine if desert varnish rock samples contained a record of recent air pollution. A major component of desert varnish, a coloured coating found on rocks in arid environments, is windblown clay. As the concentrations of As, Cr, Pb and Zn, elements commonly found in fly ash, were significantly higher in samples collected downwind from two power plants than in unvarnished substrate rock, it was concluded that desert varnish could indeed be utilised as a passive environmental monitor to investigate recent air pollution (over the last 20–30 years). The potential⁵⁷ of using commercially available carbon adhesive tabs, typically used to mount samples for SEM analysis, in TXRF analysis was tested by sprinkling small quantities of particles (*ca.* 0.5 mg) onto these carbon substrates mounted on quartz reflectors. Good agreement with certified values was obtained for a number of powdered CRMs including NIST SRM 1648 (urban particulate matter). For quantification, a chosen certified element was taken as an internal standard. For unknown particulate samples, elements were normalised to the most abundant element so only elemental concentration ratios and not absolute concentrations could be measured. This procedure was advocated for the analysis of atmospheric fall-out particulate matter by swabbing surfaces to collect settled dust.

Solid-state speciation analysis gives an insight into the chemical composition of airborne particles. The XAS analysis⁵⁸ of airborne particulate matter, vehicle brake lining and brake pad wear residues showed that brake pads contain appreciable levels of Sb, typically 1–2% (m/m), mostly as Sb^{III} derived from the use of stibnite (Sb₂S₃) as a lubricant to reduce vibrations and to improve friction stability. The other major form was Sb^{III} derived from Sb₂O₃. However, the finding that the majority of wear residues, airborne particles and suspended road dust contained Sb₂O₄, an admixture of Sb^{III} and Sb^V oxides, supported the findings from thermogravimetric experiments that during braking brake pads may indeed reach temperatures high enough to induce oxidation. The authors concluded that Sb could be used as a tracer of motor vehicle emissions in source apportionment studies. The XAS technique is indeed powerful and is increasingly being used in diverse air pollution applications such as the speciation and bioaccumulation of S in camphor tree leaves⁵⁹ and Zn speciation in flue dust arising from the generation of waste during the production of carbon steel in blast furnaces.⁶⁰ The HR-PIXE analysis⁶¹ of aerosols collected in Budapest clearly identified the major Cl component as NaCl. Readers are directed to our companion Update for further information on developments and applications in reviews of X-ray spectrometry.⁴



1.4.5 Combustion and spectrometric techniques. *New instrumentation* is being developed to measure the carbon content in airborne particles that can impact greatly upon both climate and human health. A major contributor to aerosols in the workplace is DEEE which WHO have recently classified as a Group One carcinogen. A new real-time personal monitor⁶² measured the elemental carbon content of DPM captured on a Teflon filter. The instrument worked on the principle of light extinction, a combination of light absorption and scattering, using a laser at 650 nm. In the case of DPM collected on a filter, absorption was the dominant process. A calibration function was generated by exposing the instrument to DEEE in a controlled chamber alongside filter samples which were subsequently analysed using a reference combustion method (NIOSH 5040). For each data pair, the optical density, determined by taking the inverse log of the transmission (instrumental voltage reading), was plotted against the elemental carbon result obtained by the combustion method to derive a linear calibration plot ($r^2 = 0.98$) over the range 20–400 $\mu\text{g m}^{-3}$. For a 15 min integration period, the LOD was 10 $\mu\text{g m}^{-3}$. The instrument was not prone to interferences from humidity or oil mists. Potential light scattering effects due to other particles could be minimised by selectively sampling DPM over larger sized interferent particles through the use of a 1 μm size-selective sampler inlet. Although rarely present in the workplace nowadays, cigarette smoke could cause a positive bias in results. This instrument is currently being tested in underground mines, where worker exposure to DEEE can be a concern. Another instrument,⁶³ the multi-wavelength absorbance analyser, has been developed to measure light absorption by ambient air particulate matter collected on filters and hence to derive the black and brown carbon contents. This system used switchable low-power laser diodes at 405, 635 and 850 nm wavelengths thereby offering the possibility to apportion black and brown/organic carbon sources. Whilst the laser beam was collimated to illuminate only a small (*ca.* 1 mm^2) area of the filter, the instrument could automatically scan up to 2 \times 2 cm^2 in about 10 min. A 16-position filter wheel allowed unattended operation. Results correlated well with those obtained using other established photometric techniques (MAAP and a polar photometer) and with elemental carbon results obtained using a TOT method following the EUSAAR_2 protocol.

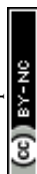
Evaluation of the analytical steps within TOT methods is another fertile area of interest. A step-wise solvent extraction method⁶⁴ for characterising carbonaceous aerosols allowed organic material to be separated into distinct fractions. Three punches taken from each filter were extracted with solvents of increasing polarity. The first was extracted in hexane (100%), the second in hexane–methylene chloride (1 : 1 by volume) and the third by a mixture of hexane–methylene chloride–acetone (1 : 1 : 1 by volume). In summary, the method fractionated organic aerosol into extractable and non-extractable OC and then further separated the extractable OC into three fractions defined as non-polar, low-polar and high-polar OC. It is hoped that this new methodology could assist atmospheric scientists to gain a better insight into the formation of secondary organic

aerosols for which knowledge of precursors, production pathways and atmospheric evolution is lacking. The outcome of a study⁶⁵ on the effects of different thermal treatments on radio-carbon measurements of OC and EC fractions in the atmospheric aerosol was suggested improvements to existing thermal protocols. One such improvement was the addition of a thermal step at high temperature in a helium atmosphere, after the traditional O_2 precombustion step, to remove more fully the refractory fraction of OC. By doing so, the potential for carry over of charred OC into the EC determination step was minimised. A study⁶⁶ was undertaken to ascertain the effect of increasing Fe content in laboratory-produced soot aerosol on its composition, structure and thermo-chemical properties. The temperature-programmed oxidation profiles showed a main peak ascribed to the evolution of CO_2 and a shoulder peak which was assigned to the combustion of iron carbides which became more pronounced as the concentration of Fe increased. The temperature of maximum CO_2 emission was found to decrease exponentially with increasing Fe content. Such a finding casts doubt on the feasibility of commonly used thermo-optical techniques for the quantification of OC and EC in carbonaceous particles if they are substantially contaminated with inorganic compounds, given that the distinction between the carbon forms using thermal techniques requires an operationally defined combustion temperature split-point.

1.5 Data analysis and quality

Evaluation of methodologies and instrumental techniques through *interlaboratory comparisons* is recognised as a valuable tool amongst measurement scientists. The divergent sampling techniques for respirable dust and the analyses for crystalline silica are an important issue amongst industrial occupational hygienists. In a comprehensive comparison study,⁶⁷ the workplace atmosphere multi-sampler, a rotating device in which 12 samplers could be exposed to the same dust environment concurrently, was used to compare the performance of six respirable dust samplers. The samplers were exposed to airborne dusts in four workplace settings (enamel production, sand extraction, foundry and brickworks) and the resultant filter samples analysed in seven participating laboratories using FTIR or XRD spectrometries.

It is possible for particles to deposit on surfaces in air samplers rather than fully on the filters. An *acid-soluble internal capsule digested with the filter* has been proposed as a possible solution to the incomplete sampling of airborne particles. An interlaboratory study⁶⁸ with 10 participants evaluated the suitability of cellulosic capsule inserts in the determination of trace elements in airborne samples. Prototype inserts were spiked with: aqueous solutions of Pb, Pb-containing soil RMs or aerosol samples (As, Cd, Co, Cr, Cu, Fe, Pb, Mn and Ni) generated using a desolvated nebuliser system. For these elements evaluated, the interlaboratory precision and mean recoveries were similar to those that could be expected if only filter samples were digested and analysed. As such this extra cellulose material should not present undue analytical complications but it remains to be seen whether such inserts can be produced commercially.



In a simple method⁶⁹ for generating *matched filter sets with known OC and EC contents*, carbon black particles were dispersed in water and nebulised, dried and desolvated in a test chamber to provide a reference EC particle aerosol. A saturated alginic acid solution was used as the starting material for preparing an OC-containing aerosol. Analysis in seven participating laboratories using the NIOSH 5040 combustion method gave a laboratory repeatability of <10%, 11% and 12% RSD for TC, OC and EC, respectively. Within-laboratory repeatability was <12%. This relatively simple generation system was considered suitable for method-performance studies.

Comparisons of instrumental techniques for measuring the same chemical moieties are interesting to read. Aerosols of ultrafine TiO₂ particles⁷⁰ with an agglomerate mean diameter of 67 nm were loaded (3–578 µg) onto PTFE filters and analysed independently using FTIR, LIBS and portable XRF procedures. The LODs (3σ) were 108, 0.03 and 11.8 µg, respectively, for the three procedures. The greatest dynamic range was given by the portable XRF instrumentation. In summary, XRF spectrometry could be a useful field measurement tool but further tests are required to test its performance on real matrix-containing samples. Robust methods to detect and characterise engineered NPs in environmental samples are urgently needed. The combination of ICP-MS with a size separation method holds promise in this context. Hence, the comparison⁷¹ of the HDC and AF4 techniques coupled to ICP-MS for detection, quantification and characterisation of NPs was welcome. The LODs, resolution and recoveries for both techniques were determined using Au NPs. The AF4 system was capable of separating mixtures of 5, 20, 50 and 100 nm particles with greater resolution than the HDC system, particularly in the smaller size range. Higher sample recoveries were noted for the HDC system (77–96%) than for the AF4 system (4–89%). The LOD for both techniques was *ca.* 5 µg L⁻¹. An additional benefit of HDC over AF4 was that it has a capability of separating a dissolved-sample signal from a NP signal.

2 Water analysis

2.1 Sample preparation

As noted in last year's review,¹ the determination of Hg in natural waters remains a challenge due to preservation and stability problems. In order to investigate the *stability and behaviour of Hg²⁺* spiked at natural levels in water samples, Guevara and Horvat⁷² irradiated an enriched ¹⁹⁶Hg²⁺ solution to produce a ¹⁹⁷Hg²⁺ radiotracer solution that was used to spike filtered and unfiltered marine, coastal lagoon, lake, river and rain waters at 3 to 13 ng L⁻¹ with and without acidification (1% v/v HCl). Subsequent storage was at room temperature or at 5 °C. The ¹⁹⁷Hg²⁺ was stable for over 10 days in unfiltered and unacidified marine and lake waters but 20% of the spike was lost, probably to the walls of the container (the authors did not specify), from the particulate and dissolved phases of river and lagoon waters. In refrigerated samples, the ¹⁹⁷Hg²⁺ partitioned between the dissolved and solid fractions as above but reached equilibrium more slowly. The ¹⁹⁷Hg²⁺ spike in samples acidified to 1% v/v HCl was stable at room temperature and at 5 °C when

stored in PTFE or borosilicate glass bottles, but significant (20–30%) losses occurred at all temperatures when the samples were stored in polyethylene bottles. The authors did not speculate on the fate of the lost mercury and did not carry out speciation analysis, so unfortunately we do not know if species inter-conversion occurred.

2.2 Sample preconcentration and extraction

Review articles published this year examined preconcentration methods from environmental matrices including waters. Of particular interest was a review⁷³ (52 references) of recent developments in SPE of elemental species from aqueous solutions. Two reviews focussed on the use of CNTs as SPE sorbents. One concentrated on their use prior to atomic spectrometric detection of trace elements⁷⁴ (140 references) and the other more specifically on the chemical modification of CNTs⁷⁵ (78 references). Given the explosion of interest in liquid microextraction techniques, a review of DLLME coupled with atomic absorption spectrometry⁷⁶ (126 references) was timely. Tables 1 and 2 summarise the most significant developments for analyte preconcentration prior to water analysis in this Update period.

2.3 Speciation

A *review* on the speciation of As, Cr, Hg, Sb, Se and Sn by coupled techniques⁷⁷ (79 references) included analysis of air, drinking water and soil matrices.

In a field-separation-based method for the *speciation analysis of arsenic*,⁷⁸ As^V was selectively retained on an anion-exchange resin and the eluent containing other cationic or neutral species collected. The As^V was then eluted with 5% HNO₃ and the As content of both eluents determined by ICP-SFMS operating in medium resolution mode. The method accuracy was assessed by analysis of NIST SRM 1640 (natural water). In another offline method,⁷⁹ the As^{III} in drinking water and snow was complexed with APDC and retained on polymeric microbeads. The adsorbed As was eluted with 0.25 M HNO₃ and quantified by ETAAS. The enrichment factor was 86 and the LOD for As^{III} 10 ng L⁻¹. The method was validated by carrying out spiking experiments (recovery varied from 96–100%) and analysis of water RM SEM 2011 from a Turkish national QA scheme.

Non-chromatographic methods⁸⁰ for the *speciation analysis of Cr in natural waters* have been reviewed (87 references). Addition⁸¹ of the ionic liquid 1-butyl-3-methylimidazolium tetrafluoroborate ([C4MIM]BF₄) to water samples improved the DDTC extraction of Cr^{VI} complexes during hollow-fibre liquid-phase-extraction. The Cr^{VI} in the eluate was determined by FAAS. The improvement in enrichment factor from 50 in the absence of ionic liquids to 175 resulted in a LOD of 0.7 ng mL⁻¹. Results for IERM CRM GSBZ5027-94 (environmental water) were in good agreement with the certified values. The dye dimethyl indocarbocyanide, an ion pairing agent⁸² that complexes Cr^{VI} under acid conditions, was used in a colorimetric method for the determination of Cr^{VI} by ETAAS. The complex was back extracted into toluene from the sample and



Table 1 Preconcentration methods using liquid phase extraction for the analysis of water

Analyte(s)	Matrix	Method	Reagent(s)	Detector	Attributes LOD ($\mu\text{g L}^{-1}$) unless otherwise stated	CRMs or other validation approaches	Reference
Al, Bi, Cd, Co, Cu, Fe, Ga, In, Ni, Pb, Tl and Zn	Water	Ultrasonic LLME	APDC, CCl_4	ICP-AES	LODs 0.13 (Al) to 0.52 (Tl), Enrichment factor 17–20	NRCC SLRS-4 (riverine water), HPS TMDW-500 (drinking water)	123
Au, Tl	Water	SFODME	1-Undecanol, benzyldimethyltetradecyl ammonium chloride dihydrate	ETAAS	Enrichment factors 441 (Au) and 443 (Tl); LODs 0.66 (Au) and 4.67 (Tl) ng L^{-1}	NIST SRM 1643 d (trace elements in water)	124
B	Water, seawater	DLLME	Aliquat® 336, trichloromethane	ICP-MS	Preconcentration factor 18, LOD 0.3	Spike recovery and comparison with ISO 9390:1990; azomethine-H method	125
Cd, Co, Mn, Ni	Water	Ultrasonic LLME	Tetrachloroethene, NaCl	ICP-AES	Sample pH12, LODs 0.13 (Co) to 0.28 (Ni)	NRCC SLRS-4 (river water), HPS TMDW-500 (drinking water)	126
Cd, Cr, Cu, Pb	Water	CPE	APDC, Triton X-114®	ID-ETV-ICP-MS	Preconcentration factor 14, LODs 1 (Pb) to 4 (Cr) pg mL^{-1}	NRCC SLRS-4 (river water) and SLEW-3 (estuarine water)	127
Cd, Co, Cu, Ni, Pb and Zn	Water	CPE	8-Hydroxyquinoline, Triton X-114®, back extraction into aqueous phase	ICP-AES	Enrichment factors 9.95–22.16, LODs 0.01 (Co, Pb) to 0.34 (Zn)	Spike recovery	128
Cd, Cu, Mn, Ni, Pb	Water and CPE effluent	CPE	APDC, Triton X-114®	ETAAS	Preconcentration factor 10, LODs 5 (Cu) to (80) Pb pg mL^{-1}	NIST 1640a (trace elements in natural water), IRMM BCR-713 (effluent waste water), BCR-715 (industrial effluent waste water) and BCR-609 (ground water)	129
Cd, Hg, Sb	Water	CPE	APDC, Triton X-114®	FI-VG-ID-ICP-MS	10 mL of sample, LODs 0.0006 (Sb) to 0.002 (Cd) ng mL^{-1}	NRCC SLRS-4 (river water) and SLEW-3 (estuarine water)	130
Co, Cu, Fe, Se, Pb and Zn	Water	DLLME	DDTC, CCl_4	EDXRF	5 mL sample, LODs 1.5 (Co) to 3.9 (Pb) ng mL^{-1}	Spike recovery and comparison with FAAS and ETAAS results	117
Cu, Pb	Water	DLLME	APDC, MIBK	FAAS	Enrichment factors 310 (Cu) and 187 (Pb), LODs 0.12 (Cu) and 1.2 (Pb).	NIST SRM 1643 e (trace elements in water)	131

the Cr determined by ETAAS. The LOD was $0.25 \mu\text{g L}^{-1}$ for a 3 mL water sample. Both coprecipitation and DLLME were used⁸³ in the determination of total Cr and Cr^{VI} in water, effluent and soils. The total Cr concentration was determined by FAAS after oxidation with $\text{Ce}(\text{SO}_4)_2$ in H_2SO_4 and coprecipitation with APDC. The Cr^{VI} was complexed with APDC and extracted by DLLME before quantification and the Cr^{III} was determined by difference. The enrichment factor for a 40 mL sample was 400 for the DLLME extraction and 100 for the coprecipitation approach. The LODs were 0.037 (Cr^{VI}) and $2.13 \mu\text{g L}^{-1}$ (total Cr). The method was validated by recovery of a spike from drinking water and the determination of total Cr in the NRCC CRM GBW-07309 (stream sediment).

Chromatographic methods for the determination of halogen species continue to receive attention. A method for fluorine speciation analysis⁸⁴ used molecular absorption spectrometry (CS-AAS) to detect F via the stable GaF molecule at 211.248 nm.

Offline RP LC with a C_8 column and a water-methanol (1 + 1) mobile phase separated the two model compounds trifluorobenzoic acid and 5-fluoroindol-5-carboxylic acid. The method LOD was *ca.* 1 ng mL^{-1} (100 pg absolute) and species identification was verified by ESI-MS. The authors postulated that this method approach could be suitable for the identification and quantification of unknown fluorinated organic compounds in environmental water samples. A new method⁸⁵ using the ion pairing agent tetraethylammonium hydroxide allowed the separation of the iodine species I^- , IO_3^- , 3-iodotyrosine and 3,5-diiodotyrosine in a single chromatographic run and was tested on seawater and seaweed samples. The LODs using an ICP-MS detector were 0.061 (IO_3^-) to 0.24 (3,5-diiodotyrosine) $\mu\text{g L}^{-1}$ and the recoveries 90–110%. The coupling of ion exchange chromatography with ICP-MS for the inorganic speciation analysis of Br and I in only 0.3 mL of Antarctic ice⁸⁶ gave LODs of 5–9 pg g^{-1} for the individual species.



Table 2 Preconcentration methods using solid phase extraction for the analysis of water

Analyte(s)	Matrix	Substrate	Substrate coating or modifying agent	Detector	Attributes LOD ($\mu\text{g L}^{-1}$) unless otherwise stated	CRMs or other validation approaches	Reference
Al, Be, Cd, Co, Cr, Cu, Fe, Mn, Ni, Pb, Ti	Water	Porous silica		ICP-AES	LODs 0.03 (Be) to 0.48 (Fe), 15 mL sample	NIST SRM 1643e (trace elements in water)	132
Cd and Pb	Water	Oxidised MWCNT	APDC	TXRF	LODs 1.0 (Cd) and 2.1 (Pb) ng mL^{-1} , 20 mL sample	Spike recovery	133
Cd, Co, Cu, Pb, Zn	Seawater and urine	PVC packed beads		ICP-MS	LOD 0.7 (Co) to 7.0 (Pb) ng L^{-1} , Enrichment factor of 10	NRCC SLEW-3 (estuarine water), NASS-2 (seawater) and NIST SRM 2670a (human urine)	134
Cd, Cu, and Pb	Natural waters and mussel tissue	Bond Elut® Plexa™ PCX polymer resin		FAAS	Enrichment factors of 90–95, LODs of 0.1 (Cd) to 0.5 (Pb)	NIST SRM 1643e (trace elements in water) and IRMM BCR 278r (mussel tissue)	135
Co, Cr, Cu, Mn, Ni and Zn	Water	Oxidised MWCNT	Electrochemically assisted sorption	EDXRF	LODs 1 (Cr and Cu) to 8 (Zn) ng mL^{-1} 100 mL sample	Spike recovery, comparison with ICP-AES	136
Cs	Estuarine and coastal waters	Separation using an AG50W-8X ion exchange resin	Adsorption onto ammonium molybdophosphate	ICP-MS	LOD 1.0 ng L^{-1} , 20 mL sample volume	NRCC SLEW-3 (estuarine water), CASS-4 (near shore seawater) and NASS-5 (seawater) even though not certified for Cs	137
Hg^{2+}	Drinking water	Activated carbon	Aliquat® 336	XRF	1700-fold enrichment factor, LOD 1 ng L^{-1}	Spike recovery of 98.5–100.6% at unrealistic spike levels ($\mu\text{g L}^{-1}$ level)	138
Ir, Pd and Pt	Sediments, water	Aminopropyl-controlled pore glass	1,5-bis(2-pyridyl)-3-sulphophenyl methylene]thiocarbonylhydrazide	ICP-MS	Enrichment factors of 43 (Ir) to 2.3 (Pd), LODs 0.1 (Ir) to 78.5 (Pt) ng L^{-1}	NIST SRM 2557 (autocatalyst)	139
REEs	Seawater	TSK™ Polymer beads	MWCNT	ICP-MS	LOD 0.01 (Lu) –0.16 (Ce) pg mL^{-1} , 100 mL sample	Spike recovery and comparison with another method	140
^{99}Tc	Seawater	Eichrom Teva	$\text{Fe}(\text{OH})_2$ coprecipitation	ICP-MS	LOD 11.5 pg m^{-3} for a 200 L sample (equivalent to 7.5 mBq m^{-3})	Comparison with standard method	141

The determination of *gadolinium-based MRI contrast agents* in biological and environmental samples remains a hot topic with a review⁸⁷(79 references) and two new significant articles being published recently. Detection of three unknown species in sewage sludge and waste water⁸⁸ indicated that species transformation can occur during anaerobic sludge treatment. The presence of the proprietary MRI agents⁸⁹ DotaremA® and GadovistaA® in water samples and river plants 5 km downstream of treatment works near Berlin was confirmed by coupling HILIC with ICP-MS and comparing retention times with those of standards. This finding supports concerns that

certain emerging pollutants may not be fully captured in traditional water treatment processes.

The *fractionation of trace elements in water* has become more feasible with the ever increasing proliferation of SEC and FFF instruments. The transport and fate of REEs⁹⁰ and 16 other trace elements⁹¹ in Alaskan rivers and the extent of their binding to organic and iron-rich nanocolloids was studied by directly coupling FFF to ICP-MS. It was noted that the distribution of these elements within these fractions was dependent on seasonal variations. The trace elements associated with marine dissolved organic matter have been characterised⁹² by SEC



followed by AEC. Using SEC it was demonstrated that marine dissolved organic matter, following ultra-filtration with a 10 000 Da cut off filter, ranged from 6.5–16 kDa. The AES-UV analysis (absorbance at 205 nm) of this mass fraction revealed the presence of 4 sub-fractions. With an elemental ICP-MS detector it was demonstrated that Sr and Zn containing complexes were associated with the first fraction, Mn was bound to the second and Co was detected in the third fraction.

2.4 Instrumental analysis

2.4.1 Atomic absorption spectrometry. *Improvements in the use of AAS* have been reported. The use of the slotted quartz tube as an atom trap⁹³ has been resurrected by some workers for the preconcentration of Bi on the surface of the quartz tube before release of the trapped atoms with 50 μL of methyl ethyl ketone. The use of the slotted tube resulted in a 2.9-fold improvement in sensitivity over an AAS system without this slotted tube, but by trapping on the tube a 256-fold improvement in sensitivity was achieved. This resulted in a LOD of 1.6 ng mL^{-1} when pre-concentrating a nominal 36 mL sample. The same research group⁹⁴ then modified this method for the determination of Sb. The optimal conditions of a nominal 25 mL sample volume and the use of MIBK as the releasing solvent resulted in a 369-fold sensitivity enhancement and a LOD of 3.9 $\mu\text{g L}^{-1}$. Use of quartz atom traps improved the LODs in the CVG of Ag.^{95,96} In the first paper,⁹⁵ the LOD of 0.7 ng mL^{-1} for Ag following trapping for 120 s was a significant improvement to that (10 ng mL^{-1}) for a similar system without this integration step. In the second paper,⁹⁶ the LOD of 0.11 ng mL^{-1} with 150 s trapping was better than that (1 ng mL^{-1}) for CVG using a multi-atomiser. The best combination of chemical modifiers⁹⁷ for the ETAAS determination of As, Cr, Cu and Mn in thermal spring waters was a ternary mixture of Ni, Pd and citric acid. Results for NIST SRM 1643e (trace elements in water) were in good agreement with certified values. The use of continuum source ETAAS⁹⁸ to measure Br gave an absolute LOD of 78 pg (7.8 $\mu\text{g L}^{-1}$ for a 10 μL injection). Bromine was detected as CaBr at the molecular absorption line of 625.315 nm after *in situ* formation in the pyrolytic graphite tube in the presence of an excess of Ca and Zr used as a permanent modifier. Careful selection of the absorption bands (less sensitive for high concentrations to more sensitive for low concentrations) made a linear working range of 10 $\mu\text{g L}^{-1}$ to 1 g L^{-1} possible. The method was considered suitable for the determination of Br^- , Br-containing whirlpool disinfectant agents and polybrominated flame retardants in waters.

2.4.2 Inductively coupled plasma atomic emission spectrometry. Some *novel uses of the ICP technique* have been reported. A review⁹⁹ (67 references) of current methods for the determination of chlorine in inorganic substances compared ICP-AES methods for the determination of Cl species (Cl , Cl^- and ClO_4^-) in aqueous media to the traditionally used titrimetric and chromatographic methods. In an interesting variation¹⁰⁰ of the procedure that uses $\text{K}_2\text{Cr}_2\text{O}_7$ for the determination of COD in waste waters, the sample refluxing step was initiated using a microwave-assisted reaction. The resultant Cr^{III}

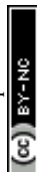
generated by the reduction of the Cr_2O_7^- was determined by FI-ICP-AES rather than the more traditional spectrophotometric endpoint. The linear range was 2.78–850 $\text{mg O}_2 \text{ L}^{-1}$ with an LOD of 0.94 $\text{mg O}_2 \text{ L}^{-1}$ and the results obtained correlated well with those obtained using the standard method. A miniaturised analytical CCD-AES system¹⁰¹ for the cold vapour determination of Hg in water was modified to use a gold filament preconcentration system to increase sensitivity. The LOD of 0.02 ng L^{-1} was sufficient for the determination of Hg in natural waters. Recoveries of $101 \pm 2\%$ ($n = 5$) for Hg in IRMM CRM ERM®-CA615 (Groundwater) were obtained.

2.4.3 Inductively coupled plasma mass spectrometry. Two *review papers* surveyed the use of ICP-MS analysis in the wider environmental (198 references)¹⁰² and life sciences arenas (42 references).¹⁰³ More specifically, in the second review, the determination of radionuclides in drinking water using ICP-MS techniques was compared against traditional radiometric techniques. A review of recent advances in vapour generation coupled with atomic spectrometry¹⁰⁴ (119 reference) covered the non-chromatographic speciation analysis of As, Bi, Cd, Ge, Hg, Ni, Pb, Sb, Se, Sn and Te in environmental samples including waters.

On account of its sensitivity, ICP-MS is well placed to meet *regulatory monitoring requirements for emerging pollutants* likely to be imposed in the future. Over 88 and 69% of Gd and Pt, respectively, discharged in hospital waste water was not removed¹⁰⁵ by a waste water treatment plant and was consequently discharged into the river Seine. The ETV-ICP-MS LOD¹⁰⁶ was 0.12 $\mu\text{g L}^{-1}$ when Au was used as a modifier in the determination of Hg in production waters arising from crude oil extraction processes. The average spike recovery was 106% for a production water sample which had been spiked with a Biorad Level 1 urine control material to produce a realistic saline matrix simulant. Reduction in argon consumption¹⁰⁷ to a mere 1.5 L min^{-1} as a move to reduce the cost of regulatory measurements was achieved with a novel low-flow ion source/sampling cone geometry. Even at these low flow rates, there was sufficient analytical sensitivity as judged by the good recoveries obtained for NIST SRM 1643e (trace elements in water).

In a *HG-ICP-MS* procedure for the simultaneous separation, preconcentration and determination of As, Bi and Sn in waters,¹⁰⁸ the analytes were retained on a functionalised silica column prior to quantification. Under optimum conditions of a sample loading flow rate of 1.9 mL min^{-1} , a 0.5% (m/v) NaBH_4 solution and a carrier gas flow rate of 0.98 L min^{-1} , the enrichment factors ranged from 2.5 (Sn) to 7.0 (Bi) and the LODs from 0.142 (Sn) to 0.002 (Bi) $\mu\text{g L}^{-1}$. Results for NWRI CRMs TMDA-54.4 and TM-24.3 (both fortified lake waters) were in good agreement with certified values. The volatile generation of Cd^{109} and Pb^{110} species was improved 15- and 17-fold, respectively, by the addition of $\text{K}_3\text{Cr}(\text{CN})_6$ and $\text{K}_3\text{Mn}(\text{CN})_6$, to the NaBH_4 reductant prior to ICP-MS detection.

The use of *isotope dilution analysis* in intercomparison exercises can generate data with a high degree of precision. An exact-matching ID-ICP-MS approach¹¹¹ was used for the determination of Cd, Ni and Pb in a NRCC candidate RM SIM-QM-S2 (trace elements in drinking water). Exact matching was



achieved by carrying out an initial analysis of the water using an external calibration approach to ascertain elemental concentrations in the test sample and then adding equal quantities of enriched isotopes to prepare 1 : 1 spiked solutions. Such ratios are optimal for counting statistics and for achieving the best possible measurement precisions. Results were in good agreement with values generated by other NMIs as part of an intercomparison exercise involving this candidate material.

The use of ICP-MS for *isotopic analysis* continues to be reported. As part of an interlaboratory analysis¹¹² of CRM IAEA-443 (natural and artificial radionuclides in seawater from the Irish sea), the MC-ICP-MS results for ²³⁹Pu, ²⁴⁰Pu, and ²⁴¹Pu activities and activity ratios were in good agreement with the radiometric data from 12 other laboratories. Such studies demonstrate the usefulness of ICP-MS as an alternative to traditional but slower radiometric techniques. The use of high-efficiency cones and desolvating nebulisers allowed the ¹⁴³Nd/¹⁴⁴Nd ratio to be determined on trace levels (1–5 ng) of Nd.¹¹³ Used in conjunction with a high-yield column preconcentration step, the long term measurement precision of the ¹⁴³Nd/¹⁴⁴Nd ratio was (± 0.000016 , 2 SD), comparable to that of TIMS analysis. An anion-exchange-resin-based clean-up method¹¹⁴ for the measurement of $\delta^{34}\text{S}$ required only 2 μg of sample and allowed a method precision of 0.24–0.34‰ (2 σ) to be achieved. This precision was comparable to that achieved using a previously reported cation-exchange clean-up methodology which, however, required 500 μg of sample.

2.4.4 X-ray fluorescence spectrometry. A number of papers advocated the use of *XRF techniques* for water analysis. The use of SR-TXRF spectrometry¹¹⁵ to determine trace element concentrations in Brazilian groundwater seems to this reviewer to be using a sledge hammer to crack a nut but there may be some merit to this approach as sample preconcentration was not required. The passive sample collection method DGT¹¹⁶ was used with EDXRF to determine the labile concentrations of Co, Cu, Mn, Ni, Pb and Zn in river water. The DGT samplers were analysed directly and gave results similar to those obtained by the SR-TXRF analysis of filtered samples from the same rivers. The use of DLLME extraction and dried spot EDXRF spectrometry¹¹⁷ for the determination of Co, Cu, Fe, Ni, Pb, Se and Zn in nominal 5 mL water samples gave LODs of between 1.5 (Co) and 3.9 (Pb) ng mL⁻¹. An alternative procedure,¹¹⁸ used to extract Se from aqueous samples, involved the use of MWCNTs in dispersive SPME mode. Mean spike recoveries were 97% and the LOD using EDXRF was 0.06 ng mL⁻¹.

2.4.5 Laser induced breakdown spectroscopy. Although the use of LIBS for water analysis remains hampered by the *lack of sensitivity*, hardware commonly used elsewhere in atomic spectrometry such as USN¹¹⁹ or HG¹²⁰ have now been combined with LIBS in an attempt to boost sensitivity. Alternative approaches advocated the use of absorbents such as printing¹²¹ or filter paper¹²² in an attempt to preconcentrate water samples. Papers were soaked in the sample, dried and then ablated. By preconcentrating a 40 g sample, LODs for Cr and Pb of 18 and 75 $\mu\text{g L}^{-1}$ were achievable.

3 Analysis of soils, plants and related materials

3.1 Review papers

Reviews of *analytical methods for the determination of specific analytes* included a critical evaluation¹⁴² of techniques for the measurement of Se in mushrooms (53 references); a summary¹⁴³ of methods for the determination of Re in various sample matrices including soils and plants (65 references); and overviews of radiochemical and ICP-MS procedures for measuring Th¹⁴⁴ (129 references) and ²³⁹Np¹⁴⁵ (227 references) in environmental samples.

Reviews on *specific sample types and applications* included the use of chemometrics in authentication of herbal medicines¹⁴⁶ by chromatographic, genetic and spectroscopic methods (196 references); the speciation and fractionation of trace elements in tea infusions¹⁴⁷ to assess bioaccessibility (60 references); and the capabilities and limitations¹⁴⁸ of INAA, XRF spectrometry, ICP-AES, ICP-MS and AAS in plant ionomics research (290 references).

3.2 Reference materials

A *brown rice flour CRM* (NMIJ CRM 7531-a) was certified¹⁴⁹ containing 0.280, 0.308, 4.34, 11.7, 27.6 and 31.8 mg kg⁻¹ As, Cd, Cu, Fe, Mn, and Zn, respectively.

3.3 Sample preparation

3.3.1 Sample dissolution and extraction. Rezić¹⁵⁰ presented a *comparison of digestion and extraction methods* for over 20 elements in cellulosic fibre materials (cotton, flax and hemp) as part of an assessment of the suitability of these materials as biosorbents. Microwave-assisted digestion of 0.5 g samples with 10 mL of 7 M HNO₃ gave better accuracy than dry ashing or open-vessel digestion when used in the analysis of CRM IAEA-V-9 (cotton cellulose); whilst ultrasound-assisted extraction in dilute mixed mineral acid solution recovered higher concentrations of analytes than liquid solid extraction or microwave-assisted extraction from fibres that had been steeped in a multi-element solution overnight. For the determination of P in soils, Ivanov *et al.*¹⁵¹ recommended digestion with 60% HClO₄ instead of *aqua regia* in either the ISO 11466 or EPA Method 3052 procedures because the *aqua regia* method underestimated *P* values for soil CRMs. In the determination of phytoavailable *P* extracted either in 0.04 M calcium lactate at pH 3.5 (the Egner Riehm soil test) or in 0.5 M sodium bicarbonate at pH 8.5 (method ISO 11263:2002), ICP-MS yielded higher concentrations than colorimetry. The relative differences were greater in soils with lower *P* concentrations. The determination of Ti in environmental studies is gaining importance as a means of estimating concentrations of engineered TiO₂ nanoparticles in the environment. In the analysis of a range of materials¹⁵² (stream sediment, bentonite, kaolinite and humic acid spiked with anatase, brookite and rutile), a novel muffle-furnace-based KOH fusion method yielded much higher Ti recoveries than microwave-assisted digestion. For example, results obtained



when Method EPA 3051A was applied to pure samples of the TiO₂ polymorphs were <10% of theoretical values, whilst recoveries of *ca.* 90% could be obtained with fusion.

Microwave-assisted digestion with a 5 : 4 HNO₃–H₂O₂ mixture gave better precision,¹⁵³ but similar recoveries, to those obtained by either *aqua regia* or reverse *aqua regia* digestion in the determination of 20 analytes in plants by ICP-AES. Disposable, screw-capped polypropylene tubes¹⁵⁴ were used as a cheaper alternative to PTFE vessels in the digestion of sediments with 30% HNO₃ + 5% HF. Recoveries similar to EPA Method 3052 were obtained for 26 elements, but the approach was unsuitable for Rb, REEs, Th, U or Zr.

*Microwave-assisted EDTA extraction*¹⁵⁵ was a viable alternative to *aqua regia* extraction for the estimation of pseudototal Cd, Cu, Mn and Pb concentrations in selected soil and compost samples, but gave poor recoveries for As, Ba, Be, Co, Cr, Ni, V and Zn. Unfortunately, even for the analytes successfully determined, the method may not prove transferable to other types of substrate. Microwave-assisted extraction with EDTA did provide¹⁵⁶ the basis for a successful IC-ICP-MS method for the determination of Cr^{VI} in solid samples including soil and welding dust. The analyte was extracted quantitatively with 50 mM EDTA at pH 10 in only 10 minutes (5 min at 90 °C + 5 min at 100 °C). Application of a double spike ID procedure showed that species interconversion – the bane of Cr speciation measurement – was inhibited by the formation of a stable Cr^{III}–EDTA complex.

A *ultrasound-assisted extraction* method¹⁵⁷ for the determination of S in mine tailing by ICP-AES – optimised by the use of a two-level, three-factor, full factorial design – involved sonication of 0.1 g samples for 20 minutes at 80 °C in 1 mL HCl + 1 mL HNO₃. Sonication¹⁵⁸ for 15 min in 0.05 M EDTA solution followed by quantification by ICP-AES was the basis of a fast screening method for estimation of mobile and potentially mobile Cu, Pb and Zn in sediment samples.

Sequential extraction protocols generally specify the use of air-dried samples. However, evidence has emerged that this may underestimate metal availability in flooded field conditions. Researchers in China¹⁵⁹ applied the BCR procedure to soils from rice paddies, extracting one portion of each sample at field moisture capacity under N₂ and another after air drying. A significant shift of Cd, Cr, Cu and Ni (but not Pb) from acid exchangeable and reducible to residual forms occurred on drying. Huang *et al.*¹⁶⁰ spiked soils with ²⁰²Hg and then used ICP-MS to measure the ²⁰²Hg/²⁰⁰Hg isotope ratio in the fractions obtained from an eight-step modified Tessier procedure. After two weeks equilibration at room temperature, the tracer was recovered predominantly in the first four fractions: water-soluble, exchangeable, and associated with fulvic and humic acids. Kozak and Niedzielski¹⁶¹ adapted their reactor manifold previously used for water analysis to perform *in situ* extraction of water-leachable, exchangeable and 2 M HCl-leachable forms of As and Sb in sediment, with quantification by on-line HG-AAS.

Interest has continued in improving *physiologically-based extraction tests* to assess human bioaccessibility of elements following ingestion. A round-robin study¹⁶² compared no fewer

than 17 different procedures for assessment of the bio-accessible content of up to 24 elements in NIST SRM 2710 (Montana soil). No preferred method emerged, but several gave results consistent with *in vivo* testing for As (swine and mouse) and Pb (swine only). The pH of the extractant(s) was found to have a strong influence on results. A modified version¹⁶³ of the European Standard Toy Safety Protocol EN-71 (sample : extractant ratio 1 : 2000) extracted similar amounts of As, Cd, Cr, Cu, Ni, Pb and Zn as the well-established SBET method (0.4 M glycine at pH 1.5) from NIST SRMs 2710 and 2711 (both Montana soils) and 2583 and 2584 (both indoor dusts). The modified EN-71 extraction was therefore recommended for use as a simple and rapid soil screening test.

3.3.2 Sample preconcentration. *Analyte preconcentration procedures* continue to be developed because they remove potential interferents and allow workers who have access only to techniques such as FAAS to improve their LODs substantially. Methods for the analysis of soils, plants or related materials, or those developed for other sample matrices that used soil or plant CRMs for validation, are summarised in Tables 3–5.

A *combination of preconcentration approaches*⁸³ was used successfully for Cr speciation in soil extracts and water by FAAS. The Cr^{VI} concentration was determined following DLLME using APDC, carbon tetrachloride and ethanol as chelating agent, extraction solvent and disperser solvent, respectively. The total Cr concentration was determined by coprecipitation following oxidation of the sample with 0.02% Ce(SO₄)₂ in 0.07 M H₂SO₄. The Cr^{III} concentration was estimated by difference. A four-step procedure¹⁶⁴ reduced interference from Mo and Sn in the determination of Cd in rice and sediments by ICP-MS. The steps were: thiourea SPE for removal of the majority of matrix elements; coprecipitation with Mg(OH)₂ to eliminate Mo; acid dissolution of the precipitate; and strong anion exchange SPE to remove Sn.

3.4 Instrumental analysis

3.4.1 Atomic absorption spectrometry. A thermal desorption AAS method¹⁶⁵ used a commercial total Hg analyser for *rapid identification of Hg species in solid samples*. The procedure was applied successfully to soil and sediment samples and CRMs BCR CRM 142 R (light sandy soil), RTC CRM 021 (sandy loam) and NRCC MESS-3 and PACS-2 (both marine sediments).

Developments in AAS included a method for the determination of Ag that introduced a new design⁹⁵ of CVG integrated-atom-trap. A 2 min *in situ* preconcentration gave a 143-fold improvement in sensitivity over conventional FAAS and an LOD of 0.7 µg L⁻¹. A method¹⁶⁶ for the determination of Cd in soil extracts combined high-speed self-reversal background correction with HG-AAS. The LOD was 1 ng mL⁻¹ and the RSD 5% (*n* = 10). Results were statistically similar to those obtained by ETAAS using a Pd/MgNO₃ matrix modifier. Li *et al.*¹⁶⁷ more than doubled both sensitivity and linear range for the determination of Cu and Zn in plants by coating the inner wall of a slotted quartz tube atomiser with SiO₂ nanoparticles. Recoveries of analytes from NIST SRMs 1515 (apple leaves) and 1573 (tomato leaves) were in the range 95–102%.



Table 3 Preconcentration methods involving liquid-phase extraction used in the analysis of soils, plants and related materials

Analyte(s)	Matrix	Method	Reagent(s)	Detector	Attributes LOD ($\mu\text{g L}^{-1}$) unless otherwise stated	CRMs or other validation approaches	Reference
Au, Pd, Pt	Soil	CPE	Tergitol TMN-6 and ammoniumpyrolysine dithiocarbamate	FAAS	1.2, 1.4, 2.8 for Au, Pd, Pt, respectively	Spike recovery	221
Bi	Ash, coal, metals, ointment, soil, urine, water	CPE	Triton X-114® and iodide + thiourea	HG-ICP-AES	0.01	Spike recovery	222
Cd, Co, Ni, Pb	Water	DLLME	2-(2'-Benzothiazolylazo)-p-cresol in trichloroethylene and ethanol	ICP-AES	0.2–0.7	NIST SRM 1944 (waterway sediment)	223
Hg species	Sediment	VALLME	L-Cysteine and carbontetrachloride	HPLC-cold vapour-AFS	0.028 ng g ⁻¹ for MeHg ⁺ , 0.057 ng g ⁻¹ for EtHg ⁺ , and 0.029 ng g ⁻¹ for Hg ²⁺ .	IRMM ERM-CC580 and IAEA-405 (both estuarine sediments) for MeHg, spike recovery for other analytes	224
Mn	Fish, mollusc, water	SDME	1-(2-Pyridylazo)-2-naphthol in chloroform	ETAAS	0.03	NIST SRMs 1515 (apple leaves), 1570a (spinach leaves), 1577 (bovine liver), IRMM ERM CE 278k (mussel tissue)	225
Pb, Pd	Catalytic converter, radiology waste, soil, street dust, urban aerosol	CPE	Triton X-114® and dimethylglyoxime	FAAS	1.4 for Pb, 1.0 for Pd	NIST SRM 2711 (Montana soil), 2704 (Buffalo river sediment), and IRMM BCR CRM 142R (light sandy soil)	226
Pd	Anode slime, catalytic converter, road sediment, water	DLLME	2,2'-Furyldioxime in chloroform and methanol	FAAS	0.04	CDN-PGMS-10 (platinum group ore)	227
Zn	Hair, rice, soil, tea, waters	LLE	Ethyl-2-(4-methoxybenzoyl)-3-(4-methoxyphenyl)-3-oxopropanoylcarbamate in MIBK	FAAS	0.2	LGC 6019 (river water), NIST SRM 1547 (peach leaves)	228

Developments in ETAAS included a new chemical modifier¹⁶⁸ of 6 $\mu\text{g Pb}$ + 1600 μg citric acid that overcame chloride interference in the determination of Ag in *aqua regia* digests of soils, sediments and sludges, and a procedure¹⁶⁹ for the simultaneous determination of As, Cd, Cu, Cr, Ni, Pb and Tl in sediment digests and extracts, optimised *via* a 3³ Box-Behnken factorial design. Interest in slurry sample introduction continued. One reported method¹⁷⁰ used Ir as a permanent modifier in the measurement of Cd and Pb in medicinal plants. Another¹⁷¹ used

dimethylglyoxime-impregnated activated carbon to preconcentrate Co and Ni from plant CRMs prior to introduction to the graphite tube as a carbon slurry. Although good recoveries were obtained (105–114% for Co and 95–100% for Ni), before the sorbent could be added the samples had to be digested in HNO₃ and the digests taken to near dryness, reconstituted in de-ionised water, and adjusted to pH 7 with sodium hydroxide. This is a disadvantage relative to conventional slurry sample introduction that can be applied directly to solid samples.

Table 4 Preconcentration methods involving precipitation used in the analysis of soils, plants and related materials

Analyte(s)	Matrix	Carrier	Detector	Attributes LOD ($\mu\text{g L}^{-1}$) unless otherwise stated	CRMs or other validation approaches	Reference
Cd, Co, Cr, Cu, Fe, Mn, Ni, Pb	Food, soil	Holmium hydroxide	AAS		IRMM BCR CRM 141R (calcareous loam soil), CRM 025-050 (soil)	229
Cd, Co, Pb, Zn	Baby food, dried eggplant, water	Mo(VI)-diethyldithiocarbamate	FAAS	1.1–2.2	NWRI TMDW-500 (drinking water)	230
Cr species ^a	Soil, water	Copper-violuric acid	FAAS	1.2	Spike recovery	231

^a Coprecipitation of Cr^{III}, then reduction with sulfuric acid and ethanol, determination of total Cr, and estimation of Cr^{VI} by difference.



Table 5 Preconcentration methods involving solid phase extraction used in the analysis of soils, plants and related materials

Analyte(s)	Matrix	Substrate	Substrate coating or modifying agents	Detector	Attributes LOD ($\mu\text{g L}^{-1}$) unless otherwise stated	CRMs or other validation approaches	Reference
Au	Water	Alumina nanoparticles	9-Acridinylamine	FAAS	13		232
Cd, Co, Mn, Ni, Pb	Street sediment, tea, water	Poly(2-thiozylmethacrylamide-co-divinylbenzene-co-2-acrylamido-2-methyl-1-propanesulfonic acid)		FAAS	0.23–1.1	NWRI TMDA-70 (fortified lake water), SPS-WW1 batch 111 (waste water), NIST SRM 8704 (Buffalo River sediment), NRCCRM GBW 07605 (tea)	233
Co, Cu, Fe, Pb	Table salt	MWCNT	Violuric acid	FAAS	0.15–0.43 $\mu\text{g g}^{-1}$	NWRI TMDA 54.4 (fortified lake water), HR-1 (Humber River sediment) NIST SRM 1515 (apple leaves)	234
Cu, Fe, Ni, Pb	Animal feed, water	Single walled carbon nanotube discs	2-(5-Bromo-2-pyridylazo)-5-diethylaminophenol	FAAS	0.3–4.6	NWRI TMDA 54.4 (fortified lake water), NWRI HR-1 (Humber River sediment)	235
Cu, Zn	Vegetables, water	Silica-coated Fe_3O_4 nanoparticles	2,6-Diaminopyridine	AAS	0.14 for Cu, 0.22 for Zn	NRCCRM GBW 08301 (river sediment), 08607 (water solution)	236
Fe, Pb	Environmental samples	MWCNT	2,9-Dimethyl-4,7-diphenyl-1,10-phenanthroline	FAAS	1.3 for Fe, 2.9 for Pb	NWRI TMDA 54.4 (fortified lake water), HR-1 (Humber River sediment)	237
Hg	Liver, lotus leaf, water	Silica gel	Diethylenetriamine and thiourea	ICP-AES	0.023	NRCCRM GBW 08301 (river sediment), 09101 (hair powder)	238
Ir, Pd, Pt	Sediment, water	Aminopropyl-controlled pore glass	1,5-bis(2-pyridyl)-3-sulfophenyl methylene thiocarbonohydrazide	ICP-MS	0.0001 for Ir, 0.056 for Pd, 0.079 for Pt	NIST SRM 2557 (autocatalyst)	139
La, Nd, Pr, Sm	Soil	Carbon ferrite magnetic nanocomposite	4-(2-Pyridylazo) resorcinol	ICP-AES	0.5–10	IAEA Soil-7	239
Mo	Vegetables, water	Amino-functionalised silica	2,6-Diacetylpyridine-			monosalicyloylhydrazone	FAAS
0.5 Ni	Fish, plants, soil, water	Pyridine-functionalised MCM-41 and MCM-48		FAAS	3.5	Spike recovery	241
Ni	Fish, sediment, vegetables, water	Nanostructured ion imprinted polymer		FAAS	0.15	NACIS DC 73323 (soil), OREAS BG 326 (ore polymetallic gold)	242
Pb	Water	MWCNT	3-Mercaptopropyl trimethoxysilane	FAAS	1.7	NRCC PACS-2 marine sediment	243
Pb	Fish, sediment, soil, water	Magnetic metal-organic framework		FAAS	0.37	NRCCRM GBW 07293 (platinum ore), inter-laboratory comparison	244
Pd	Soil, water	Pyridine-functionalised magnetic nanoparticles		FAAS	0.15	Spike recovery, inter-laboratory comparison	245
Pd, Pt, Rh	Soil	Activated alumina		ICP-AES	0.3–2.1	Spike recovery	246

High-resolution continuum-source AAS has seen use with both flame and electrothermal atomisers. Researchers in Romania¹⁷² developed a fast sequential method for determination of Ag, Cd, Co, Cr, Cu, Ni, Pb and Zn in soil digests by HR-CS-FAAS. This was shown by the Bland and Altman statistical method to have accuracy, precision and LODs statistically similar to those obtained using ICP-AES. Researchers in Brazil, who have long championed CS-AAS, reported methods for the determination of Cr¹⁷³ and Pb¹⁷⁴ in medicinal plants by HR-CS-ETAAS with direct solid sampling. Both procedures yielded accurate results, at the 95% confidence level, for analysis of RMs including NIST

SRM 1515 (apple leaves), 1547 (peach leaves) and 1575a (pine needles). The use of wavelength-integrated absorbance and/or summation of absorbance at different lines enhanced¹⁷⁵ sensitivity in the determination of B, P and S in plant digests by HR-CS-FAAS.

3.4.2 Atomic emission spectrometry. Use of a flow-blurring® multiple nebuliser¹⁷⁶ increased analyte transport into the plasma by >40% relative to a standard sample introduction system and also meant that an internal standard (1 mg L⁻¹ In) could be mixed with samples and standards in the spray chamber, thereby reducing interference from Ca, K, Mg and Na in the



determination of As and Se by ICP-AES. Recovery of As from BCR CRM 280R (lake sediment) was 96% compared with 116% with a conventional nebuliser. The LODs were *ca.* 50 $\mu\text{g L}^{-1}$ for both analytes compared with 91 $\mu\text{g L}^{-1}$ for As and 130 $\mu\text{g L}^{-1}$ for Se when using a conventional nebuliser.

In contrast, lower plasma loading and sample consumption was achieved¹⁷⁷ in the development of a *high-temperature, single-pass spray chamber* (also called a torch-integrated sample introduction system, see Section 3.4.4). Combined with segmented sample injection into an air carrier gas and single point standard addition, it was used in the ICP-AES analysis of marine samples including CRMs GBW 07313 and ISS-A1 (both marine sediment). Matrix interferences from Al, Ca, K and Na on the analytes Ag, Al, Cd, Mn and Zn were reduced.

Multivariate optimisation using two-level factorial design¹⁷⁸ allowed *development of a method for the determination of mercury by FI-cold vapour-ICP-AES* with a LOD of 0.11 $\mu\text{g L}^{-1}$. The recovery was 99% for NIST SRM 2704 (Buffalo River sediment) and 98% for CRM IAEA 085 (human hair).

3.4.3 Atomic fluorescence spectrometry. A new method¹⁷⁹ for the *speciation of Sb in vegetables* by HPLC-HG-AFS involved ultrasound-assisted extraction with 10 mM EDTA at pH 2.5. It gave the highest yield (70% of the total Se present) of all the extraction reagents tested. This extractant was compatible with the HPLC mobile phase used and, importantly, prevented oxidation of Sb^{III} to Sb^V. The LODs were 0.07, 0.08 and 0.9 $\mu\text{g L}^{-1}$ for Sb^{III}, Sb^V, and trimethyl Sb^V, respectively.

A simplified method¹⁸⁰ for *determination of mercury species in sediments* by HPLC-cold vapour-AFS used 0.1% mercaptoethanol microwave-assisted extraction. Results similar to certified values were obtained for MeHg⁺ in CRMs ERM-C580 and IAEA 405 (both estuarine sediments). The LODs were 0.5, 1.1 and 0.5 ng g^{-1} for MeHg⁺, EtHg⁺ and Hg²⁺, respectively.

3.4.4 Inductively coupled plasma mass spectrometry. Grotti *et al.*¹⁸¹ optimised a *torch-integrated total-consumption sample introduction system* for ICP-MS. Using a chamber temperature of 150 °C, a nebuliser gas flow rate of 0.7 L min^{-1} , a sheathing gas flow rate of 0.35 L min^{-1} and a sample uptake rate of 20 $\mu\text{L min}^{-1}$, the apparatus was between 2 and 8 times more sensitive than a conventional micronebuliser and mini spray chamber system for the measurement of 30 analytes. Results for a set of CRMs, including NIST SRM 1570a (spinach leaves), were in good agreement with certified values (*t*-test at 95% probability).

The *accuracy of the determination of lanthanides in plants* by ICP-MS was improved¹⁸² by the removal of silica and fluoride by volatilisation as SiF₄ and BF₃ after microwave digestion of the sample. The low recoveries obtained if this was omitted were attributed to the formation of tiny silica particles that could act as analyte sorbents and interfere with ion production.

Claverie *et al.*^{183,184} developed a *LA-ICP-MS method with a fast spinning platform* on which samples and standards, prepared as lithium metaborate fused beads, were ablated alternately. The standard was spiked with Gd isotopically enriched in ¹⁵⁷Gd, whilst the sample was spiked with Gd of natural isotopic abundance. Differences in ablation rates between the two materials could therefore be calculated from analysis of the

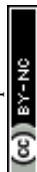
mixed aerosol. In one set of experiments¹⁸³ the two glasses were mounted symmetrically about the spin axis; in another¹⁸⁴ they were positioned on the platform such that it was possible to ablate either only the sample or, by moving the laser farther off-axis, an increasing proportion of standard, thus performing in-cell standard additions. The approach was used successfully to determine Ba, Cu, Ni, Sr, Pb and Zn in glass, rock, sediment and soil SRMs.

The excellent *review of hyphenated techniques involving ICP-MS* (89 references) presented by Maher *et al.*¹⁸⁵ predominantly concerned HPLC-ICP-MS but also covered HPLC-HG-ICP-MS, cryogenic trapping ICP-MS, and GC-ICP-MS. Example applications were discussed, challenges highlighted, and recommendations for future work provided. Articles featuring HPLC-ICP-MS published since 1978 were reviewed by Shoaib and Al-Swaidan⁷⁷ (79 references).

Various procedures involving *chromatographic separation coupled to ICP-MS* have been reported for specific analytes. A gradient elution HPLC-ICP-MS method¹⁸⁶ successfully separated organoarsenic feed additives and other As species present in the 0.5 M H₃PO₄ extracts of soil and sediment from the vicinity of pig farms in China. Complementary SEC-ICP-MS and CZE-ICP-MS methods¹⁸⁷ were developed and applied to the characterisation of low-, medium- and high-molecular weight complexes of cadmium with glutathione and phytochelatin in model solutions and extracts of thale cress (*Arabidopsis thaliana*). Gadolinium-based contrasting agents⁸⁹ used in MRI were detected in river water and aquatic plants near Berlin by hydrophilic interaction chromatography ICP-MS. Application of a variety of techniques¹⁸⁸ including HPLC-ICP-MS gave a comprehensive characterisation of low molecular weight (<5 kDa) selenometabolites in rice, wheat and maize grown on soils naturally rich in Se. A speciation method¹⁸⁹ involving on-line preconcentration IC-ICP-MS gave LODs for both selenite and selenate in Se deficient soils of <10 pg.

3.4.5 Accelerator mass spectrometry. Several AMS facilities reported *new or enhanced analytical capabilities* during the review period. The Centre for Isotopic Research on Cultural and Environmental Heritage in Italy¹⁹⁰ used a new beam line dedicated to actinide measurement for analysis of soils from around the Garigliano power plant, which is currently undergoing decommissioning. The Gliwice Absolute Dating Methods Centre in Poland¹⁹¹ improved its sample throughput for radio-carbon measurement to around 400 targets per year. The Xi'an AMS Centre in China¹⁹² demonstrated that its methods for measurement of ¹²⁹I can be applied to sequential extracts of soil to aid understanding of I migration in loess profiles. The research group at the Vienna Environmental Research Accelerator in Austria¹⁹³ developed a method to measure ²³⁹Pu, ²⁴⁰Pu, ²⁴¹Pu, ²⁴²Pu and ²⁴⁴Pu on a single target. This allowed more precise assessment of the origin of Pu in environmental samples than was previously possible.

3.4.6 Laser induced breakdown spectroscopy. A comprehensive¹⁹⁴ *review of LIBS* (312 references) explained the fundamentals of the technique, described specific approaches including double pulse and fs LIBS and summarised applications in a range of fields. Another review¹⁹⁵ (84 references)



provided an authoritative overview of developments and applications of LIBS relevant to the analysis of plants. Together with animal and microbial samples, plants were also the subject of a wider review¹⁹⁶ of the biological applications of LIBS.

The first application of LA-LIBS to soil analysis has been published.¹⁹⁷ In this technique, the processes of solid sample ablation and generation of the LIBS plasma for analyte measurement are performed separately, allowing each to be optimised independently, although both can be performed with the same laser following beam-splitting. The LA-LIBS and conventional LIBS procedures were compared for the measurement of K in soils spiked with N-P-K fertiliser. Superior linearity was obtained with LA-LIBS ($r^2 = 0.861$ cf. $r^2 = 0.665$). Although acceptable results were obtained for only Ca, Fe, K and Mg in the analysis of 65 soil samples with known concentrations of Ca, Fe, K, Mg, Mn and Na, there is considerable scope for further development of the approach.

Another interesting innovation was *the application of microwave-assisted LIBS to soil analysis*.¹⁹⁸ The LIBS signal intensity could be increased markedly by application of microwave radiation to extend plasma emission lifetime. The sensitivity for measurement of Cu was thereby increased 23-fold and concentrations as low as 30 mg kg⁻¹ could be measured. Additional analytes such as Ag, undetectable using conventional LIBS analysis, could be detected.

Applications of LIBS to plant analysis included the development of a method¹⁹⁹ for measurement of Cu in algae by standard additions, and a detailed investigation²⁰⁰ of how laser fluence and focusing affected the determination of Al, B, Ca, Cu, Fe, K, Mg, Mn, P and Zn in pellets of plant material. Best results were obtained when the Q-switched Nd:YAG laser (1064 nm) was operated at 50 J cm⁻¹ with a spot size of 750 μm.

Research has continued to improve *the performance of LIBS for analysis of soils*. Methods have been reported for the determination of Pb,²⁰¹ Zn,²⁰² and Ca, Cu and Zn,²⁰³ all with LODs <50 mg kg⁻¹. Repeatedly firing the laser at the same spot on a soil sample enhanced²⁰⁴ both signal intensity and signal-to-background ratio for Fe, K, Mn and Ti, potentially improving LODs. Frydenvang *et al.*²⁰⁵ developed a novel approach for determining elemental ratios that combined the fundamental mathematical framework of calibration-free LIBS with empirical calibration using 22 CRMs, including NIST SRMs 2709 (San Joaquin soil), 2710 (Montana soil – highly elevated trace elements) and 2711 (Montana soil – moderately elevated trace elements). The usefulness of ANNs²⁰⁶ in overcoming matrix effects and non-linear response in LIBS was clearly illustrated when a transportable instrument was deployed at a former mining site in France. A separate ANN model was built for each analyte, if necessary incorporating lines for other elements to improve the prediction. Results obtained for Al, Ca, Cu and Fe agreed well with those obtained using ICP-AES.

3.4.7 X-ray spectrometry. Applications of μ-SR-XRF spectrometry²⁰⁷ to study *the distribution of biologically important elements in environmental matrices*, including plants and soils, were reviewed (80 references).

Plessow²⁰⁸ highlighted some major problems in the *analysis of soil* by XRF spectrometry for B, Cl and F. Fluorescence

intensities changed dramatically over time, usually increasing over replicate analyses, but occasionally decreasing, depending on the nature of the sample. He attributed this to radiolysis, suggesting that irradiation could mobilise the analytes, which could then either move into the analytical zone, or through it and be lost to the vacuum. Difficulties in the application of PIXE to soil and other thick insulating samples²⁰⁹ due to charge build-up, which contributes to the Bremsstrahlung background, were overcome by use of an electron flood gun and beam profile monitor. The utility of the approach was demonstrated by analysis of CRM IAEA Soil 7. Wovkulich *et al.*²¹⁰ ran soil column experiments in a synchrotron beam line. Both μ-XRF and μ-XANES spectrometries were used to measure changes in As concentration and speciation following treatment of the soil with oxalic acid, a potential reagent for use in the remediation of As-contaminated soil. Malherbe and Claverie²¹¹ presented the intriguing possibility of using a commercially available high-resolution WDXRF spectrometer for direct determination of Cr speciation in solid samples, including soils, based on differences in K_β transition profiles between Cr⁰, Cr^{III} and Cr^{VI}.

In the *analysis of plants*, Paltridge *et al.* confirmed the suitability of EDXRF spectrometry for measuring Fe and Zn in rice and pearl millet²¹² and Fe, Se and Zn in wheat²¹³ and recommended wider use of the technique to assess nutrient status in biofortification programmes. Other workers used μ-SR-XRF to image and quantify Fe in tomato roots²¹⁴ and to investigate the distribution of macronutrients and micronutrients in *Dioscorea balcanica*.²¹⁵ A rather unusual study²¹⁶ combined ultrasound-assisted extraction with TXRF spectrometry for the measurement of Ca, Cr, Cu, Fe, K, Mn, Ni, P, Pb and Zn in medicinal plants, spices and herbs. The optimised procedure involved 15 min sonication of 10 mg finely ground sample in 1 mL of 10% v/v HNO₃ + 10% v/v HCl + 10% v/v HF, followed by centrifugation to separate residual solid and drying of 10 μL of the supernatant onto a quartz sample carrier for analysis.

As noted in our sister review,⁴ *developments and applications of PXRF spectrometry* continue to be reported. Bosco²¹⁷ summarised presentations delivered at the James L Waters Symposium at Pittcon in 2012 and provided a fascinating insight into the commercial evolution of the technique. Researchers in Brazil²¹⁸ proposed a new method to correct for the effects of moisture in the analysis of soil based on the low energy background under the Ti K_α peak. More significantly, two groups—one in Australia and one in the UK—almost simultaneously reported the ‘first’ application of PXRF spectrometry to the analysis of plants. McLaren *et al.*²¹⁹ determined Ca, Co, Cr, Fe, K, Mn, Ni, P, S, Si and Zn in agricultural plants from New South Wales whereas Reidinger *et al.*²²⁰ focussed on the measurement of P and Si.

4 Analysis of geological materials

4.1 Reference materials

Current interest in developing suitable RMs for microanalytical and isotopic analysis was highlighted in a review²⁴⁷ of papers published in 2011 containing *analytical data for geochemical and*



environmental RMs and CRMs. The on-line version, containing all the references and supporting information in appendices, is particularly valuable because it is fully integrated with the GeoReM database (<http://georem.mpch-mainz.gwdg.de>), thereby providing the geoanalyst with access to information on approximately 2600 RMs. The IGGE has reported²⁴⁸ certified and indicative values for 18 oxides and elements in four new chromium ore CRMs with Cr₂O₃ contents between 17.6 and 57.8% m/m.

The increased use of *microanalytical techniques* in recent years has fuelled the demand for suitable reference glasses. Two soda lime reference glasses (BAM-S005-A and BAM-S005-B), initially prepared as standards for bulk analysis by techniques like XRF spectrometry, were assessed for their suitability as glass standards for microanalysis using EPMA, LA-ICP-MS and SIMS.²⁴⁹ All major and 33 trace elements were homogeneously distributed at the μm scale in both glasses but Cl, Cr, Cs, Mo and Ni were not. Information values for major elements on the original certificate were confirmed by EPMA, while LA-ICP-MS data for 18 trace elements were within the uncertainties of the certified concentrations; no explanation for the lack of agreement with the certified values for Ba, Ce, Pb and Sr could be given. New LA-ICP-MS data for a further 22 trace elements were presented and will enhance the utility of these materials. The paucity of commercially available RMs for the determination of Au and the PGEs in sulfides by LA-ICP-MS prompted a comparative study²⁵⁰ of some PGE-bearing sulfide materials employed as in-house RMs in various laboratories around the world. A new nickel sulfide RM (NiS-3) was developed and used to calibrate LA-ICP-MS measurements of the five in-house sulfide RMs. Gold and PGE concentrations were not homogeneously distributed in all the RMs tested. Calibration against different RMs did not produce consistent results for all elements, highlighting the importance of the widespread availability of well-characterised sulfide RMs.

More RMs for isotope studies are required to facilitate easy comparison between data sets. Although NIST SRM 3108 (Cd solution), certified for its Cd concentration, is not an isotopic RM *per se*, a round-robin intercalibration²⁵¹ of various in-house Cd reference solutions involving seven laboratories demonstrated that it fulfilled all reasonable criteria for its adoption as a zero-delta RM, pending the certification of another material as a proper isotopic RM for Cd. Similarly, there is no universally accepted zero-delta RM for the Mo stable isotope system, making it difficult to compare results generated in different laboratories using different analytical approaches. In an inter-laboratory calibration²⁵² of various in-house Mo standard solutions, the $\delta^{98}\text{Mo}$ values differed by up to 0.37‰, significantly exceeding the typical reproducibility of the determinations. Data from this study facilitated a rigorous assessment of previously published Mo isotope data. Mutually consistent $\delta^{98}\text{Mo}$ data for NIST SRM 3134 (Mo solution) supported the proposal by Greber *et al.*²⁵³ that the Mo-isotope community should adopt this material as the zero-delta RM. Greber *et al.* also refined the working values for Mo concentrations in NIST glass RMs SRM 610 and 612, using an ID double-spike technique, and advocated their use as solid

standards, as they have identical and homogeneous $^{98}\text{Mo}/^{95}\text{Mo}$ ratios at a test portion of 0.02 g. Despite its significantly different ablation behaviour, Darling *et al.*²⁵⁴ found that NIST SRM 610 was effective in correcting for instrumental mass fractionation during *in situ* Pb isotope analysis of a range of Fe–Ni–Cu–Zn sulfides from the Sudbury impact structure using 193 nm LA-MC-ICP-MS. Although matrix-dependent melting and condensate accumulation around the sulfide ablation pits may have reduced the sensitivity of the measurements, they did not result in any detectable isotopic fractionation.

Twelve *natural monazites* were analysed to find a suitable RM with homogeneous Sm–Nd composition and concordant U–Th–Pb age to act as a standard for *in situ* microanalysis.²⁵⁵ From determinations of trace element concentrations by quadrupole ICP-MS and of isotope ratios by LA-MC-ICP-MS, with some check data for Nd–Sm isotopes by ID-TIMS, two monazites were found to be sufficiently homogeneous to act as potential standards.

4.2 Solid sample introduction

4.2.1 Laser ablation. A succinct summary²⁵⁶ of advances in laser sampling over the past few years concluded that the benefits expected of *femtosecond LA systems*, compared to *ns* systems, have only been partially realised thus far. The wider availability of fs LA systems should facilitate future research into fs ablation processes. For those new to this field, a comprehensive review²⁵⁷ (157 references) of recent developments and future prospects for fs LA-ICP-MS should prove valuable. It addressed the fundamentals of laser–solid interactions during ablation and the characteristics of various LA systems. Most of the examples of fs LA-ICP-MS applications, including depth profiling and geochemical analysis, confirmed that the use of fs LA can greatly reduce elemental fractionation, matrix effects and the need for matrix-matched standards, compared to the use of *ns* LA. The advantages of UV over IR wavelengths for *ns* LA systems are well documented; however, these benefits were not so conclusive in studies using fs systems. In line with previous work, Kimura and Chang²⁵⁸ reported reduced laser-induced matrix effects using a 200 nm fs laser rather than a 193 nm *ns* excimer laser for the determination of 44 major and trace elements in silicate glasses by SF-ICP-MS. Velasquez *et al.*²⁵⁹ confirmed that data of similar quality could be obtained for Au and Cu concentrations in natural sulfides by NIR fs LA coupled to quadrupole ICP-MS, irrespective of whether NIST silicate glasses or sulfide RMs were used as calibrators. In a study²⁶⁰ of Th–U ratios in titanite by fs LA-MC ICP-MS, ablations were carried out at wavelengths of 800 nm (NIR) and 265 nm (UV) using a Ti-sapphire-based laser system. Elemental fractionation was significantly less using the UV single spot ablation mode compared to NIR spot analyses, but precision was limited by the lower ion signals achievable. Differences in U–Th fractionation were also observed between different titanite materials, *e.g.*, glass and minerals, even when their compositions were nearly identical, indicating that the calibration standard needed to be matched both in terms of composition and crystal structure.



Several new investigations have provided insights into causes of *elemental fractionation in LA-ICP-MS*. When silicate glasses were ablated with a 193 nm excimer laser in a single-volume ablation chamber,²⁶¹ differential responses of volatile and refractory elements (relative to ⁴³Ca) at different ablation sites were found to be correlated with the local helium gas velocity at the position of analysis. This fractionation was thought to be related to the different behaviour of these elements during condensation after ablation, as well as interaction between condensate and the carrier gas. In contrast, ablation within a two-volume sample chamber, designed to produce a uniform helium flow regime throughout the ablation cell, showed little evidence of this type of elemental fractionation. Flamigni *et al.*²⁶² used 2D optical emission spectrometry and quadrupole ICP-MS to investigate the processes involved in the vaporisation of laser-produced aerosols and particles within the ICP. They demonstrated a shift of a few mm along the axial channel in the onset and maximum positions of atomic emission, depending on whether the aerosols were produced from the ablation of silicate glasses or of metals. These shifts arose from the aerosol penetrating to different depths along the ICP axial channel, depending on its composition, resulting in varying ion extraction efficiencies through the vacuum interface. Although further work is required, these findings may influence the design of future LA-ICP-MS systems.

Hardware modifications for improving the analytical performance of LA-ICP-MS included the development of a signal-smoothing device,²⁶³ which consisted of a copper cylinder (internal volume *ca.* 94 cm³) filled with steel wire and placed between the ablation cell and the ICP torch. This device produced smooth signals at laser repetition rates as low as 1–2 Hz without any detrimental effect on the signal decay time and was successfully used for U–Pb dating of zircons. The development of a spinning ablation cell platform enabled ID¹⁸³ and standard addition¹⁸⁴ techniques to be implemented with LA-ICP-MS. Two samples were placed close together in a sample holder on a rotating platform in the ablation cell and ablated using a stationary laser beam, allowing quasi-simultaneous ablation of the materials. Isotope dilution¹⁸³ was performed on four NIST SRMs, two soils and two sediments, prepared as lithium borate fusions spiked with a natural Gd solution. By ablating an isotopically spiked glass, containing known amounts of ¹³⁵Ba, ¹⁵⁷Ga, ²⁰⁶Pb, ⁸⁶Sr, and ⁶⁷Zn, alongside each sample on the spinning platform, a homogeneous aerosol was produced after a period of equilibration. The main advantage of this method was the possibility of analysing a large number of samples with the same isotopically spiked glass RM, which could be reused after polishing to remove previous ablations. The spinning platform was employed in a similar manner to determine Ba, Cu, Ni, Pb, Sr and Zn concentrations in geological materials by standard addition.¹⁸⁴ A glass RM, prepared by spiking lithium borate flux with a multielement solution containing the elements of interest and a solution of ¹⁵⁷Gd, was mounted alongside the fused sample in an off-axis alignment so that it was possible to increase the proportion of standard in the aerosol mix by performing the ablation further from the axis of rotation. The validity of the proposed method for the direct and

fast analysis of solid samples of different matrices by standard additions using a single standard sample was demonstrated using NIST SRMs. A new design²⁶⁴ of skimmer and sample cones with addition of nitrogen to the central gas flow enhanced signal intensities for LA-MC-ICP-MS measurements. This modification was utilised for the *in situ* determination of Hf isotope ratios in zircons using Faraday detectors, for which large ions beams are necessary for precise and accurate results.

Laser ablation ICP-MS is now considered an essential tool for analysing individual *fluid inclusions*. The main limitation in determining Br and Cl by LA-ICP-MS is their high first ionisation energies, which result in low signal intensities. Using well-characterised natural scapolite standards, Hammerli *et al.*²⁶⁵ routinely achieved LODs of 8 µg g^{−1} for Br and 500 µg g^{−1} for Cl during multi-element analysis of individual fluid inclusions by quadrupole ICP-MS coupled to a 193 nm ArF excimer laser. Corrections for polyatomic interferences on the Br signal were required, particularly when analysing K-bearing minerals, with measurements at mass ⁸¹Br recommended in preference to ⁷⁹Br. In most fluid inclusion analysis by LA-ICP-MS, microthermometric measurements are used to provide an absolute concentration for one major element, usually Na, which is then applied as an internal standard to the LA-ICP-MS data. Recently, concerns have been voiced about the thermodynamic and numerical models used to estimate the absolute concentration of the internal standard from the microthermometric data, particularly for complex fluids containing salts other than NaCl. Microthermometric measurements of two phase transitions allowed Schlegel *et al.*²⁶⁶ to quantify absolute concentrations of CaCl₂ and NaCl in Ca–Na dominated brine inclusions. Using this approach, accurate Na concentrations for internal standardisation of LA-ICP-MS data could be obtained irrespective of the host mineral, *e.g.*, quartz or calcium-rich minerals like fluorite or carbonate. Leisen *et al.*²⁶⁷ presented an improved method for calculating cation concentrations in quartz-hosted fluid inclusions of low to moderate salinity. When combined with a signal processing protocol, this enabled them to estimate analytical uncertainties for each major and trace element determined in a single inclusion. The method was validated against concentrations in materials previously analysed by LIBS or crush-leach methods, and was applied as part of a wider strategy²⁶⁸ involving microthermometry and LA-ICP-MS for the determination of Br, Cl and Na concentrations in individual fluid inclusions of variable size and bulk salinity. The calculated uncertainty on Cl/Br and Na/Br ratios was found to be between 30 and 38%, regardless of the salinity of the inclusion.

The application of LA-ICP-MS to *U–Pb geochronology* continues to be a major growth area. Nemchin *et al.*²⁶⁹ summarised the state-of-the-art capability of LA-ICP-MS and SIMS for resolving age variations in U and Th-bearing minerals at the µm-scale. A review²⁷⁰ of the development of LA-ICP-MS for U–Pb dating of accessory minerals illustrated how recent advances have increased the precision and accuracy of such analysis. Included was a typical workflow for the *in situ* analysis of accessory minerals in standard 30 µm polished thin sections by 193 nm ArF excimer LA-ICP-MS. Data reduction was performed



using Iolite™ and VizualAge™. The latter is a new software tool²⁷¹ developed for reducing and visualising U–Pb geochronology data obtained by LA-ICP-MS. In addition, it provides computational tools to correct for the presence of common lead. In a recent zircon dating study,²⁷² systematic differences observed in ²⁰⁶Pb/²³⁸U data obtained by LA-ICP-MS and TIMS were related to differences in radiation damage in the RM and samples. Annealing unknown and reference zircons to the same state prior to analysis appeared to overcome this problem. A modified protocol²⁷³ based on single shot LA-ICP-MS, with semi-automated data reduction and robust error propagation, offered rapid sample throughput for analysing detrital zircon and monazite grains without compromising data quality. The time taken to analyse 120 sample grains and associated RMs was reduced from *ca.* 2 h using conventional LA protocols with continuous laser pumping to 20 min, with only a modest increase in uncertainty from 2% to 4%. Significant matrix effects were encountered during *in situ* U–Pb dating of titanite²⁷⁴ by 193 nm LA coupled to quadrupole ICP-MS. Consistent ages were obtained when titanite RMs rather than zircons were used for external calibration.

The *suitability of various RMs for LA-ICP-MS multi-element analysis* of Roman and late Iron Age glasses²⁷⁵ was evaluated. Standards from the Corning Museum of Glass were considered to be more appropriate for this purpose than the NIST SRM 600 series of glass RMs in terms of their matrix composition and concentration range of trace elements, but the former were not as well characterised as the NIST ones in terms of element concentrations and their homogeneity. Quantification was achieved by adopting a strategy developed by previous workers, in which an average response factor for each analyte was calculated from a set of glass RMs. Comparison of individual response factors obtained from different standards provided an indication of any standard that suffered from specific issues, so that any deemed unsuitable could be discarded. Calibration using sets of response factors produced more accurate results than single-point calibrations and enabled the quantification of trace elements in glasses with very different compositions. As an alternative to the glass RMs currently available, Ulrich and Kamber²⁷⁶ proposed the use of natural obsidian glass as an inexpensive and abundant QC material for LA-ICP-MS analysis of silicates and oxides. The obsidian samples were homogeneous at the 40 µm scale for many trace elements including REEs. Silicon was recommended as the internal standard for these matrices.

The *suitability of carbon as the internal standard* for biological and medical applications has long been a matter of debate. A fundamental study²⁷⁷ on the ablation behaviour of carbon revealed a matrix-dependent partitioning of carbon into gaseous species and particles, whereas trace elements were exclusively transported in the particulate phase. Calcium carbonate powder and diamonds used as cutting tool tips were included in the 12 common carbon matrices examined.

4.2.2 Laser induced breakdown spectroscopy. Recent developments in *LIBS instrumentation and analytical performance* are covered in a sister Update.³ Much of the current research into geological applications of LIBS has been directed

towards improving the performance of the ChemCam instrument on the Mars Science Laboratory *Curiosity* rover.^{278,279} The possibility of developing a LIBS instrument for *in situ* K–Ar geochronology for Mars has also been explored.²⁸⁰ A laboratory-built portable LIBS instrument²⁸¹ was used to identify tephra layers in lacustrine sediments and fossilisation processes in ammonites. An optimised calibration procedure for determining elemental ratios by LIBS, as advocated by Frydenvang *et al.*,²⁰⁵ was better than empirical methods at coping with matrix effects. Their procedure was a hybrid between an empirical approach, based on calibration curves using 22 NIST and USGS RMs spanning a wide range of rock compositions, and the mathematical framework of the theoretical calibration-free LIBS method often employed.

4.3 Sample preparation

4.3.1 Sample dissolution. Although the principles of *green chemistry*²⁸² can be applied to every step of the analytical process, techniques that involve *in situ* measurements with little or no sample preparation or dissolution, *e.g.*, LIBS and PXRF spectrometry, can be considered to be the most environmentally friendly. However, there is still scope to simplify the reagents and digestion conditions used in methods where complete sample digestion is a prerequisite. Thus, a dissolution procedure²⁸³ employing ammonium bifluoride (NH₄HF₂) was developed for the ICP-MS multielement analysis of rocks. Ultrapure NH₄HF₂, prepared using a standard PFA sub-boiling distillation system, has a higher boiling point than mineral acids such as HF, HNO₃ and HCl so digestions could be carried out at higher temperatures than usual, facilitating the decomposition of refractory mineral phases. Digestion (2–3 h at 230 °C) with 200 mg of NH₄HF₂ in a screw top Teflon vial was sufficient to digest 50 mg of the USGS RM GSP-2 (granodiorite), one of the more challenging samples to dissolve because of its 550 µg g^{−1} Zr content. This was six times faster than a conventional acid digestion in a high pressure PTFE bomb at 190 °C. In addition, the NH₄HF₂ digestion was not hampered by the formation of insoluble fluorides, making it an effective, simple, economical and comparatively safe method of dissolution. A new simple design of sub-boiling still²⁸⁴ may be of interest to many geochemical laboratories. It consisted of two Teflon bottles connected at right angles, with one acting as the feed bottle and heated by IR radiation on its upper surface, and the other in a cold water bath acting as the condenser and receiver. Compared to commercially available stills with a similar performance, this still was easy and inexpensive to construct, had a smaller footprint, much larger yield (up to 500 mL of mineral acid per day) and lower energy consumption.

In a systematic reassessment of the optimum conditions for *high pressure digestion of felsic rocks* in HF–HNO₃ acids, Zhang *et al.*²⁸⁵ concluded that the use of HF alone was more effective in dissolving refractory phases, such as zircon, than the use of a mixture of HF with other minerals acids. It was recommended that a test portion of ≤100 mg of ultrafine powder (<30 µm nominal particle size) be taken to prevent the formation of



insoluble fluorides even though this might result in unrepresentative subsampling.

4.3.2 Sample separation and preconcentration. A review²⁸⁶ of methods for the *dissolution of geological materials for the determination of REEs* by ICP-MS presented the strengths and weaknesses of both alkali fusion and acid digestion procedures. Alkali fusions are preferred by many laboratories because they are relatively rapid and digest totally the resistant accessory minerals, but they result in a solution with high TDS content. Singh *et al.*²⁸⁷ compared two fusion procedures for the dissolution of zircon prior to the measurement of the REEs, Th and U: one based on sodium peroxide and the other using a 3 + 1 mixture of KHF₂ and NaF. Unfortunately, certified values were unavailable for both of the two zircons analysed, although data from both methods were comparable with each other and any available published data. The TDS of the final solution was, in fact, not a problem as the sensitivity of modern ICP-MS instruments allows such solutions to be analysed at high dilutions.

For samples with low REE content or matrix components that cause severe polyatomic interferences, *separation and preconcentration of REEs* prior to analysis is desirable; the determination of the REEs and Th at ng kg⁻¹ levels in ultramafic rocks being one such case. Preconcentration methods are often based on ion-exchange resins, as in that developed by Sun *et al.*²⁸⁸ in which anion exchange and inorganic co-precipitation were used to separate and preconcentrate REEs from a HF-HNO₃ digest treated with boric acid to prevent the formation of insoluble fluorides. In a novel approach, Fedyunina *et al.*²⁸⁹ used a chelating sorbent, Pol-DETATA (cross-linked polystyrene grafted with diethylene-triaminetetraacetate groups), to extract REEs from lithium metaborate fusions of rock CRMs. Because Pol-DETATA sorbs metals ions other than the REEs, 5-sulfosalicylic acid was added as a masking agent to minimise the retention of Fe, which would otherwise reduce REE sorption. Flow injection of 50 µL of eluate in 1 M HNO₃ into the ICP-MS instrument was deemed a reasonable compromise between maximising analytical sensitivity and minimising the risk of corrosion of the interface. Data obtained were within 15% of the reference value for most REEs in the four CRMs analysed. The authors claimed that the method was faster, required less reagent and provided lower LODs than more conventional preconcentration methods based on ion-exchange or extraction chromatography.

4.4 Instrumental analysis

4.4.1 Atomic emission spectrometry. A review²⁵⁶ of recent developments in *geochemical analysis by ICP-AES* confirmed that most advances have focussed on improved sample pretreatment, sample introduction and calibration. The determination of U isotopes by ICP-AES was particularly novel although unlikely to replace ICP-MS as the technique of choice for these measurements. In a modified sample introduction system²⁹⁰ for ICP-AES, the heater/condenser of a commercial USN system was replaced with a pre-evaporation tube and sheathing device. On leaving the USN, the aerosol was heated to 400 °C by IR heating before entering the ICP. The increased amount of water vapour

introduced by this configuration improved the plasma excitation conditions and robustness such that analysis of geological samples could be carried out by simple calibration, without matrix-matching, using an argon emission line as the internal standard. A 10–25 fold improvement in sensitivity and LODs, compared to conventional pneumatic nebulisation, was reported. Volatile elements such as B and Hg, normally lost in the heating phase of a conventional USN, could also be determined.

4.4.2 Inductively coupled plasma mass spectrometry. Several noteworthy reviews of *recent developments in ICP-MS* are available. A summary of improvements in ICP-MS hardware²⁵⁶ covered developments in ion detectors, TOF and Mattauch-Herzog designs of ICP-MS instruments, the concept of distance-of-flight MS and the introduction of the first commercial ICP triple-quadrupole mass spectrometer. The update³ on atomic spectrometry described new approaches to sample preparation for isotope ratio measurements by ICP-MS, as well as novel instrument features and applications. Baxter *et al.*²⁹¹ published a detailed tutorial (184 references) on fundamental aspects of isotope abundance ratio measurements by SF-ICP-MS. A more general overview¹⁰² focussed on progress in coupling different separation techniques to ICP-MS for quantitative analysis in environmental and life sciences. It is always instructive to view the history of ICP-MS developments through the eyes of one of its leading practitioners; Longerich's perspective²⁹² is relevant to anyone engaged in geochemical analysis.

While quadrupole ICP-MS is firmly established as a routine workhorse for elemental determinations, improvements in isotope ratio measurements by MC-ICP-MS continue to support advances in geochemical research. The emphasis is often on novel *methods for chemical separation and purification* to improve the accuracy of isotope ratio measurements. A one-step separation²⁹³ of Mg from matrix elements using AG50W-X8 cation-exchange resin in a purification process taking about 5 h gave recoveries of ≥97% for Mg whereas ≤0.2% of the matrix components were recovered. The total procedural blank of <3 ng Mg was considered to be negligible. Magnesium isotope measurements were made by MC-ICP-MS under cool plasma conditions using a high-sensitivity skimmer cone (X-cone) to maximise signal intensity and to reduce background interferences. Although the samples contained significant Ca concentrations, Ca : Mg ratios of up to 100 : 1 had little impact on the measured Mg isotope data. The accuracy of the procedure was confirmed through the analysis of seven rock RMs. The analytical precision was 0.03–0.09‰ (2σ). In a method for the isolation of Sb from stibnite ores,²⁹⁴ care was taken not to change the oxidation state which could influence the Sb isotope ratio. After *aqua regia* digestion, separation was achieved using a combination of cation-exchange chromatography on Dowex AG50-X8 resin and AEC on Amberlite IRA 743 resin. Indium was used to correct for instrument-induced mass bias during measurements of ¹²³Sb/¹²¹Sb by MC-ICP-MS at medium resolution (*R* = 4000). Variations in Sb isotope ratios in stibnite ores of 0.1%, compared to a measurement reproducibility of 0.01%, demonstrated the potential of this method for provenance studies of Roman glasses. Lithium isotope ratios²⁹⁵ in three RMs were measured by MC-ICP-MS after a three-step separation



technique employing cation-exchange chromatography on AG50W-X8, with 2.8 M HCl, 0.15 M HCl and 0.5 M HCl in 30% ethanol as eluants at each of the three stages. The precision of the technique (± 0.72 – 1.04% , 2σ) was similar to that obtained by other MC-ICP-MS laboratories.

A method²⁹⁶ for the simple and rapid *determination of Os and Re isotope ratios* by MC-ICP-MS was based on Carius tube digestion and sparging introduction of Os. Measurement times were reduced significantly by employing four channeltron multi-ion counters for simultaneous measurement of the Os isotopes. Because the amplification efficiencies of the multi-ion counters differed from one another and varied with time, Os isotope ratios were corrected using the sample-standard bracketing method. Rhenium isotopes were measured by means of eight Faraday cups with solution nebulisation *via* a USN. The method was sufficiently sensitive to determine Re–Os isotope systematics in samples such as chert with low concentrations. Precisions for $^{187}\text{Os}/^{188}\text{Os}$ ratios for RMs JMS-2, JCh-1 (GSJ sedimentary rock RMs) and DROSS (Durham Romil Os solution) were 0.35–0.71, 1.56–3.31 and 0.99–1.28% RSD, respectively, depending on the ion intensities. These precisions were considered to be adequate for reconstructing changes in marine Os isotope compositions. Lawley and Selby²⁹⁷ proposed a room-temperature chemical separation technique using HF to isolate ultrafine (<50 μm) molybdenite grains for Re–Os geochronology. Exposure to HF had no effect on the Re–Os molybdenite systematics. The procedure allowed the determination of reproducible ages for ultrafine samples that were unsuitable for Re–Os determinations using traditional physical mineral separation techniques.

Kramchaninov *et al.*²⁹⁸ sought to refine the procedure for *Sr isotope measurements by MC-ICP-MS* to achieve performance data to rival those obtainable by TIMS. By correcting for mass bias effects using a combination of normalisation to zirconium isotope ratios and standard-sample bracketing, they obtained precisions of ± 0.015 – $\pm 0.05\%$ for $^{88}\text{Sr}/^{86}\text{Sr}$, depending on sample composition. These precisions were better than those reported previously by similar protocols based on MC-ICP-MS but worse than those achievable by double spike TIMS ($\pm 0.02\%$). The advantages cited were greater productivity (5–6 times higher) and the ability to measure $^{88}\text{Sr}/^{86}\text{Sr}$ and $^{87}\text{Sr}/^{86}\text{Sr}$ simultaneously with high precision. However, at least 95% Sr recovery from the chromatographic column was essential for accurate results. Building on earlier work using a heated torch integrated spray chamber, Paredes *et al.*²⁹⁹ demonstrated that it was possible to measure Sr isotope ratios at a continuous liquid flow rate of $<10\ \mu\text{L min}^{-1}$ with a repeatability of *ca.* 40 ppm on the $^{87}\text{Sr}/^{86}\text{Sr}$ ratio measured in NIST SRM 987 (strontium carbonate). This figure of merit was similar to that (30–50 ppm) previously reported for liquid flows rates 5 to 10 times higher. The new instrumental setup allowed a sheathing gas to be introduced and included a semi-automated FI sample-delivery system to minimise manipulation of small sample volumes.

Several new procedures for the *measurement of Nd isotopes by MC-ICP-MS* have been published. Huang *et al.*¹¹³ employed a combination of high-sensitivity cones and a new generation desolvator (Aridus II or APEX-IR), together with column

chemistry based on Eichrom LN resin, to achieve optimal conditions for Nd isotope determination in a variety of sample matrices with low Nd content, including carbonates and seawater. The long-term precision of ± 0.000016 (2SD) for $^{143}\text{Nd}/^{144}\text{Nd}$ in a sample size of *ca.* 1.25 ng Nd, was a factor of 5 better than that for existing MC-ICP-MS methods using <2 ng Nd. Their column separation chemistry provided yields ($>92\%$) similar to those of more traditional multi-step separations but was simpler and more rapid, with negligible procedural blanks. As a practical alternative to ID-TIMS, Sanchez-Lorda *et al.*³⁰⁰ proposed an MC-ICP-MS procedure for determining $^{143}\text{Nd}/^{144}\text{Nd}$ and $^{147}\text{Sm}/^{144}\text{Nd}$ ratios on solutions of silicate rocks without resorting to ID or separating Nd and Sm from each other. The LREEs were separated from matrix elements with yields of $\geq 97\%$ by cation-exchange on Dowex AG50W followed by extraction chromatography on Eichrom TRU resin. Oxide formation, a major cause of mutual fractionation of Nd and Sm in the ICP, was minimised by introducing the sample into the ICP *via* a commercially available two-step desolvation system. After correction for instrumental mass bias effects and isobaric interferences, the overall reproducibility for $^{147}\text{Sm}/^{144}\text{Nd}$ was 0.2–0.7% RSD. Although this performance cannot compete with that achievable by TIMS (typically 0.1% RSD), the precision and accuracy were sufficient for many geological applications. Interestingly, the within-run uncertainty of 0.000014 for $^{143}\text{Nd}/^{144}\text{Nd}$ in a depleted basalt (GSJ JB-2), was similar to the long-term precision reported by Huang *et al.*¹¹³ In a study of isotopic fractionation of Ce and Nd in geological samples by MC-ICP-MS, Ohno and Hirata³⁰¹ employed a similar two-step separation scheme to isolate the LREEs before further purification on an Ln Spec column to separate Ce and Nd. Mass discrimination effects were corrected by means of an external correction technique based on an exponential law, using $^{149}\text{Sm}/^{147}\text{Sm}$ and $^{153}\text{Eu}/^{151}\text{Eu}$ ratios to correct the isotope data for Ce and Nd, respectively. The reproducibilities of the measurements for $^{142}\text{Ce}/^{140}\text{Ce}$, $^{146}\text{Nd}/^{144}\text{Nd}$ and $^{148}\text{Nd}/^{144}\text{Nd}$ were 0.08‰ (2SD, $n = 25$), 0.06‰ (2SD, $n = 39$) and 0.12‰ (2SD, $n = 39$), respectively. With this level of precision it was possible to demonstrate that the Ce and Nd isotope ratios in two igneous and two sedimentary rocks were the same, within analytical uncertainty, whereas the ratios for both elements were significantly higher in a carbonate RM.

The 100th anniversary of the publication of “Age of the Earth” in 1913 by Arthur Holmes, the first person to use radioactivity to date rocks, has been marked by various conferences and *review articles on isotope geochronology* and its future. An issue of *Elements* (volume 9, number 1) dedicated to this theme contained perspectives on various aspects of modern geochronology by some of the leading practitioners in the field. In his review of the evolution of U–Pb geochronology as a robust dating technique, Corfu³⁰² focussed on the causes and implications of discordance between the $^{206}\text{Pb}/^{238}\text{U}$ and $^{207}\text{Pb}/^{235}\text{U}$ decay systems. Although targeted at the nuclear industry, a guide³⁰³ to the fundamental concepts and recent applications of U chronometry may also be of interest to some geochemists.

An article on *high precision geochronology*³⁰⁴ highlighted the continuing efforts of the EARTHTIME community ([38 | J. Anal. At. Spectrom., 2014, 29, 17–50](http://</p>
</div>
<div data-bbox=)



www.earth-time.org) to identify and mitigate inter-laboratory biases through group inter-calibration experiments. Important developments in the application of U–Pb dating to speleothems were discussed by Woodhead and Pickering.³⁰⁵ Although the mechanisms for the transport and incorporation of Pb and U in speleothem calcite remain a matter of debate, LA-ICP-MS and autoradiography were considered ideal screening methods for reconnaissance studies.³⁰⁶ On the basis of exploratory studies already undertaken, this is likely to be a major growth area in the next decade as the potential palaeoclimatic information contained within selected speleothems offers insights in many fields of research.

4.4.3 Other mass spectrometric techniques

4.4.3.1 Thermal ionisation mass spectrometry. The analytical capabilities of the current generation of TIMS instruments have renewed the debate²⁵⁶ over the best strategies for achieving the lowest uncertainties and best accuracy for geological applications, as well as choice of the most appropriate RM.

As noted in Section 4.3.2, double spike TIMS is the method of choice when the best precision for *Nd isotope determinations* is required. Wakaki and Tanaka³⁰⁷ refined this procedure by including internal normalisation and an iterative calculation procedure to improve precision and to minimise possible systematic bias during data analysis. The average $^{143}\text{Nd}/^{144}\text{Nd}$ ratio for GSJ JNdi-1 (neodymium oxide) was 0.512106 ± 0.000010 (2SD, $n = 44$). Significant mass-dependent isotope fractionation occurred during the analysis of commercial high-purity Nd oxide reagents and the La Jolla RM, relative to JNdi-1, suggesting that these data should always be normalised to JNdi-1 rather than the La Jolla RM, which is often used for this purpose. By replacing the $10^{11} \Omega$ resistors in the feedback loop with $10^{12} \Omega$ resistors to reduce the noise in the Faraday cup current amplifiers, Koornneef *et al.*³⁰⁸ achieved a two-fold improvement in the analytical precision on $^{143}\text{Nd}/^{144}\text{Nd}$ and $^{87}\text{Sr}/^{86}\text{Sr}$ ratio measurements. Their data suggested that it should be possible to resolve the variability in the fourth decimal place for Nd and Sr isotope ratios in geological samples as small as 100 pg. The $10^{12} \Omega$ resistors were expected to provide a similar improvement in S/Ns when used in MC-ICP-MS detection systems, although any limitations imposed by the slower response time of the $10^{12} \Omega$ resistors would need to be investigated. Normally, the determination of $^{143}\text{Nd}/^{144}\text{Nd}$ and $^{147}\text{Sm}/^{144}\text{Nd}$ ratios by TIMS requires purified Nd and Sm fractions to be loaded onto different filaments because of severe isobaric interferences, making the procedure lengthy and laborious. Li *et al.*³⁰⁹ proposed a new method, using a mixed ^{152}Sm – ^{148}Nd spike rather than the traditional ^{149}Sm – ^{150}Nd spike, in which both ratios and concentrations of Nd and Sm were measured simultaneously on the same filament loading. Measurements of ten silicate rock CRMs confirmed that neither precision nor accuracy of the results had been compromised.

One of the major problems in the measurement by TIMS of *boron isotope ratios* in organic-rich natural samples, such as fossil carbonates, is interference from isobaric ions from the organic matter. Characterisation of natural biocarbonates³¹⁰ confirmed these isobaric interferences originated from organic compounds with an acylamino group ($-\text{CO}_2-\text{NH}_2$). However,

total elimination of organic matter by pretreating the samples is still a considerable challenge. A method³¹¹ for the determination of B isotope composition of tourmalines employed K_2CO_3 fusion and a three-column ion-exchange procedure to achieve full recovery of B prior to measurement by positive ionisation TIMS and MC-ICP-MS. Although the $\delta^{11}\text{B}$ values obtained by the two techniques were generally in good agreement, some discrepancies observed for a couple of samples were thought to be due to interferences from isobaric ions formed from trace organic matter during ion-exchange. Thus, it would appear that MC-ICP-MS may be preferred over TIMS for organic-rich samples.

Experiments³¹² were performed to assess whether an approach to *U–Pb dating of monazite* involving multi-step chemical abrasion plus TIMS could reveal complexities in either age or composition that might be masked by single-step analysis. It was recommended that high temperature annealing should not be used for monazite because the annealing induced recrystallisation that affected the style of dissolution and produced age and composition data that were more variable than those for unannealed samples. Instead, slow partial dissolution of monazite in weak acid proved suitable for obtaining consistent information on complex samples.

An investigation³¹³ into the suitability of various *commercial silica gels* as emission activators for the ionisation of Pb in TIMS concluded that the emitter produced by Sigma-Aldrich was an excellent alternative to Merck silica gel, which is no longer manufactured.

4.4.3.2 Secondary ion mass spectrometry. An authoritative overview of the current state of *SIMS technology* formed part of a more wide-ranging review²⁵⁶ of recent developments in geochemical analysis. Applications of SIMS to geochronology, palaeoclimate studies and quantification of volatile elements were highlighted, together with the increased popularity of NanoSIMS due to its capability for high-spatial-resolution imaging. The main applications of NanoSIMS within the Earth sciences continue to be imaging and isotope ratio determinations on presolar grains. For a detailed account of the technical aspects and application of NanoSIMS in cosmochemistry and biogeochemistry, a critical review (170 references) by Hoppe *et al.*³¹⁴ is recommended.

The increased capabilities of SIMS have resulted in more research projects using the technique to resolve *variations in the growth of biocarbonate structures at the μm scale*. Vetter *et al.*³¹⁵ conducted experiments in which planktonic foraminifera were grown at a constant temperature and transferred every 12 h between unmodified seawater and seawater with modified Ba/Ca and $\delta^{18}\text{O}$ chemistry to produce time-resolved bands of shell calcite with predictable geochemistries. Elemental (Ba/Ca) data were obtained by LA-ICP-MS and cross-correlated with $\delta^{18}\text{O}$ measurements by SIMS with a $3 \mu\text{m}$ spot and average precision of 0.6‰ (2 SD). The finding that Ba and $\delta^{18}\text{O}$ tracers were incorporated into the shell calcite synchronously demonstrated the power of SIMS, in combination with high resolution LA-ICP-MS, to measure chemical variations in daily growth increments in the fossil record. NanoSIMS³¹⁶ was used to study the skeletal structures of a coral exposed to ^{86}Sr -enriched seawater at



intervals of 48 h interspersed with 5 days of growth under normal seawater conditions. Images of the $^{86}\text{Sr}/^{44}\text{Ca}$ ratio in the skeleton formed during the experiment allowed the growth rate of components of the coral skeleton to be calculated.

New approaches to *U–Pb geochronology by SIMS* have taken advantage of the high spatial resolution that can be achieved. Schmitt and Zack³¹⁷ used an O_2^+ primary ion beam coupled with surficial O_2 gas deposition (so-called O_2 flooding) for *U–Pb* dating of rutile. Natural and synthetic rutiles were conductive under O_2^+ bombardment so higher sputter rates were possible than by conventional SIMS with a O_2^- beam, without incurring detrimental effects due to sample charging. Both *Pb–Pb* and *U–Pb* ages generated were accurate to within <1% for Early Paleozoic to Archean rutile, without evidence of any significant bias due to crystal orientation. The coupling of two new approaches enabled Ault *et al.*³¹⁸ to analyse zircons too small to be dated by standard SIMS and TIMS methods. Automated mineralogy was used instead of mineral separation to identify rapidly sub-20 μm zircons in a single thin Section. A modified SIMS protocol then preferentially collected secondary ions emitted from a domain a few μm in size within the *ca.* 20 μm diameter analysis pit. In this manner, *in situ* *U–Pb* data were acquired for zircons grains with dimensions of <10 μm .

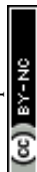
Other novel *geological applications of SIMS* included high precision *in situ* measurements of Mg isotopes in meteoritic materials³¹⁹ using 30–40 μm analytical spots. The data reduction procedure was critical for achieving the level of precision required, typically ± 5 ppm. By modelling factors such as Faraday cup background drift and instrumental fractionation induced by the sample matrix, the fully corrected Mg isotopic data attained the levels of precision and accuracy needed to establish the chronology of events in the early solar system based on the decay of ^{26}Al to ^{26}Mg . Following an evaluation of methods for correcting the significant instrumental mass fractionation observed during *in situ* determination of oxygen isotopes in magmatic glasses,³²⁰ a simple correction scheme based on the SiO_2 content of appropriate standards spanning a compositional range from basalt to rhyolite was recommended. Using this method, the $\delta^{18}\text{O}$ values of a range of glass RMs were reproduced to within $\pm 0.4\text{‰}$ of their nominal value. An unusual approach³²¹ to the quantification of abundant volatile elements (Cl, F and H) in apatites by SIMS was based on the stoichiometric constraint that the sum of the volatile elements must closely approach 100% occupancy of their collective structure sites. The main advantage of this procedure is that it does not require any independently known homogeneous RMs. Whitehouse³²² demonstrated the potential of SIMS for high spatial resolution measurements of all four S isotopes in sulfides. In addition, two sulfides from SW Greenland and Minas Gerais, Brazil were shown to be sufficiently homogenous to be used as secondary RMs to monitor the accuracy of $\Delta^{33}\text{S}$ measurements by SIMS.

The use of *TOF-SIMS* for quantitative analysis of geological materials is still in its infancy. Marques *et al.*³²³ studied a single melt inclusion in a single phenocryst to evaluate the advantages and limitations of this technique for elemental and isotopic determinations. Two basalt glass RMs (USGS BCR-1 and GSJ JB-

2) with similar matrix composition and physical properties to the melt inclusion were used for quantification. The composition of an ore-metal sublimate on the wall of an exposed vapour bubble inside the melt inclusion could be determined as well as the composition of its host clinopyroxene. Results for the melt inclusion and the clinopyroxene were close to those obtained previously by EPMA and LA-ICP-MS. Values for B, Cl, Li, O and S isotope ratios in the two glass RMs differed significantly from literature values so the authors concluded that more research was necessary to establish whether these discrepancies related to sample heterogeneity at the nanoscale or to analytical factors such as matrix effects in SIMS analysis.

4.4.3.3 Accelerator mass spectrometry. A review of *advances in AMS*²⁵⁶ noted that the focus of current geochemical applications has shifted from extraterrestrial materials to tectonics and climate research, and hot topics now include archaeometry and anthropology. The precision and accuracy of cosmogenic ^3He measurements by AMS are dependent on the passive He blank from the extraction apparatus. A new high temperature single vacuum furnace³²⁴ was capable of extracting He from minerals such as apatite, pyroxene and olivine with virtually 100% recovery. After heating at 1450 °C for 20 min, the blanks of 3.7×10^{-21} mole for ^3He and 1.1×10^{-15} mole for ^4He were an order of magnitude better than those of a conventional double vacuum furnace. Large accelerators are normally necessary to separate ^{36}Cl from its stable isobar ^{36}S but these measurements can now be performed with modern 5 MeV AMS instruments using gas stripping to produce the highest quality beams. A protocol³²⁵ for the accurate determination of ^{36}Cl included ID for stable Cl measurement and separation from ^{36}S on a relatively small automated spectrometer using 30 MeV ions. Improvements in AMS measurement precisions and low Pt machine backgrounds contributed to the first reported observation that the $^{198}\text{Pt}/^{195}\text{Pt}$ ratio in two presolar nanodiamonds³²⁶ from the Allende meteorite may be enhanced by 6–7%. Although they require verification, these results may shed light on nucleosynthesis processes taking place in the parent star.

Ten laboratories participated in the first international interlaboratory comparison³²⁷ for the measurement of the *long-lived radionuclide* ^{10}Be . The results for three samples ($^{10}\text{Be}/^{11}\text{Be} = 10^{-12}$ – 10^{-14}) were made traceable to NIST SRM 4325 (beryllium chloride solution) to avoid discrepancies from the use of different calibration materials. Multi-variate statistical analysis of the data indicated that participating AMS facilities fell into two distinct groups, with maximum discrepancies of 6–31% depending on the absolute $^{10}\text{Be}/^{11}\text{Be}$ value. Various issues were discussed openly in the paper because the laboratories had waived their right to anonymity. Unfortunately, NIST SRM 4325 is no longer available, so another material of the same metrological quality is required in the very near future. Instead of following the common practice of adding stable ^9Be as a carrier during sample preparation prior to ^{10}Be AMS measurements, researchers at ETH Zurich advocated³²⁸ a two-step leaching procedure for the measurement of $^{10}\text{Be}/^{11}\text{Be}$ in marine sediments without the addition of ^9Be carrier. An elaborate procedure was necessary to separate authigenic Be from detrital Be while keeping contamination from ^9Be to a minimum. In a



procedure³²⁹ for measuring ^{10}Be in small amounts of sediments, 1–10 mg of sediment were spiked with several hundred μg of ^9Be carrier. The ^{10}Be values obtained by this method agreed within 3–5% with values previously determined on much larger 200 mg samples at the same AMS facility at the University of Tokyo. Efficient extraction and purification of quartz from rocks, soils and sediments are essential for *in situ* AMS measurement of cosmogenic nuclides such as ^{26}Al and ^{10}Be in the determination of surface exposure ages, erosion rates and burial ages. The use of hot phosphoric acid,³³⁰ which preferentially dissolved silicates but not quartz, was considered an alternative to the usual procedure involving repetitive etching in dilute HF. This method was particularly effective at recovering quartz from samples with very low quartz abundance or with cryptocrystalline silica, e.g., greywacke and chert.

4.4.4 X-ray spectrometry. For up-to-date information on instrumental developments and *applications of X-ray techniques*, the Update on XRF⁴ should be consulted. A review³³¹ (203 references) of synchrotron photon-based techniques focussed on the main methodological developments and trends in their use for the characterisation of ancient and historical materials.

Polarised-beam EDXRF instruments are routinely used for the determination of major and trace elements in a wide range of materials including soils and sediments³³² and chert artefacts.³³³ Redus and Huber³³⁴ suggested that a suitable figure of merit for comparison of EDXRF instruments would be the time required to achieve a given statistical uncertainty and they demonstrated how this could be used to select the optimum detector and spectrometer configuration for a specific application. A comparison³³⁵ of EDXRF detectors concluded that CdTe detectors generally gave better precision and accuracy for K lines greater than 20 or 25 keV but that high resolution silicon drift detectors were superior at lower energies. For applications requiring accurate measurement of high Z elements in complex matrices, instruments with a combined or dual detector system provided both high resolution and high efficiency.

The popularity of *XRF core scanning* for obtaining elemental data from sediment cores has increased, particularly for applications such as paleoclimate studies in which relative rather than absolute element concentrations are required. The capabilities of a new core scanner,³³⁶ with a resolution of 0.8 mm, were compared with ICP-AES and ICP-MS analysis after acid digestion of discrete samples collected at 1 mm intervals on a 5 m marine sediment core. Scanning was suitable for obtaining an overview on the chemical patterns along the core and so identifying the most appropriate sampling locations to take discrete samples for ICP analysis to address specific paleoclimatic questions. Errors calculated by the core scanner software were underestimated, especially at high count rate, so it was recommended that the XRF data should always be compared with quantitative data from discrete samples for calibration purposes. Hennekam and de Lange³³⁷ noted the measurement variability caused by different thicknesses of the water film underneath the plastic foil during XRF core scanning and suggested ways of correcting for this.

Recent applications of *PXRF devices*, in use for over a decade, included mudrock chemostratigraphy in drill cores,³³⁸

characterisation of stoneware ceramics³³⁹ and the provenancing of glass beads.³⁴⁰ The user-friendly nature of the technique means that handheld and portable bench-top instruments are regularly employed in activities such as mineral prospecting, ore-grade evaluation and contaminated land surveys by operators with very limited knowledge of the underlying spectrometry. A cautionary tale in relation to the use of PXRF devices in mineral exploration³⁴¹ was highlighted in a study commissioned by the Canadian Mining Industry Research Organisation (CAMIRO), in which the performance of three handheld and two benchtop models were evaluated. No reliance could be placed on preset factory calibrations so recalibration of portable instruments with well-characterised RMs was recommended. The CAMIRO Phase I report, which is available at <http://www.appliedgeochemists.org>, gives a detailed picture of the performance of this type of instrumentation and should be essential reading for anyone interested in using PXRF instrumentation.

5 Glossary of terms

2D	Two-dimensional
A4F	Asymmetrical flow field flow fractionation
AAS	Atomic absorption spectrometry
AEC	Anion exchange chromatography
AES	Atomic emission spectrometry
AFS	Atomic fluorescence spectrometry
ALF	Artificial lysosomal fluid
ANN	Artificial neural network
AMS	Accelerator mass spectrometry
APDC	Ammonium pyrrolidine dithiocarbamate
ASU	Atomic spectrometry update
aTOF-MS	Aerosol time of flight mass spectrometry
BAM	Federal Institute for Materials Research and Testing (Germany)
BCR	Community Bureau of Reference (<i>of the European Community</i>) now IRMM
CCD	Charge coupled detector
CDN	CDN Resource Laboratories Ltd (Canada)
CI	Confidence interval
CNT	Carbon nanotube
COD	Chemical oxygen demand
CPC	Condensation particle counter
CPE	Cloud point extraction
CRM	Certified reference material
CRS	Cavity ringdown spectroscopy
CS	Continuum source
CVG	Chemical vapour generation
CZE	Capillary zone electrophoresis
DDTC	Diethyldithiocarbamate
DEEE	Diesel engine exhaust emission
DGT	Diffusion gradient in thin films
DLLME	Dispersive liquid liquid microextraction
DPM	Diesel particulate matter
DRC	Dynamic reaction cell
EC	Elemental carbon
ED	Energy dispersive



EDS	Energy dispersive spectrometry	LREE	Light rare earth element
EDTA	Ethylidiaminetetraacetic acid	MAAP	Multiangle absorption photometer
EDXRF	Energy dispersive X-ray fluorescence	MC	Multicollector
EN	European standard	MIBK	Methyl isobutyl ketone
EPA	Environmental Protection Agency (USA)	MOUDI	Micro orifice uniform deposition impactor
EPMA	Electron probe microanalyser	MRI	Magnetic resonance imaging
ERM	European Reference Material	MS	Mass spectrometry
ES	Electrospray	MWCNT	Multiwalled carbon nanotube
ESI-MS	Electrospray ionisation mass spectrometry	NACIS	National Analysis Centre for Iron and Steel (China)
ETAAS	Electrothermal atomic absorption spectrometry	NCS	China National Analysis Centre for Iron and Steel
ETV	Electrothermal vaporisation	NDIRS	Non-dispersive infrared spectroscopy
EUSAAR	European Supersites for Atmospheric Aerosol Research	Nd:YAG	Neodymium doped:yttrium aluminum garnet
FAAS	Flame atomic absorption spectrometry	NIOSH	National Institute of Occupational Safety and Health (USA)
FFF	Field flow fractionation	NIR	Near infrared
FI	Flow injection	NIST	National Institute of Standards and Technology (USA)
fs	Femto second	NMI	National Measurement Institute
FTIR	Fourier transform infrared	NMIJ	National Metrology Institute of Japan
GC	Gas chromatography	NP	Nanoparticle
GSJ	Geological Survey of Japan	NRCC	National Research Council of Canada
HDC	Hydrodynamic chromatography	NRCCRM	National Research Centre for Certified Reference Materials (China)
HEN	High efficiency nebuliser	ns	Nano-second
HG	Hydride generation	NTIMS	Negative thermal ionisation mass spectrometry
HILIC	Hydrophilic liquid interaction chromatography	NWRI	National Water Research Institute (Canada)
HPLC	High performance liquid chromatography	OC	Organic carbon
HPS	High Purity Standards (USA)	OES	Optical emission spectrometry
HR	High resolution	OREAS	Ore Research and Exploration Pty Ltd Assay Standards (Australia)
IAEA	International Atomic Energy Agency	PFA	Perfluoroalkyl
IC	Ion chromatography	PGE	Platinum group element
ICP	Inductively coupled plasma	PIXE	Particle induced X-ray emission
ICP-AES	Inductively coupled plasma atomic emission spectrometry	PM _{0.07-0.34}	Particulate matter (with an aerodynamic diameter of between 0.07 and 0.34 µm)
ICP-MS	Inductively coupled plasma mass spectrometry	PM _{0.34-1.15}	Particulate matter (with an aerodynamic diameter of between 0.34 and 1.15 µm)
ICP-SF-MS	Inductively coupled plasma sector field mass spectrometry	PM _{1.15-2.5}	Particulate matter (with an aerodynamic diameter of between 1.15 and 2.5 µm)
ID	Isotope dilution	PM _{2.5}	Particulate matter (with an aerodynamic diameter of up to 2.5 µm)
IERM	Institute for Environmental Reference Materials (of Ministry of Environmental Protection, China)	ppbv	Part per billion volume
IGGE	Institute of Geophysical and Geochemical Exploration (China)	ppm	Part per million
IMPROVE	Interagency Monitoring for Protected Visual Environments	PTFE	Poly(tetrafluoroethylene)
INAA	Instrumental neutron activation analysis	PXRF	Portable X-ray fluorescence
INCT	Institute of Nuclear Chemistry and Technology (Poland)	QA	Quality assurance
IR	Infrared	QC	Quality control
IRMM	Institute for Reference Materials and Measurements	REE	Rare earth element
IRMS	Isotope ratio mass spectrometry	rf	Radio frequency
ISO	International Organisation for Standardization	RM	Reference material
ISS	Istituto Superiore di Sanita (Italy)	RP	Reversed phase
ITU	Institute for Transuranium Elements	RSD	Relative standard deviation
LA	Laser ablation	RTC	Resource Technology Corporation (USA)
LC	Liquid chromatography	SBET	Simplified bioaccessibility extraction test
LGC	Laboratory of the Government Chemist (UK)	SD	Standard deviation
LIBS	Laser induced breakdown spectroscopy	SDME	Single drop microextraction
LLE	Liquid liquid extraction	SEC	Size exclusion chromatography
LLME	Liquid liquid microextraction	SEM	Scanning electron microscopy
LOD	Limit of detection	SF	Sector field



SFE	Supercritical fluid extraction
SFODME	Solidification of floating organic drop microextraction
SIMS	Secondary ion mass spectrometry
SMPS	Scanning mobility particle sizer
S/N	Signal-to-noise ratio
SPE	Solid phase extraction
SPME	Solid phase microextraction
SR	Synchrotron radiation
SRM	Standard reference material
TC	Total carbon
TDS	Total dissolved solid
TEM	Transmission electron microscopy
TEOM	Tapered element oscillating microbalance
TGA	Thermal gravimetric analysis
TIMS	Thermal ionisation mass spectrometry
TOF	Time of flight
TOT	Thermal optical transmission
TSP	Total suspended particles
TXRF	Total reflection X-ray fluorescence
USGS	United States Geological Survey
USN	Ultrasonic nebuliser
UV	Ultra violet
VALLME	Vortex-assisted liquid liquid microextraction
VG	Vapour generation
VOC	Volatile organic compound
WDXRF	Wavelength dispersive X-ray fluorescence
WHO	World Health Organisation
XANES	X-ray absorption near edge structure
XAS	X-ray absorption spectrometry
XRD	X-ray diffraction
XRF	X-ray fluorescence
z	Atomic number
σ	Population standard deviation

References

- O. T. Butler, W. R. L. Cairns, J. M. Cook and C. M. Davidson, *J. Anal. At. Spectrom.*, 2013, **28**(2), 177–216.
- A. Taylor, M. P. Day, S. Hill, J. Marshall, M. Patriarca and M. White, *J. Anal. At. Spectrom.*, 2013, **28**(4), 425–459.
- E. H. Evans, M. Horstwood, J. Pisonero and C. M. M. Smith, *J. Anal. At. Spectrom.*, 2013, **28**(6), 779–800.
- M. West, A. T. Ellis, P. J. Potts, C. Streli, C. Vanhoof, D. Wegrynek and P. Wobrauschek, *J. Anal. At. Spectrom.*, 2013, **28**(10), 1544–1590.
- S. Carter, A. S. Fisher, M. W. Hinds and S. Lancaster, *J. Anal. At. Spectrom.*, 2013, **28**(12), 1814–1869.
- P. Negrel, M. Blessing, R. Millot, E. Petelet-Giraud and C. Innocent, *TrAC, Trends Anal. Chem.*, 2012, **38**, 143–153.
- F. Drewnick, *Anal. Bioanal. Chem.*, 2012, **404**(8), 2127–2131.
- B. R. Bzdek, M. R. Pennington and M. V. Johnston, *J. Aerosol Sci.*, 2012, **52**, 109–120.
- P. Kumar, L. Pirjola, M. Ketzler and R. M. Harrison, *Atmos. Environ.*, 2013, **67**, 252–277.
- I. van der Veen and J. de Boer, *Chemosphere*, 2012, **88**(10), 1119–1153.
- A. Mukhtar and A. Limbeck, *Anal. Chim. Acta*, 2013, **774**, 11–25.
- E. R. Lennox, N. M. Kreisberg and L. D. Montoya, *Aerosol Sci. Technol.*, 2013, **47**(6), 626–633.
- J. S. Kang, K. S. Lee, K. H. Lee, H. J. Sung and S. S. Kim, *Aerosol Sci. Technol.*, 2012, **46**(9), 966–972.
- B. R'Mili, O. L. C. Le Bihan, C. Dutouquet, O. Aguerre-Charriol and E. Frejafon, *Aerosol Sci. Technol.*, 2013, **47**(7), 767–775.
- A. L. Miller, P. L. Drake, N. C. Murphy, J. D. Noll and J. C. Volkwein, *J. Environ. Monit.*, 2012, **14**(1), 48–55.
- A. L. Miller, P. L. Drake, N. C. Murphy, E. G. Cauda, R. F. LeBouf and G. Markevicius, *Aerosol Sci. Technol.*, 2013, **47**(7), 724–733.
- C. N. Liu, A. Awasthi, Y. H. Hung and C. J. Tsai, *Atmos. Environ.*, 2013, **69**, 325–333.
- R. Cucciniello, A. Proto, D. Alfano and O. Motta, *Atmos. Environ.*, 2012, **60**, 82–87.
- M. Arashiro and D. Leith, *J. Aerosol Sci.*, 2013, **57**, 181–184.
- S. A. Einstein, C. H. Yu, G. Mainelis, L. C. Chen, C. P. Weisel and P. J. Lioy, *J. Environ. Monit.*, 2012, **14**(9), 2411–2420.
- C. Isaxon, K. Dierschke, J. Pagels, J. Londahl, A. Gudmundsson, I. Hagerman, M. Berglund, A. Wierzbicka, E. Assarsson, U. B. Andersson, B. A. G. Jonsson, M. E. Messing, J. Nielsen and M. Bohgard, *Aerosol Sci. Technol.*, 2013, **47**(1), 52–59.
- C. Isaxon, K. Dierschke, J. H. Pagels, A. Wierzbicka, A. Gudmundsson, J. Londahl, I. Hagerman, M. Berglund, E. Assarsson, U. B. Andersson, B. A. G. Jonsson, J. K. Nojgaard, A. Eriksson, J. Nielsen and M. Bohgard, *J. Aerosol Sci.*, 2013, **60**, 55–66.
- E. Vo and Z. Q. Zhuang, *J. Aerosol Sci.*, 2013, **61**, 50–59.
- B. O. Meuller, M. E. Messing, D. L. J. Engberg, A. M. Jansson, L. I. M. Johansson, S. M. Norlen, N. Tureson and K. Deppert, *Aerosol Sci. Technol.*, 2012, **46**(11), 1256–1270.
- L. Stabile, A. Ruggiero, G. Iannitti and G. Buonanno, *J. Aerosol Sci.*, 2013, **55**, 66–77.
- A. Mamakos, I. Khalek, R. Giannelli and M. Spears, *Aerosol Sci. Technol.*, 2013, **47**(8), 927–936.
- J. Aldabe, C. Santamaria, D. Elustondo, E. Lasheras and J. M. Santamaria, *Anal. Methods*, 2013, **5**(2), 554–559.
- J. J. Niu, P. E. Rasmussen and M. Chenier, *Int. J. Environ. Anal. Chem.*, 2013, **93**(6), 661–678.
- X. Hu, Y. Zhang, Z. H. Ding, T. J. Wang, H. Z. Lian, Y. Y. Sun and J. C. Wu, *Atmos. Environ.*, 2012, **57**, 146–152.
- C. Puls, A. Limbeck and S. Hann, *Atmos. Environ.*, 2012, **55**, 213–219.
- F. Zereini, C. L. S. Wiseman and W. Puttmann, *Environ. Sci. Technol.*, 2012, **46**(18), 10326–10333.
- R. G. O. Araujo, F. Vignola, I. N. B. Castilho, B. Welz, M. G. R. Vale, P. Smichowski, S. L. C. Ferreira and H. Becker-Ross, *Microchem. J.*, 2013, **109**, 36–40.
- S. Atilgan, S. Akman, A. Baysal, Y. Bakircioglu, T. Szigeti, M. Ovari and G. Zaray, *Spectrochim. Acta, Part B*, 2012, **70**, 33–38.



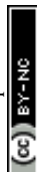
- 34 I. Gaona, P. Lucena, J. Moros, F. J. Fortes, S. Guirado, J. Serrano and J. J. Laserna, *J. Anal. At. Spectrom.*, 2013, **28**(6), 810–820.
- 35 C. B. Stipe, A. L. Miller, J. Brown, E. Guevara and E. Cauda, *Appl. Spectrosc.*, 2012, **66**(11), 1286–1293.
- 36 J. H. Kwak, G. Kim, Y. J. Kim and K. Park, *Aerosol Sci. Technol.*, 2012, **46**(10), 1079–1089.
- 37 C. Dutouquet, G. Wattieaux, L. Meyer, E. Frejafon and L. Boufendi, *Spectrochim. Acta, Part B*, 2013, **83–84**, 14–20.
- 38 T. Tjarnhage, P. A. Gradmark, A. Larsson, A. Mohammed, L. Landstrom, E. Sagerfors, P. Jonsson, F. Kullander and M. Andersson, *Opt. Commun.*, 2013, **296**, 106–108.
- 39 P. Sahay, S. T. Scherrer and C. J. Wang, *Rev. Sci. Instrum.*, 2012, **83**(9), 14.
- 40 N. Spada, A. Bozlaker and S. Chellam, *Anal. Chim. Acta*, 2012, **735**, 1–8.
- 41 T. Pulles, H. D. van der Gon, W. Appelman and M. Verheul, *Atmos. Environ.*, 2012, **61**, 641–651.
- 42 S. A. Pergantis, T. L. Jones-Lepp and E. M. Heithmar, *Anal. Chem.*, 2012, **84**(15), 6454–6462.
- 43 S. Elzey, D. H. Tsai, L. L. Yu, M. R. Winchester, M. E. Kelley and V. A. Hackley, *Anal. Bioanal. Chem.*, 2013, **405**(7), 2279–2288.
- 44 Y. Suzuki, H. Sato, K. Hiyoshi and N. Furuta, *Spectrochim. Acta, Part B*, 2012, **76**, 133–139.
- 45 M. Sakata, T. Ishikawa and S. Mitsunobu, *Atmos. Environ.*, 2013, **67**, 296–303.
- 46 F. Gueguen, P. Stille, V. Dietze and R. Giere, *Atmos. Environ.*, 2012, **62**, 631–645.
- 47 S. Kappel, S. F. Boulyga and T. Prohaska, *J. Environ. Radioact.*, 2012, **113**, 8–15.
- 48 M. Kraiem, S. Richter, N. Erdmann, H. Kuhn, M. Hedberg and Y. Aregbe, *Anal. Chim. Acta*, 2012, **748**, 37–44.
- 49 H. E. Hocking, L. W. Burggraf, X. F. F. Duan, J. A. Gardella, B. P. Yatzor and W. A. Schuler, *Surf. Interface Anal.*, 2013, **45**(1), 545–548.
- 50 E. Barkan and B. Luz, *Rapid Commun. Mass Spectrom.*, 2012, **26**(23), 2733–2738.
- 51 Z. C. Wu, Y. F. Zhou, N. Xu, L. Tao and H. W. Chen, *J. Anal. At. Spectrom.*, 2013, **28**(5), 697–701.
- 52 E. S. Cross, A. Sappok, E. C. Fortner, J. F. Hunter, J. T. Jayne, W. A. Brooks, T. B. Onasch, V. W. Wong, A. Trimborn, D. R. Worsnop and J. H. Kroll, *J. Eng. Gas Turbines Power*, 2012, **134**(7), 072801.
- 53 D. Salcedo, A. Laskin, V. Shutthanandan and J. L. Jimenez, *Aerosol Sci. Technol.*, 2012, **46**(11), 1187–1200.
- 54 A. Wastl, F. Stadlbauer, J. Prost, C. Horntrich, P. Kregsamer, P. Wobrauschek and C. Streli, *Spectrochim. Acta, Part B*, 2013, **82**, 71–75.
- 55 S. Yarkin and M. Gerboles, *Atmos. Environ.*, 2013, **73**, 159–168.
- 56 P. Nowinski, V. F. Hodge and S. Gerstenberger, *Environ. Chem.*, 2012, **9**(4), 379–388.
- 57 C. Cantaluppi, M. Natali, F. Ceccotto and A. Fasson, *X-Ray Spectrom.*, 2013, **42**(4), 213–219.
- 58 D. Varrica, F. Bardelli, G. Dongarra and E. Tamburo, *Atmos. Environ.*, 2013, **64**, 18–24.
- 59 J. R. Zeng, G. L. Zhang, L. M. Bao, S. L. Long, M. G. Tan, Y. Li, C. Y. Ma and Y. D. Zhao, *J. Environ. Sci.*, 2013, **25**(3), 605–612.
- 60 L. H. Wang, X. M. Lu, X. J. Wei, Z. Jiang, S. Q. Gu, Q. Gao and Y. Y. Huang, *J. Anal. At. Spectrom.*, 2012, **27**(10), 1667–1673.
- 61 Z. Kertesz, E. Furu and M. Kavcic, *Spectrochim. Acta, Part B*, 2013, **79–80**, 58–62.
- 62 J. Noll, S. Janisko and S. E. Mischler, *Anal. Methods*, 2013, **5**(12), 2954–2963.
- 63 D. Massabo, V. Bernardoni, M. C. Bove, A. Brunengo, E. Cuccia, A. Piazzalunga, P. Prati, G. Valli and R. Vecchi, *J. Aerosol Sci.*, 2013, **60**, 34–46.
- 64 Y. Cheng, K. B. He, F. K. Duan, Z. Y. Du, M. Zheng and Y. L. Ma, *Atmos. Environ.*, 2012, **59**, 551–558.
- 65 V. Bernardoni, G. Calzolari, M. Chiari, M. Fedi, F. Lucarelli, S. Nava, A. Piazzalunga, F. Riccobono, F. Taccetti, G. Valli and R. Vecchi, *J. Aerosol Sci.*, 2013, **56**, 88–99.
- 66 H. Bladt, J. Schmid, E. D. Kireeva, O. B. Popovicheva, N. M. Perseantseva, M. A. Timofeev, K. Heister, J. Uihlein, N. P. Ivleva and R. Niessner, *Aerosol Sci. Technol.*, 2012, **46**(12), 1337–1348.
- 67 S. Verpaele and J. Jouret, *Ann. Occup. Hyg.*, 2013, **57**(1), 54–62.
- 68 M. Harper and K. Ashley, *J. Occup. Environ. Hyg.*, 2013, **10**(6), 297–306.
- 69 M. Chai, M. E. Birch and G. Deye, *Ann. Occup. Hyg.*, 2012, **56**(8), 959–967.
- 70 R. F. LeBouf, A. L. Miller, C. Stipe, J. Brown, N. Murphy and A. B. Stefaniak, *Environ. Sci. Processes Impacts*, 2013, **15**(6), 1191–1198.
- 71 E. P. Gray, T. A. Bruton, C. P. Higgins, R. U. Halden, P. Westerhoff and J. F. Ranville, *J. Anal. At. Spectrom.*, 2012, **27**(9), 1532–1539.
- 72 S. R. Guevara and M. Horvat, *Anal. Methods*, 2013, **5**(8), 1996–2006.
- 73 D. Das, U. Gupta and A. K. Das, *TrAC, Trends Anal. Chem.*, 2012, **38**, 163–171.
- 74 C. H. Latorre, J. A. Mendez, J. B. Garcia, S. G. Martin and R. M. P. Crecente, *Anal. Chim. Acta*, 2012, **749**, 16–35.
- 75 R. Sitko, B. Zawisza and E. Malicka, *TrAC, Trends Anal. Chem.*, 2012, **37**, 22–31.
- 76 V. Andruch, I. S. Balogh, L. Kocurova and J. Sandrejova, *J. Anal. At. Spectrom.*, 2013, **28**(1), 19–32.
- 77 M. Shoaib and H. M. Al-Swaidan, *J. Chem. Soc. Pak.*, 2012, **34**(6), 1585–1593.
- 78 E. Sugar, E. Tatar, G. Zaray and V. G. Mihucz, *Microchem. J.*, 2013, **107**, 131–135.
- 79 S. Doker, L. Uzun and A. Denizli, *Talanta*, 2013, **103**, 123–129.
- 80 K. Pyrzynska, *Int. J. Environ. Anal. Chem.*, 2012, **92**(11), 1298–1311.
- 81 C. J. Zeng, Y. Lin, N. Zhou, J. T. Zheng and W. Zhang, *J. Hazard. Mater.*, 2012, **237**, 365–370.
- 82 R. Karosi, K. Boruzs, A. Beni, J. Posta, J. Balogh and V. Andruch, *Anal. Methods*, 2012, **4**(8), 2361–2364.



- 83 J. A. Baig, A. Hol, A. Akdogan, A. A. Kartal, U. Divrikli, T. G. Kazi and L. Elci, *J. Anal. At. Spectrom.*, 2012, **27**(9), 1509–1517.
- 84 Z. W. Qin, D. McNee, H. Gleisner, A. Raab, K. Kyeremeh, M. Jaspars, E. Krupp, H. Deng and J. Feldmann, *Anal. Chem.*, 2012, **84**(14), 6213–6219.
- 85 X. Han, L. H. Cao, H. Y. Cheng, J. H. Liu and Z. G. Xu, *Anal. Methods*, 2012, **4**(10), 3471–3477.
- 86 A. Spolaor, P. Vallelonga, J. Gabrieli, N. Kehrwald, C. Turetta, G. Cozzi, L. Poto, J. M. C. Plane, C. Boutron and C. Barbante, *Anal. Bioanal. Chem.*, 2013, **405**(2–3), 647–654.
- 87 L. Telgmann, M. Sperling and U. Karst, *Anal. Chim. Acta*, 2013, **764**, 1–16.
- 88 L. Telgmann, C. A. Wehe, M. Birka, J. Kunemeyer, S. Nowak, M. Sperling and U. Karst, *Environ. Sci. Technol.*, 2012, **46**(21), 11929–11936.
- 89 U. Lindner, J. Lingott, S. Richter, N. Jakubowski and U. Panne, *Anal. Bioanal. Chem.*, 2013, **405**(6), 1865–1873.
- 90 B. Stolpe, L. D. Guo, A. M. Shiller and G. R. Aiken, *Geochim. Cosmochim. Acta*, 2013, **105**, 221–239.
- 91 B. Stolpe, L. D. Guo and A. M. Shiller, *Geochim. Cosmochim. Acta*, 2013, **106**, 446–462.
- 92 N. Garcia-Otero, P. Bermejo-Barrera and A. Moreda-Pineiro, *Anal. Chim. Acta*, 2013, **760**, 83–92.
- 93 E. Kilinc, S. Bakirdere, F. Aydin and O. Y. Ataman, *Spectrochim. Acta, Part B*, 2012, **73**, 84–88.
- 94 S. Titretir, A. I. Sik, Y. Arslan and O. Y. Ataman, *Spectrochim. Acta, Part B*, 2012, **77**, 63–68.
- 95 H. Matusiewicz and M. Krawczyk, *Spectrosc. Lett.*, 2012, **45**(7), 487–499.
- 96 S. Musil, J. Kratzer, M. Vobecky and T. Matousek, *J. Anal. At. Spectrom.*, 2012, **27**(9), 1382–1390.
- 97 O. Acar, O. M. Kalfa, O. Yalcinkaya and A. R. Turker, *Anal. Methods*, 2013, **5**(3), 748–754.
- 98 T. Limburg and J. W. Einax, *Microchem. J.*, 2013, **107**, 31–36.
- 99 G. I. Bebesko and Y. A. Karpov, *Inorg. Mater.*, 2012, **48**(15), 1341–1348.
- 100 C. A. Almeida, P. Gonzalez, M. Mallea, L. D. Martinez and R. A. Gil, *Talanta*, 2012, **97**, 273–278.
- 101 T. Frentiu, A. I. Mihaltan, E. Darvasi, M. Ponta, C. Roman and M. Frentiu, *J. Anal. At. Spectrom.*, 2012, **27**(10), 1753–1760.
- 102 D. Profrock and A. Prange, *Appl. Spectrosc.*, 2012, **66**(8), 843–868.
- 103 S. Caroli, M. Forte, C. Nuccetelli, R. Rusconi and S. Risica, *Microchem. J.*, 2013, **107**, 95–100.
- 104 Z. Long, C. Chen, X. D. Hou and C. B. Zheng, *Appl. Spectrosc. Rev.*, 2012, **47**(7), 495–517.
- 105 J. P. Goulle, E. Saussereau, L. Mahieu, D. Cellier, J. Spiroux and M. Guerbet, *Bull. Environ. Contam. Toxicol.*, 2012, **89**(6), 1220–1224.
- 106 T. D. Saint-Pierre, R. C. C. Rocha and C. B. Duyck, *Microchem. J.*, 2013, **109**, 41–45.
- 107 T. Pfeifer, R. Janzen, T. Steingrobe, M. Sperling, B. Franze, C. Engelhard and W. Buscher, *Spectrochim. Acta, Part B*, 2012, **76**, 48–55.
- 108 A. C. Fornieles, A. G. de Torres, E. I. V. Alonso and J. M. C. Pavon, *J. Anal. At. Spectrom.*, 2013, **28**(3), 364–372.
- 109 V. Yilmaz, L. Rose, Z. Arslan and M. D. Little, *J. Anal. At. Spectrom.*, 2012, **27**(11), 1895–1902.
- 110 V. Yilmaz, Z. Arslan and L. Rose, *Anal. Chim. Acta*, 2013, **761**, 18–26.
- 111 S. Y. Ng, A. Zou, L. P. Sim, Y. Ding, K. L. Yuen, R. Y. C. Shin and T. K. Lee, *Int. J. Mass Spectrom.*, 2012, **321**, 19–24.
- 112 J. Zheng and M. Yamada, *Appl. Radiat. Isot.*, 2012, **70**(9), 1944–1948.
- 113 K. F. Huang, J. Blusztajn, D. W. Oppo, W. B. Curry and B. Peucker-Ehrenbrink, *J. Anal. At. Spectrom.*, 2012, **27**(9), 1560–1567.
- 114 A. Das, C. H. Chung, C. F. You and M. L. Shen, *J. Anal. At. Spectrom.*, 2012, **27**(12), 2088–2093.
- 115 G. C. Justen, F. R. Espinoza-Quinones, A. N. Modenes and R. Bergamasco, *Water Sci. Technol.*, 2012, **66**(5), 1029–1035.
- 116 E. de Almeida, V. F. do Nascimento and A. A. Menegario, *Spectrochim. Acta, Part B*, 2012, **71–72**, 70–74.
- 117 K. Kocot, B. Zawisza and R. Sitko, *Spectrochim. Acta, Part B*, 2012, **73**, 79–83.
- 118 R. Skorek, E. Turek, B. Zawisza, E. Margui, I. Queralt, M. Stempin, P. Kucharski and R. Sitko, *J. Anal. At. Spectrom.*, 2012, **27**(10), 1688–1693.
- 119 N. Aras, S. U. Yesiller, D. A. Ates and S. Yalcin, *Spectrochim. Acta, Part B*, 2012, **74–75**, 87–94.
- 120 S. U. Yesiller and S. Yalcin, *Anal. Chim. Acta*, 2013, **770**, 7–17.
- 121 H. G. Qian and W. D. Zhou, *Spectrosc. Spectral Anal.*, 2012, **32**(10), 2820–2823.
- 122 Y. Lee, S. W. Oh and S. H. Han, *Appl. Spectrosc.*, 2012, **66**(12), 1385–1396.
- 123 H. Sereshti, Y. E. Heravi and S. Samadi, *Talanta*, 2012, **97**, 235–241.
- 124 H. Fazilrad and M. A. Taher, *Talanta*, 2013, **103**, 375–383.
- 125 K. Chandrasekaran, D. Karunasagar and J. Arunachalam, *J. Anal. At. Spectrom.*, 2013, **28**(1), 142–149.
- 126 M. Karimi, H. Sereshti, V. Khojeh and S. Samadi, *Int. J. Environ. Anal. Chem.*, 2013, **93**(4), 401–415.
- 127 Y. Z. Yi, S. Y. Wu, S. J. Jiang and A. C. Sahayam, *At. Spectrosc.*, 2013, **34**(2), 39–47.
- 128 L. L. Zhao, S. X. Zhong, K. M. Fang, Z. S. Qian and J. R. Chen, *J. Hazard. Mater.*, 2012, **239**, 206–212.
- 129 N. N. Meeravali and S. J. Kumar, *Anal. Methods*, 2012, **4**(8), 2435–2440.
- 130 P. H. Liao, S. J. Jiang and A. C. Sahayam, *J. Anal. At. Spectrom.*, 2012, **27**(9), 1518–1524.
- 131 A. N. Anthemidis, C. Mitani, P. Balkatzopoulou and P. D. Tzanavaras, *Anal. Chim. Acta*, 2012, **733**, 34–37.
- 132 G. Bauer, M. A. Neouze and A. Limbeck, *Talanta*, 2013, **103**, 145–152.
- 133 K. Kocot, B. Zawisza, E. Margui, I. Queralt, M. Hidalgo and R. Sitko, *J. Anal. At. Spectrom.*, 2013, **28**(5), 736–742.
- 134 C. K. Su, T. W. Lee and Y. C. Sun, *J. Anal. At. Spectrom.*, 2012, **27**(9), 1585–1590.
- 135 A. N. Anthemidis, S. Xidia and G. Giakissikli, *Talanta*, 2012, **97**, 181–186.



- 136 B. Zawisza and R. Sitko, *Analyst*, 2013, **138**(8), 2470–2476.
- 137 H. Takata, T. Aono, J. Zheng, K. Tagami, J. Shirasaka and S. Uchida, *Anal. Methods*, 2013, **5**(10), 2558–2564.
- 138 P. R. Aranda, L. Colombo, E. Perino, I. E. De Vito and J. Raba, *X-Ray Spectrom.*, 2013, **42**(2), 100–104.
- 139 M. L. A. Castillo, A. G. de Torres, E. V. Alonso, M. T. S. Cordero and J. M. C. Pavon, *Talanta*, 2012, **99**, 853–858.
- 140 J. Cho, K. W. Chung, M. S. Choi and H. J. Kim, *Talanta*, 2012, **99**, 369–374.
- 141 K. L. Shi, J. X. Qiao, W. S. Wu, P. Roos and X. L. Hou, *Anal. Chem.*, 2012, **84**(15), 6783–6789.
- 142 J. Falandysz, *Food Chem.*, 2013, **138**(1), 242–250.
- 143 O. V. Evdokimova, N. V. Pechishcheva and K. Y. Shunyaev, *J. Anal. Chem.*, 2012, **67**(9), 741–753.
- 144 I. A. Bhatti, M. A. Hayat and M. Iqbal, *J. Chem. Soc. Pak.*, 2012, **34**(4), 1012–1022.
- 145 P. Thakur and G. P. Mulholland, *Appl. Radiat. Isot.*, 2012, **70**(8), 1747–1778.
- 146 H. A. Gad, S. H. El-Ahmady, M. I. Abou-Shoer and M. M. Al-Azizi, *Phytochem. Anal.*, 2013, **24**(1), 1–24.
- 147 M. Welna, A. Szymczycha-Madeja, E. Stelmach and P. Pohl, *Crit. Rev. Anal. Chem.*, 2012, **42**(4), 349–365.
- 148 R. Djingova, V. Mihaylova, V. Lyubomirova and D. L. Tsalev, *Appl. Spectrosc. Rev.*, 2013, **48**(5), 384–424.
- 149 S. Miyashita, K. Inagaki, T. Narukawa, Y. B. Zhu, T. Kuroiwa, A. Hioki and K. Chiba, *Anal. Sci.*, 2012, **28**(12), 1171–1177.
- 150 I. Rezić, *Microchem. J.*, 2013, **107**, 63–69.
- 151 K. Ivanov, P. Zaprianova, M. Petkova, V. Stefanova, V. Kmetov, D. Georgieva and V. Angelova, *Spectrochim. Acta, Part B*, 2012, **71**–72, 117–122.
- 152 R. G. Silva, M. N. Nadagouda, J. Webster, S. Govindaswamy, K. D. Hristovski, R. G. Ford, C. L. Patterson and C. A. Impellitteri, *Environ. Sci. Processes Impacts*, 2013, **15**(3), 645–652.
- 153 E. J. dos Santos, L. M. Baika, A. B. Herrmann, S. Kulik, C. S. Sato, A. B. dos Santos and A. J. Curtius, *Braz. Arch. Biol. Technol.*, 2012, **55**(3), 457–464.
- 154 M. V. B. Krishna, K. Chandrasekaran, G. Venkateswarlu and D. Karunasagar, *Anal. Methods*, 2012, **4**(10), 3290–3299.
- 155 S. Oztan and R. A. During, *Talanta*, 2012, **99**, 594–602.
- 156 N. Fabregat-Cabello, P. Rodriguez-Gonzalez, A. Castillo, J. Malherbe, A. F. Roig-Navarro, S. E. Long and J. I. G. Alonso, *Environ. Sci. Technol.*, 2012, **46**(22), 12542–12549.
- 157 A. H. Khan, J. Q. Shang and R. Alam, *J. Hazard. Mater.*, 2012, **235**, 376–383.
- 158 J. Blaskova, V. Vojtekova, J. Novakova, D. Mackovych, Y. Bazel, L. Lapcik, Z. Popernikova and A. M. M. Abusenaina, *Cent. Eur. J. Chem.*, 2013, **11**(7), 1201–1212.
- 159 B. Wang, B. Huang, Y. B. Qi, W. Y. Hu and W. X. Sun, *Chin. Chem. Lett.*, 2012, **23**(11), 1287–1290.
- 160 Z. Y. Huang, D. P. Qin, X. C. Zeng, J. Li, Y. L. Cao and C. Cai, *Geoderma*, 2012, **189**, 243–249.
- 161 L. Kozak and P. Niedzielski, *Int. J. Environ. Anal. Chem.*, 2012, **92**(9), 1093–1105.
- 162 I. Koch, K. J. Reimer, M. I. Bakker, N. T. Basta, M. R. Cave, S. Denys, M. Dodd, B. A. Hale, R. Irwin, Y. W. Lowney, M. M. Moore, V. Paquin, P. E. Rasmussen, T. Repaso-Subang, G. L. Stephenson, S. D. Siciliano, J. Wragg and G. J. Zagury, *J. Environ. Sci. Health, Part A: Toxic/Hazard. Subst. Environ. Eng.*, 2013, **48**(6), 641–655.
- 163 M. Dodd, P. E. Rasmussen and M. Chenier, *Hum. Ecol. Risk Assess.*, 2013, **19**(4), 1014–1027.
- 164 R. Q. Thompson and S. J. Christopher, *Anal. Methods*, 2013, **5**(5), 1346–1351.
- 165 A. T. Reis, J. P. Coelho, S. M. Rodrigues, R. Rocha, C. M. Davidson, A. C. Duarte and E. Pereira, *Talanta*, 2012, **99**, 363–368.
- 166 C. Waterlot, A. Pelfrene and F. Douay, *Can. J. Chem.*, 2012, **90**(10), 874–879.
- 167 S. X. Li, F. Y. Zheng, Y. C. Li, T. S. Cai and J. Z. Zheng, *J. Agric. Food Chem.*, 2012, **60**(47), 11691–11695.
- 168 I. Urbanova, L. Husakova and J. Sramkova, *Environ. Monit. Assess.*, 2013, **185**(4), 3327–3337.
- 169 M. A. Alvarez and G. Carrillo, *Talanta*, 2012, **97**, 505–512.
- 170 F. M. Fortunato, J. A. G. Neto and G. P. G. Freschi, *At. Spectrosc.*, 2012, **33**(4), 138–142.
- 171 R. Dobrowolski and M. Otto, *J. Food Compos. Anal.*, 2012, **26**(1–2), 58–65.
- 172 T. Frentiu, M. Ponta and R. Hategan, *Chem. Cent. J.*, 2013, **7**, 10.
- 173 A. Virgilio, J. A. Nobrega, J. F. Rego and J. A. G. Neto, *Spectrochim. Acta, Part B*, 2012, **78**, 58–61.
- 174 J. F. Rego, A. Virgilio, J. A. Nobrega and J. A. G. Neto, *Talanta*, 2012, **100**, 21–26.
- 175 M. A. Bechlin, J. A. G. Neto and J. A. Nobrega, *Microchem. J.*, 2013, **109**, 134–138.
- 176 C. D. Pereira, M. A. Aguirre, J. A. Nobrega, M. Hidalgo and A. Canals, *J. Anal. At. Spectrom.*, 2012, **27**(12), 2132–2137.
- 177 F. Ardini, M. Grotti, R. Sanchez and J. L. Todoli, *J. Anal. At. Spectrom.*, 2012, **27**(9), 1400–1404.
- 178 V. C. G. dos Santos, M. T. Grassi, M. S. de Campos, P. G. Peralta-Zamora and G. Abate, *Analyst*, 2012, **137**(19), 4458–4463.
- 179 D. Olivares, M. Bravo, J. Feldmann, A. Raab, A. Neaman and W. Quiroz, *J. AOAC Int.*, 2012, **95**(4), 1176–1182.
- 180 G. Leng, L. Feng, S. B. Li, P. Yang and D. Z. Dan, *Spectroscopy*, 2013, **28**(2), 54–67.
- 181 M. Grotti, F. Ardini and J. L. Todoli, *Anal. Chim. Acta*, 2013, **767**, 14–20.
- 182 E. Bulska, B. Danko, R. S. Dybczynski, A. Krata, K. Kulisa, Z. Samczynski and M. Wojciechowski, *Talanta*, 2012, **97**, 303–311.
- 183 F. Claverie, J. Malherbe, N. Bier, J. L. Molloy and S. E. Long, *Anal. Bioanal. Chem.*, 2013, **405**(7), 2289–2299.
- 184 F. Claverie, J. Malherbe, N. Bier, J. L. Molloy and S. E. Long, *Anal. Chem.*, 2013, **85**(7), 3584–3591.
- 185 W. Maher, F. Krikowa, M. Ellwood, S. Foster, R. Jagtap and G. Raber, *Microchem. J.*, 2012, **105**, 15–31.
- 186 X. P. Liu, W. F. Zhang, Y. N. Hu and H. F. Cheng, *Microchem. J.*, 2013, **108**, 38–45.



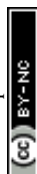
- 187 A. Miszczak, M. Roslon, G. Zbroja, K. Brama, E. Szalacha, H. Gawronska and K. Pawlak, *Anal. Bioanal. Chem.*, 2013, **405**(14), 4667–4678.
- 188 F. Aureli, L. Ouerdane, K. Bierla, J. Szpunar, N. T. Prakash and F. Cubadda, *Metallomics*, 2012, **4**(9), 968–978.
- 189 M. Lenz, G. H. Floor, L. H. E. Winkel, G. Roman-Ross and P. F. X. Corvini, *Environ. Sci. Technol.*, 2012, **46**(21), 11988–11994.
- 190 M. De Cesare, L. K. Fifield, C. Sabbarese, S. G. Tims, N. De Cesare, A. D'Onofrio, A. D'Arco, A. M. Esposito, A. Petraglia, V. Roca and F. Terrasi, *Nucl. Instrum. Methods Phys. Res., Sect. B*, 2013, **294**, 152–159.
- 191 N. Piotrowska, *Nucl. Instrum. Methods Phys. Res., Sect. B*, 2013, **294**, 176–181.
- 192 M. Y. Luo, X. L. Hou, W. J. Zhou, C. H. He, N. Chen, Q. Liu and L. Y. Zhang, *J. Environ. Radioact.*, 2013, **118**, 30–39.
- 193 P. Steier, E. Hrnccek, A. Priller, F. Quinto, M. Srncik, A. Wallner, G. Wallner and S. Winkler, *Nucl. Instrum. Methods Phys. Res., Sect. B*, 2013, **294**, 160–164.
- 194 F. J. Fortes, J. Moros, P. Lucena, L. M. Cabalin and J. J. Laserna, *Anal. Chem.*, 2013, **85**(2), 640–669.
- 195 D. Santos, L. C. Nunes, G. G. A. de Carvalho, M. D. Gomes, P. F. de Souza, F. D. Leme, L. G. C. dos Santos and F. J. Krug, *Spectrochim. Acta, Part B*, 2012, **71–72**, 3–13.
- 196 J. Kaiser, K. Novotny, M. Z. Martin, A. Hrdlicka, R. Malina, M. Hartl, V. Adam and R. Kizek, *Surf. Sci. Rep.*, 2012, **67**(11–12), 233–243.
- 197 J. Pareja, S. Lopez, D. Jaramillo, D. W. Hahn and A. Molina, *Appl. Opt.*, 2013, **52**(11), 2470–2477.
- 198 Y. Liu, B. Bousquet, M. Baudalet and M. Richardson, *Spectrochim. Acta, Part B*, 2012, **73**, 89–92.
- 199 M. Garcimuno, D. M. D. Pace and G. Bertuccelli, *Opt. Laser Technol.*, 2013, **47**, 26–30.
- 200 G. G. A. de Carvalho, D. Santos, L. C. Nunes, M. D. Gomes, F. D. Leme and F. J. Krug, *Spectrochim. Acta, Part B*, 2012, **74–75**, 162–168.
- 201 J. Kwak, K. W. Kim, M. Park, J. Kim and K. Park, *Environ. Technol.*, 2012, **33**(18), 2177–2184.
- 202 A. M. Popov, M. O. Kozhnov, T. A. Labutin, S. M. Zaytsev, A. N. Drozdova and N. A. Mityurev, *Tech. Phys. Lett.*, 2013, **39**(1), 81–83.
- 203 V. K. Unnikrishnan, R. Nayak, K. Aithal, V. B. Kartha, C. Santhosh, G. P. Gupta and B. M. Suri, *Anal. Methods*, 2013, **5**(5), 1294–1300.
- 204 J. Z. Chen, Z. Y. Chen, J. Sun, X. Li, Z. C. Deng and Y. L. Wang, *Appl. Opt.*, 2012, **51**(34), 8141–8146.
- 205 J. Frydenvang, K. M. Kinch, S. Husted and M. B. Madsen, *Anal. Chem.*, 2013, **85**(3), 1492–1500.
- 206 J. El Haddad, M. Villot-Kadri, A. Ismael, G. Gallou, K. Michel, D. Bruyere, V. Laperche, L. Canioni and B. Bousquet, *Spectrochim. Acta, Part B*, 2013, **79–80**, 51–57.
- 207 S. Majumdar, J. R. Peralta-Videa, H. Castillo-Michel, J. Hong, C. M. Rico and J. L. Gardea-Torresdey, *Anal. Chim. Acta*, 2012, **755**, 1–16.
- 208 A. Plessow, *X-Ray Spectrom.*, 2013, **42**(1), 19–32.
- 209 I. M. Ismail and M. S. Rihawy, *Nucl. Instrum. Methods Phys. Res., Sect. B*, 2013, **296**, 50–53.
- 210 K. Wovkulich, B. J. Mailloux, B. C. Bostick, H. L. Dong, M. E. Bishop and S. N. Chillrud, *Geochim. Cosmochim. Acta*, 2012, **91**, 254–270.
- 211 J. Malherbe and F. Claverie, *Anal. Chim. Acta*, 2013, **773**, 37–44.
- 212 N. G. Paltridge, L. J. Palmer, P. J. Milham, G. E. Guild and J. C. R. Stangoulis, *Plant Soil*, 2012, **361**(1–2), 251–260.
- 213 N. G. Paltridge, P. J. Milham, J. I. Ortiz-Monasterio, G. Velu, Z. Yasmin, L. J. Palmer, G. E. Guild and J. C. R. Stangoulis, *Plant Soil*, 2012, **361**(1–2), 261–269.
- 214 R. Terzano, M. Alfeld, K. Janssens, B. Vekemans, T. Schoonjans, L. Vincze, N. Tomasi, R. Pinton and S. Cesco, *Anal. Bioanal. Chem.*, 2013, **405**(10), 3341–3350.
- 215 T. Ducic, M. Borchert, A. Savic, A. Kalauzi, A. Mitrovic and K. Radotic, *J. Synchrotron Radiat.*, 2013, **20**, 339–346.
- 216 I. De La Calle, M. Costas, N. Cabaleiro, I. Lavilla and C. Bendicho, *Food Chem.*, 2013, **138**(1), 234–241.
- 217 G. L. Bosco, *TrAC, Trends Anal. Chem.*, 2013, **45**, 121–134.
- 218 R. O. Bastos, F. L. Melquiades and G. E. V. Biasi, *X-Ray Spectrom.*, 2012, **41**(5), 304–307.
- 219 T. I. McLaren, C. N. Guppy and M. K. Tighe, *Soil Sci. Soc. Am. J.*, 2012, **76**(4), 1446–1453.
- 220 S. Reidinger, M. H. Ramsey and S. E. Hartley, *New Phytol.*, 2012, **195**(3), 699–706.
- 221 Y. P. Lian, W. Zhen, Z. G. Tai, Y. L. Yang, J. Song and Z. H. Li, *Rare Met.*, 2012, **31**(5), 512–516.
- 222 M. M. Hasssanien and A. A. Z. Ali, *Arabian J. Sci. Eng.*, 2012, **37**(5), 1271–1282.
- 223 E. D. Silva, L. O. Correia, L. O. dos Santos, E. V. D. Vieira and V. A. Lemos, *Microchim. Acta*, 2012, **178**(3–4), 269–275.
- 224 G. Leng, H. Yin, S. B. Li, Y. Chen and D. Z. Dan, *Talanta*, 2012, **99**, 631–636.
- 225 V. A. Lemos and U. S. Vieira, *Microchim. Acta*, 2013, **180**(5–6), 501–507.
- 226 D. Bakircioglu, *Environ. Sci. Pollut. Res.*, 2012, **19**(6), 2428–2437.
- 227 S. Sacmaci, S. Kartal and S. Dural, *J. Braz. Chem. Soc.*, 2012, **23**(6), 1033–1040.
- 228 S. Sacmaci, S. Kartal and M. Sacmaci, *Int. J. Environ. Anal. Chem.*, 2012, **92**(14), 1626–1637.
- 229 S. Saracoglu, M. Soylak, D. Cabuk, Z. Topalak and Y. Karagozlu, *J. AOAC Int.*, 2012, **95**(3), 892–896.
- 230 M. Tufekci, V. N. Bulut, H. Elvan, D. Ozdes, M. Soylak and C. Duran, *Environ. Monit. Assess.*, 2013, **185**(2), 1107–1115.
- 231 S. Saracoglu, E. Yilmaz and M. Soylak, *Curr. Anal. Chem.*, 2012, **8**(3), 358–364.
- 232 M. Karimi, V. Amani, F. Aboufazel, H. Zhad, O. Sadeghi and E. Najafi, *J. Chem.*, 2013, 142845.
- 233 S. Turan, S. Tokalioglu, A. Sahan and C. Soykan, *React. Funct. Polym.*, 2012, **72**(10), 722–728.
- 234 M. Soylak and I. Murat, *Food Analytical Methods*, 2012, **5**(5), 1003–1009.
- 235 E. Yilmaz, Z. A. Alothman, H. M. T. Sumayli, M. Ibrahim and M. Soylak, *J. AOAC Int.*, 2012, **95**(4), 1205–1210.
- 236 Y. H. Zhai, Q. He, Q. Han and S. E. Duan, *Microchim. Acta*, 2012, **178**(3–4), 405–412.



- 237 M. Soyak and Y. E. Unsal, *J. AOAC Int.*, 2012, **95**(4), 1183–1188.
- 238 Y. Jiang, H. T. Zhang, Q. He, Z. Hu and X. J. Chang, *Microchim. Acta*, 2012, **178**(3–4), 421–428.
- 239 F. Tajabadi, Y. Yamini and M. R. Sovizi, *Microchim. Acta*, 2013, **180**(1–2), 65–73.
- 240 R. K. Sharma, A. Pandey, S. Gulati and A. Adholeya, *Chem. Eng. J.*, 2012, **210**, 490–499.
- 241 H. Ebrahimzadeh, N. Tavassoli, O. Sadeghi, M. M. Amini, S. Vahidi, S. Aghigh and E. Moazzen, *Food Analytical Methods*, 2012, **5**(5), 1070–1078.
- 242 M. Behbahani, M. Taghizadeh, A. Bagheri, H. Hosseini, M. Salarian and A. Tootoonchi, *Microchim. Acta*, 2012, **178**(3–4), 429–437.
- 243 B. F. Somera, M. Z. Corazza, M. J. S. Yabe, M. G. Segatelli, E. Galunin and C. R. T. Tarley, *Water, Air, Soil Pollut.*, 2012, **223**(9), 6069–6081.
- 244 A. Bagheri, M. Taghizadeh, M. Behbahani, A. A. Asgharinezhad, M. Salarian, A. Dehghani, H. Ebrahimzadeh and M. M. Amini, *Talanta*, 2012, **99**, 132–139.
- 245 A. Bagheri, M. Behbahani, M. M. Amini, O. Sadeghi, A. Tootoonchi and Z. Dahaghin, *Microchim. Acta*, 2012, **178**(3–4), 261–268.
- 246 E. Herincs, M. Puschenreiter, W. Wenzel and A. Limbeck, *J. Anal. At. Spectrom.*, 2013, **28**(3), 354–363.
- 247 K. P. Jochum, U. Nohl, N. Rothbarth, B. Schwager, B. Stoll and U. Weis, *Geostand. Geoanal. Res.*, 2012, **36**(4), 415–419.
- 248 Z. Cheng, H. Huang, M. Liu, T. Gu, W. Yan and M. Yan, *Geostand. Geoanal. Res.*, 2013, **37**(1), 95–101.
- 249 Q. C. Yang, K. P. Jochum, B. Stoll, U. Weis, D. Kuzmin, M. Wiedenbeck, H. Traub and M. O. Andreae, *Geostand. Geoanal. Res.*, 2012, **36**(3), 301–313.
- 250 S. Gilbert, L. Danyushevsky, P. Robinson, C. Wohlgemuth-Ueberwasser, N. Pearson, D. Savard, M. Norman and J. Hanley, *Geostand. Geoanal. Res.*, 2013, **37**(1), 51–64.
- 251 W. Abouchami, S. J. G. Galer, T. J. Horner, M. Rehkamper, F. Wombacher, Z. C. Xue, M. Lambelet, M. Gault-Ringold, C. H. Stirling, M. Schonbachler, A. E. Shiel, D. Weis and P. F. Holdship, *Geostand. Geoanal. Res.*, 2013, **37**(1), 5–17.
- 252 T. Goldberg, G. Gordon, G. Izon, C. Archer, C. R. Pearce, J. McManus, A. D. Anbar and M. Rehkamper, *J. Anal. At. Spectrom.*, 2013, **28**(5), 724–735.
- 253 N. D. Greber, C. Siebert, T. F. Nagler and T. Pettke, *Geostand. Geoanal. Res.*, 2012, **36**(3), 291–300.
- 254 J. R. Darling, C. D. Storey, C. J. Hawkesworth and P. C. Lightfoot, *Geochim. Cosmochim. Acta*, 2012, **99**, 1–17.
- 255 Z. C. Liu, F. Y. Wu, Y. H. Yang, J. H. Yang and S. A. Wilde, *Chem. Geol.*, 2012, **334**, 221–239.
- 256 M. Wiedenbeck, R. Bugoi, M. J. M. Duke, T. Dunai, J. Enzweiler, M. Horan, K. P. Jochum, K. Linge, J. Kosler, S. Merchel, L. F. G. Morales, L. Nasdala, R. Stalder, P. Sylvester, U. Weis and A. Zoubir, *Geostand. Geoanal. Res.*, 2012, **36**(4), 337–398.
- 257 M. E. Shaheen, J. E. Gagnon and B. J. Fryer, *Chem. Geol.*, 2012, **330**, 260–273.
- 258 J. I. Kimura and Q. Chang, *J. Anal. At. Spectrom.*, 2012, **27**(9), 1549–1559.
- 259 G. Velasquez, A. Y. Borisova, S. Salvi and D. Beziat, *Geostand. Geoanal. Res.*, 2012, **36**(3), 315–324.
- 260 J. M. Koornneef, L. Dorta, B. Hattendorf, G. H. Fontaine, B. Bourdon, A. Stracke, P. Ulmer and D. Gunther, *J. Anal. At. Spectrom.*, 2012, **27**(11), 1863–1874.
- 261 M. W. Loewen and A. J. R. Kent, *J. Anal. At. Spectrom.*, 2012, **27**(9), 1502–1508.
- 262 L. Flamigni, J. Koch and D. Gunther, *Spectrochim. Acta, Part B*, 2012, **76**, 70–76.
- 263 Z. C. Hu, Y. S. Liu, S. Gao, S. Q. Xiao, L. S. Zhao, D. Gunther, M. Li, W. Zhang and K. Q. Zong, *Spectrochim. Acta, Part B*, 2012, **78**, 50–57.
- 264 Z. C. Hu, Y. S. Liu, S. Gao, W. G. Liu, W. Zhang, X. R. Tong, L. Lin, K. Q. Zong, M. Li, H. H. Chen, L. Zhou and L. Yang, *J. Anal. At. Spectrom.*, 2012, **27**(9), 1391–1399.
- 265 J. Hammerli, B. Rusk, C. Spandler, P. Emsbo and N. H. S. Oliver, *Chem. Geol.*, 2013, **337**, 75–87.
- 266 T. U. Schlegel, M. Walle, M. Steele-MacInnis and C. A. Heinrich, *Chem. Geol.*, 2012, **334**, 144–153.
- 267 M. Leisen, J. Dubessy, M. C. Boiron and P. Lach, *Geochim. Cosmochim. Acta*, 2012, **90**, 110–125.
- 268 M. Leisen, M. C. Boiron, A. Richard and J. Dubessy, *Chem. Geol.*, 2012, **330**, 197–206.
- 269 A. A. Nemchin, M. S. A. Horstwood and M. J. Whitehouse, *Elements*, 2013, **9**(1), 31–37.
- 270 C. R. M. McFarlane and Y. Luo, *Geosci. Can.*, 2012, **39**(3), 158–172.
- 271 J. A. Petrus and B. S. Kamber, *Geostand. Geoanal. Res.*, 2012, **36**(3), 247–270.
- 272 C. M. Allen and I. H. Campbell, *Chem. Geol.*, 2012, **332**, 157–165.
- 273 J. M. Cottle, A. R. Kylander-Clark and J. C. Vrijmoed, *Chem. Geol.*, 2012, **332**, 136–147.
- 274 J. F. Sun, J. H. Yang, F. Y. Wu, L. W. Xie, Y. H. Yang, Z. C. Liu and X. H. Li, *Chin. Sci. Bull.*, 2012, **57**(20), 2506–2516.
- 275 M. Bertini, A. Izmer, F. Vanhaecke and E. M. Krupp, *J. Anal. At. Spectrom.*, 2013, **28**(1), 77–91.
- 276 T. Ulrich and B. S. Kamber, *Geostand. Geoanal. Res.*, 2013, **37**(2), 169–188.
- 277 D. A. Frick and D. Gunther, *J. Anal. At. Spectrom.*, 2012, **27**(8), 1294–1303.
- 278 R. B. Anderson, J. F. Bell, R. C. Wiens, R. V. Morris and S. M. Clegg, *Spectrochim. Acta, Part B*, 2012, **70**, 24–32.
- 279 M. D. Dyar, M. L. Carmosino, E. A. Breves, M. V. Ozanne, S. M. Clegg and R. C. Wiens, *Spectrochim. Acta, Part B*, 2012, **70**, 51–67.
- 280 C. B. Stipe, E. Guevara, J. Brown and G. R. Rossman, *Spectrochim. Acta, Part B*, 2012, **70**, 45–50.
- 281 J. Rakovsky, O. Musset, J. Buoncristiani, V. Bichet, F. Monna, P. Neige and P. Veis, *Spectrochim. Acta, Part B*, 2012, **74–75**, 57–65.
- 282 C. Bendicho, I. Lavilla, F. Pena-Pereira and V. Romero, *J. Anal. At. Spectrom.*, 2012, **27**(11), 1831–1857.
- 283 W. Zhang, Z. C. Hu, Y. S. Liu, H. H. Chen, S. Gao and R. M. Gaschnig, *Anal. Chem.*, 2012, **84**(24), 10686–10693.



- 284 K. Gopalan, *Geostand. Geoanal. Res.*, 2012, **36**(4), 399–405.
- 285 W. Zhang, Z. C. Hu, Y. S. Liu, L. Chen, H. H. Chen, M. Li, L. S. Zhao, S. H. Hu and S. Gao, *Geostand. Geoanal. Res.*, 2012, **36**(3), 271–289.
- 286 F. G. Pinto, R. Escalfoni and T. D. Saint-Pierre, *Anal. Lett.*, 2012, **45**(12), 1537–1556.
- 287 A. K. Singh, V. Padmasubashini and L. Gopal, *J. Radioanal. Nucl. Chem.*, 2012, **294**(1), 19–25.
- 288 Y. L. Sun, S. L. Sun, C. Y. Wang and P. Xu, *Geostand. Geoanal. Res.*, 2013, **37**(1), 65–76.
- 289 N. N. Fedyunina, K. B. Ossipov, I. F. Seregina, M. A. Bolshov, M. A. Statkus and G. I. Tsylin, *Talanta*, 2012, **102**, 128–131.
- 290 A. Asfaw, W. R. MacFarlane and D. Beauchemin, *J. Anal. At. Spectrom.*, 2012, **27**(8), 1254–1263.
- 291 D. C. Baxter, I. Rodushkin and E. Engstrom, *J. Anal. At. Spectrom.*, 2012, **27**(9), 1355–1381.
- 292 H. P. Longerich, *J. Anal. At. Spectrom.*, 2012, **27**(8), 1181–1184.
- 293 M. S. Choi, J. S. Ryu, S. W. Lee, H. S. Shin and K. S. Lee, *J. Anal. At. Spectrom.*, 2012, **27**(11), 1955–1959.
- 294 L. Lobo, V. Devulder, P. Degryse and F. Vanhaecke, *J. Anal. At. Spectrom.*, 2012, **27**(8), 1304–1310.
- 295 S. H. Tian, Z. Q. Hou, A. N. Su, K. J. Hou, W. J. Hu, Z. Z. Li, Y. Zhao, Y. G. Gao, Y. H. Li, D. Yang and Z. S. Yang, *Acta Geol. Sin.*, 2012, **86**(5), 1297–1305.
- 296 T. Nozaki, K. Suzuki, G. Ravizza, J. I. Kimura and Q. Chang, *Geostand. Geoanal. Res.*, 2012, **36**(2), 131–148.
- 297 C. J. M. Lawley and D. Selby, *Econ. Geol.*, 2012, **107**(7), 1499–1505.
- 298 A. Y. Kramchaninov, I. V. Chernyshev and K. N. Shatagin, *J. Anal. Chem.*, 2012, **67**(14), 1084–1092.
- 299 E. Paredes, D. G. Asfaha and C. R. Quetel, *J. Anal. At. Spectrom.*, 2013, **28**(3), 320–326.
- 300 M. E. Sanchez-Lorda, S. G. de Madinabeitia, C. Pin and J. I. G. Ibarguchi, *Int. J. Mass Spectrom.*, 2013, **333**, 34–43.
- 301 T. Ohno and T. Hirata, *Anal. Sci.*, 2013, **29**(1), 47–53.
- 302 F. Corfu, *Geol. Soc. Am. Bull.*, 2013, **125**(1–2), 33–47.
- 303 F. E. Stanley, *J. Anal. At. Spectrom.*, 2012, **27**(11), 1821–1830.
- 304 M. D. Schmitz and K. F. Kuiper, *Elements*, 2013, **9**(1), 25–30.
- 305 J. Woodhead and R. Pickering, *Chem. Geol.*, 2012, **322**, 290–299.
- 306 J. Woodhead, J. Hellstrom, R. Pickering, R. Drysdale, B. Paul and P. Bajo, *Quaternary Geochronology*, 2012, **14**, 105–113.
- 307 S. Wakaki and T. Tanaka, *Int. J. Mass Spectrom.*, 2012, **323**, 45–54.
- 308 J. M. Koornneef, C. Bouman, J. B. Schwieters and G. R. Davies, *J. Anal. At. Spectrom.*, 2013, **28**(5), 749–754.
- 309 C. F. Li, X. H. Li, Q. L. Li, J. H. Guo, L. J. Feng and Z. Y. Chu, *Anal. Chem.*, 2012, **84**(14), 6040–6047.
- 310 H. P. Wu, S. Y. Jiang, H. Z. Wei and X. Yan, *Int. J. Mass Spectrom.*, 2012, **328**, 67–77.
- 311 X. Yan, S. Y. Jiang, H. Z. Wei, Y. Yan, H. P. Wu and W. Pu, *Chin. J. Inorg. Anal. Chem.*, 2012, **40**(11), 1654–1659.
- 312 E. M. Peterman, J. M. Mattinson and B. R. Hacker, *Chem. Geol.*, 2012, **312**, 58–73.
- 313 M. H. Huyskens, T. Iizuka and Y. Amelin, *J. Anal. At. Spectrom.*, 2012, **27**(9), 1439–1446.
- 314 P. Hoppe, S. Cohen and A. Meibom, *Geostand. Geoanal. Res.*, 2013, **37**(2), 111–154.
- 315 L. Vetter, R. Kozdon, C. I. Mora, S. M. Eggins, J. W. Valley, B. Honisch and H. J. Spero, *Geochim. Cosmochim. Acta*, 2013, **107**, 267–278.
- 316 C. Brahmi, I. Domart-Coulon, L. Rougee, D. G. Pyle, J. Stolarski, J. J. Mahoney, R. H. Richmond, G. K. Ostrander and A. Meibom, *Coral Reefs*, 2012, **31**(3), 741–752.
- 317 A. K. Schmitt and T. Zack, *Chem. Geol.*, 2012, **332**, 65–73.
- 318 A. K. Ault, R. M. Flowers and K. H. Mahan, *Earth Planet. Sci. Lett.*, 2012, **339**, 57–66.
- 319 T. H. Luu, M. Chaussidon, R. K. Mishra, C. Rollion-Bard, J. Villeneuve, G. Srinivasan and J. L. Birck, *J. Anal. At. Spectrom.*, 2013, **28**(1), 67–76.
- 320 M. E. Hartley, T. Thordarson, C. Taylor, J. G. Fitton and EIMF, *Chem. Geol.*, 2012, **334**, 312–323.
- 321 J. W. Boyce, J. M. Eiler and M. B. Channon, *Am. Mineral.*, 2012, **97**(7), 1116–1128.
- 322 M. J. Whitehouse, *Geostand. Geoanal. Res.*, 2013, **37**(1), 19–33.
- 323 A. F. A. Marques, S. D. Scott and R. N. S. Sodhi, *Can. Mineral.*, 2012, **50**(5), 1305–1320.
- 324 L. Zimmermann, P. H. Blard, P. Burnard, S. Medynski, R. Pik and N. Puchol, *Geostand. Geoanal. Res.*, 2012, **36**(2), 121–129.
- 325 K. M. Wilcken, S. Freeman, C. Schnabel, S. A. Binnie, S. Xu and R. J. Phillips, *Nucl. Instrum. Methods Phys. Res., Sect. B*, 2013, **294**, 107–114.
- 326 A. Wallner, K. Melber, S. Merchel, U. Otte, O. Forstner, R. Golser, W. Kutschera, A. Priller and P. Steier, *Nucl. Instrum. Methods Phys. Res., Sect. B*, 2013, **294**, 496–502.
- 327 S. Merchel, W. Bremser, S. Akhmadaliev, M. Arnold, G. Aumaitre, D. L. Bourles, R. Braucher, M. Caffee, M. Christl, L. K. Fifield, R. C. Finkel, S. Freeman, A. Ruiz-Gomez, P. W. Kubik, M. Martschini, D. H. Rood, S. G. Tims, A. Wallner, K. M. Wilcken and S. Xu, *Nucl. Instrum. Methods Phys. Res., Sect. B*, 2012, **289**, 68–73.
- 328 J. Lachner, M. Christl, H. A. Synal, M. Frank and M. Jakobsson, *Nucl. Instrum. Methods Phys. Res., Sect. B*, 2013, **294**, 67–71.
- 329 K. Horiuchi, I. Oniyangi, H. Wasada and H. Matsuzaki, *Nucl. Instrum. Methods Phys. Res., Sect. B*, 2013, **294**, 72–76.
- 330 C. Mifsud, T. Fujioka and D. Fink, *Nucl. Instrum. Methods Phys. Res., Sect. B*, 2013, **294**, 203–207.
- 331 L. Bertrand, M. Cotte, M. Stapanoni, M. Thoury, F. Marone and S. Schoder, *Phys. Rep.*, 2012, **519**(2), 51–96.
- 332 U. Cevik, S. Akbulut, Y. Makarovska and R. Van Grieken, *Spectrosc. Lett.*, 2013, **46**(1), 36–46.
- 333 G. Gauthier, A. L. Burke and M. Leclerc, *J. Archaeol. Sci.*, 2012, **39**(7), 2436–2451.
- 334 R. Redus and A. Huber, *X-Ray Spectrom.*, 2012, **41**(6), 401–409.



- 335 R. Redus, A. Huber, T. Pantazis, J. Pantazis and B. Cross, *X-Ray Spectrom.*, 2012, **41**(6), 393–400.
- 336 D. Wilhelms-Dick, T. Westerhold, U. Rohl, F. Wilhelms, C. Vogt, T. J. J. Hanebuth, H. Rommermann, M. Kriews and S. Kasten, *J. Anal. At. Spectrom.*, 2012, **27**(9), 1574–1584.
- 337 R. Hennekam and G. de Lange, *Limnol. Oceanogr.*, 2012, **10**, 991–1003.
- 338 H. Rowe, N. Hughes and K. Robinson, *Chem. Geol.*, 2012, **324**, 122–131.
- 339 D. Mitchell, P. Grave, M. Maccheroni and E. Gelman, *J. Archaeol. Sci.*, 2012, **39**(9), 2921–2933.
- 340 S. Liu, Q. H. Li, F. Gan, P. Zhang and J. W. Lankton, *J. Archaeol. Sci.*, 2012, **39**(7), 2128–2142.
- 341 M. Wiedenbeck, *Elements*, 2013, **9**(1), 7–8.

